Theoretical and Experimental Studies of

Cryogenic and Hydrothermal Organic Geochemistry

by

Christopher R. Glein

A Dissertation Presented in Partial Fulfillment
of the Requirement for the Degree
Doctor of Philosophy

Approved June 2012 by the
Graduate Supervisory Committee:

Everett L. Shock, Chair
Hilairy E. Hartnett
Mikhail Y. Zolotov
Lynda B. Williams
Ian R. Gould

ARIZONA STATE UNIVERSITY

August 2012

ABSTRACT

This dissertation examines two topics of emerging interest in the field of organic geochemistry. The topic of the first portion of the dissertation is cold organic geochemistry on Saturn's moon Titan. Titan has an atmosphere and surface that are rich in organic compounds. Liquid hydrocarbons exist on the surface, most famously as lakes. Photochemical reactions produce solid organics in Titan's atmosphere, and these materials settle onto the surface. At the surface, liquids can interact with solids, and geochemical processes can occur. To better understand these processes, I developed a thermodynamic model that can be used to calculate the solubilities of gases and solids in liquid hydrocarbons at cryogenic temperatures. The model was parameterized using experimental data, and provides a good fit to the data. Application of the model to Titan reveals that the equilibrium composition of surface liquids depends on the abundance of methane in the local atmosphere. The model also indicates that solid acetylene should be quite soluble in surface liquids, which implies that acetylene-rich rocks should be susceptible to chemical erosion, and acetylene evaporites may form on Titan.

In the latter half of this dissertation, I focus on hot organic geochemistry below the surface of the Earth. Organic compounds are common in sediments. Burial of sediments leads to changes in physical and chemical conditions, promoting organic reactions. An important organic reaction in subsurface environments is decarboxylation, which generates hydrocarbons and carbon dioxide from simple organic acids. Fundamental knowledge about decarboxylation is required to better understand how the organic and inorganic

compositions of sediments evolve in response to changing geochemical conditions. I performed experiments with the model compound phenylacetic acid to obtain information about mechanisms of decarboxylation in hydrothermal fluids. Patterns in rates of decarboxylation of substituted phenylacetic acids point to a mechanism that proceeds through a ring-protonated zwitterion of phenylacetic acid. In contrast, substituted sodium phenylacetates exhibit a different kinetic pattern, one that is consistent with the formation of the benzyl anion as an intermediate. Results from experiments with added hydrochloric acid or sodium hydroxide, and deuterated water agree with these interpretations. Thus, speciation dictates mechanism of decarboxylation.

ACKNOWLEDGEMENTS

TABLE OF CONTENTS

LIST OF TABLES

LIST OF FIGURES

Figure   Page

Chapter 1

MODIFIED VAN LAAR MODEL OF NON-IDEAL SOLUTIONS IN THE CH_4-C_2H_6-C_3H_8-N_2-C_2H_2 SYSTEM ON SATURN'S MOON TITAN

1. Introduction

Saturn's giant moon, Titan, is a frigid but not entirely frozen world, as there is substantial evidence that surface liquids are present and that they erode the land (see reviews by Jaumann et al., 2009; Lunine & Lorenz, 2009). Global observations by the RADAR instrument onboard the Cassini spacecraft have revealed widespread channels with diverse morphologies (e.g., branching, meandering, braiding) that are indicative of fluvial transport and erosion (Elachi et al., 2006; Lorenz et al., 2008a; Langhans et al., 2012). Some of the channels have lengths of up to several hundred kilometers. By analogy with Earth, the presence of dendritic (tree-shaped) networks of valleys implies that rivers are supplied by a distributed source of rainfall, presumably with a methane-rich composition (Lorenz et al., 2008a). Methane (CH_4) is the second most abundant constituent of Titan's atmosphere (Niemann et al., 2010), and liquid CH_4 is volatile enough to participate in a "hydrologic" cycle. Changes in surface brightness after a cloud outburst also provide indirect evidence for recent rainfall near Titan's equator (Turtle et al., 2011a).

The RADAR instrument has also revealed surface features that are widely regarded as lakes or seas of liquid hydrocarbons (Stofan et al., 2007; Hayes et al.,

2008; Turtle et al., 2009; Stephan et al., 2010). These features are radar-dark, which means that they have smooth surfaces, they have shapes that resemble various types of lakes on Earth, and some of the features are associated with sinuous channels (presumably rivers feeding the lakes). Observed lakes and seas are generally restricted to Titan's polar regions, and they are more abundant in the north polar region than in the south (Aharonson et al., 2009). The largest seas have surface areas of up to several hundred square kilometers. Infrared spectroscopic data obtained by the Visual and Infrared Mapping Spectrometer (VIMS) on Cassini strongly suggest the presence of liquid ethane (C_2H_6) in the south polar lake Ontario Lacus (Brown et al., 2008).

Data from the Huygens probe provide more localized evidence of fluvial processes on Titan. Dendritic networks draining from highlands to lowlands were observed during the descent of the probe (Soderblom et al., 2007), and the Huygens landing site was peppered with rounded stones, which may have been abraded during earlier fluvial transport (Tomasko et al., 2005). Some liquid CH_4 and C_2H_6 appeared to be present at the landing site, as evidenced by elevated abundances of CH_4 and C_2H_6 at the surface, compared to the near-surface atmosphere (Niemann et al., 2010).

These discoveries incite many questions pertaining to geochemistry. What are the chemical compositions of liquids (e.g., rivers and lakes) on Titan? How chemically complex and diverse are the molecules dissolved in such liquids? What physical and chemical processes control liquid composition, and how do they operate over space and time? How soluble are atmospheric gases and surface

solids in liquids on Titan? Does chemical weathering occur? Are there geological features that are produced by processes involving the dissolution or precipitation of solids? And, how does fluvial geochemistry on Titan compare to that on Earth (and Mars)? While definitive answers to these questions must await future spacecraft exploration (e.g., TSSM Final Report, 2009; Coustenis et al., 2009; Stofan et al., 2010), it would be useful to begin formulating sensible hypotheses about geochemistry on Titan in preparation for future missions by doing laboratory and theoretical work. Indeed, a group at the Jet Propulsion Laboratory is measuring the solubilities of organic solids and rare gases in liquid hydrocarbons at cryogenic conditions (Hodyss et al., 2010, 2012). The time seems ripe to initiate a complementary program of theoretical research on equilibrium geochemistry. Thus, the primary goal of this study is to develop a model that can be used to quantitatively describe thermodynamic equilibria between gas, liquid, and solid phases on Titan. Knowledge of chemical equilibrium is powerful, as experience demonstrates that many geochemical phenomena on Earth can be understood in terms of equilibrium concepts (e.g., Garrels & Christ, 1965; Drever, 1997). Characterization of equilibrium is also the first step in identifying departures from equilibrium and processes that create disequilibrium.

Numerous equilibrium composition models have been developed for applications to Titan (Lunine et al., 1983; Lunine, 1985; Thompson, 1985; Raulin, 1987; Dubouloz et al., 1989; Thompson et al., 1990, 1992; Gabis, 1991; Kouvaris & Flasar, 1991; Heintz & Bich, 2009; Cordier et al., 2009, 2010, 2012). While these studies were trailblazing in drawing attention to aspects of Titan's

geochemistry, a new model is needed because existing models are too highly parameterized to specific systems, or they are not sufficiently accurate. In many cases, previous investigators did not test their model by explicit comparison with experimental data. This leads to uncertainty about how well the model of interest performs. Model parameters or other input data are also not given in some cases (references provided instead). There are barriers to studying Titan's geochemistry using existing models. Hence, an objective of this paper is to present a generalized thermodynamic framework that is both accurate and easy-to-use. Here, a model will be built using internally consistent experimental data, and the model will be tested by explicit comparison with experimental data. Another key difference between this work and previous studies is that geochemical reasoning will be demonstrated here. Making comparisons with terrestrial geochemistry gives computed values geochemical context, which helps in relating numbers from thermodynamic modeling to behaviors and occurrences of materials, and associated geological processes on Titan.

The study reported here presents an empirical model that represents, as accurately as possible, solid-liquid-vapor phase equilibrium between CH_4, C_2H_6, C_3H_8 (propane), N_2 (molecular nitrogen), and C_2H_2 (acetylene) at Titan surface conditions. N_2 and CH_4 are the major constituents of Titan's atmosphere (Niemann et al., 2010), and C_2H_6, C_2H_2, and C_3H_8 are the three most abundant products of CH_4 photochemistry in the atmosphere (Magee et al., 2009; Vinatier et al., 2010; Coustenis et al., 2010). Transport (e.g., diffusion, turbulent mixing) and condensation processes in Titan's atmosphere deliver these compounds and

others to the surface (Strobel et al., 2009), where they can participate in

geochemical processes (Lorenz & Lunine, 1996). Photochemical models (e.g.,

Yung et al., 1984; Lavvas et al., 2008a, 2008b) predict that large quantities of

liquid C_2H_6 and solid C_2H_2 (along with smaller amounts of liquid C_3H_8) would

have accumulated on Titan's surface if present-day photochemical production

rates are applicable to Titan's past (Lunine et al., 1983). However, a preliminary

survey of Titan's lakes suggested that there may be less C_2H_6 than originally

thought (Lorenz et al., 2008b). Similarly, C_2H_2 may not be as ubiquitous as once

believed, as VIMS has not detected it thus far (Clark et al., 2010). On the other

hand, C_2H_2 was detected by the Huygens Gas Chromatograph-Mass Spectrometer

(GC-MS) (Niemann et al., 2010). Reconciling the chemistries of the atmosphere

and surface is difficult (e.g., Wilson & Atreya, 2009), and will not be attempted

here. The CH_4-C_2H_6-C_3H_8-C_2H_2-N_2 system is a relevant and manageable

foundation for a geochemical model of Titan's surface, as this system features the

most important liquid hydrocarbons, possibly the most abundant organic solid,

and the dominant atmospheric species on Titan. Below, I present the

thermodynamics of the model (Section 2), I derive model parameters by

regression and correlation analyses (Section 3), I test the model and others by

comparing model predictions to independent experimental data (Section 4), and I

show how the model can be used to obtain useful information about cryogenic

hydrocarbon geochemistry on Titan (Section 5).

2. Thermodynamic relations

Thermodynamic equilibrium is the lowest energy state of a system, where physical and chemical properties of the system cease to change (Prausnitz et al., 1999; Anderson, 2005). In the absence of energy input, systems tend toward equilibrium, in accordance with the second law of thermodynamics. Phase equilibrium occurs when the temperature, pressure, and chemical potentials of system components are the same in equilibrating phases. Because chemical potentials are abstract quantities, fugacities (*f*) are more convenient variables to use in modeling, as they are proportional to partial pressures. In terms of fugacities, the phase equilibrium requirement is that the fugacities of system components be equal in equilibrating phases

$$f_k^\alpha = f_k^\beta \, , \tag{1}$$

where *k* designates component *k*, and α and β stand for separate phases. Standard states (denoted by superscript 0) must be defined before vapor-liquid and solid-liquid equilibria can be modeled. Standard states of temperature, pressure, and composition provide initial conditions for integrating thermodynamic functions to the desired state of the system. Here, I adopt conventional standard states of pure liquids and solids at the temperature and pressure of interest, and ideal gases at the temperature of interest and a pressure of 1 bar. Note that the standard state for a liquid will be hypothetical if the temperature is below the triple-point

temperature, but this is acceptable provided that the fugacity of the hypothetical liquid can be calculated.

Fugacities can be expressed as the product of the standard state fugacity and a concentration term, called activity (a). For liquids and solids, activity is defined as $a = \gamma x$, where γ signifies the (rational) activity coefficient, and x represents mole fraction; for gases, activity is defined as $a = \phi p$, where ϕ refers to the fugacity coefficient, and p corresponds to partial pressure. These definitions differ because the standard states are different. Using these quantities, Eq. (1) can be transformed into a form that is useful for evaluating vapor-liquid equilibria (Prausnitz et al., 1999)

$$\left(\phi_k p_k f_k^0 \right)^{gas} = \left(\gamma_k x_k f_k^0 \right)^{liq}. \tag{2}$$

Raoult's law can be derived from Eq. (2) by assuming that $\phi_k = \gamma_k = 1$. This is valid if gas molecules do not interact with each other, and if the average energy of interactions between molecules of k and other molecules in the liquid mixture is identical to that in pure liquid k. This phenomenon is known as ideal behavior. Real solutions may approximate ideal behavior if pressures are low, and liquid-phase molecules are similar in size, shape, and chemical nature.

A major goal here is to calculate the solubility of atmospheric gases, such as N_2, in liquids on Titan, which means that x_k must be obtained from Eq. (2). The other five quantities in Eq. (2) are specified using the following strategy. First,

$f_k^{0,gas}$ is set to 1 bar, following standard state conventions. Standard state fugacities of liquids ($f_k^{0,liq}$) are computed using the National Institute of Standards and Technology (NIST) REFPROP program (Lemmon et al., 2010), which computes thermodynamic properties using equations of state for the Helmholtz energy (CH_4: Setzmann & Wagner, 1991; C_2H_6: Bucker & Wagner, 2006; C_3H_8: Lemmon et al., 2009; N_2: Span et al., 2000). The equations in REFPROP were optimized to fit a large amount of thermal and volumetric data, and they are complex and accurate. Fugacity coefficients (ϕ_k) are also obtained from REFPROP. Partial pressures of gases (p_k) are treated as free parameters that can be compared with analytical data. This leaves the activity coefficients (γ_k).

Typically, activity coefficients are obtained from a model that has been shown to be consistent with experimental data. The general procedure is to adopt an activity coefficient model that contains empirical parameters, and then determine best-fit values of the parameters by regressing experimental data. A desirable model would have the following features: (1) a theoretical underpinning; (2) reproduces experimental data well; (3) a minimal number of adjustable parameters; (4) can be extended to multicomponent systems using binary parameters only; and (5) mathematical simplicity. A modified van Laar (MVL) model (van Laar, 1906) may satisfy these criteria best. Activity coefficients from this model can be written as (see Appendix A)

$$RT \times \ln\left(\gamma_k^{liq}\right) = -\sum_{i=1}^{n-1} \sum_{j>i}^{n} \frac{\omega_{ij} \lambda_i \lambda_j q_k}{q_i + q_j}, \tag{3}$$

where R corresponds to the molar gas constant (8.314462 J mol^{-1} K^{-1}; CODATA, 2010), T represents absolute temperature, ω_{ij} denotes the interaction energy for binary system i-j, and q_k stands for the effective volume of component k in the liquid mixture (note that ratios of q's rather than individual values are important to the thermodynamics of the non-ideal mixture). Auxiliary function λ is given in terms of effective volume fraction (z) by $\lambda_i = 1 - z_i$ when $i = k$, and $\lambda_i = -z_i$ when $i \neq k$. Effective volume fractions can be evaluated using

$$z_k = \frac{x_k q_k}{q_{mix}}, \tag{4}$$

with

$$q_{mix} = \sum_{i=1}^{n} x_i q_i. \tag{5}$$

The MVL model in the present communication was derived from the regular solution theory of Scatchard and Hildebrand (see Appendix A), which is a generalization of van Laar's original theory (see Prausnitz et al., 1999). The difference between the MVL model and Scatchard-Hildebrand theory is that the energy and volume terms in the regular-solution equations are replaced by empirical parameters. This leads to better agreement with experimental data. Other researchers have also modified van Laar's theory by introducing empirical

parameters, including Wohl (1946), Black (1958), Chien & Null (1972), Focke (2001), Holland & Powell (2003), and Peng (2010). In general, the various van Laar-type models are functionally equivalent, and they differ by how energy and volume parameters are defined. For example, the present model is nearly identical to that of Holland & Powell (2003), as Eq. (3) differs from its counterpart in Holland & Powell (2003) by a factor of two.

For reference, the activity coefficients of the components in binary 1-2 from the MVL model are given by

$$RT \times \ln\left(\gamma_1\right) = \left(\frac{\omega_{12}}{1+\frac{q_2}{q_1}}\right)\left(1+\frac{q_1 x_1}{q_2 x_2}\right)^{-2},$$

(6)

and

$$RT \times \ln\left(\gamma_2\right) = \left(\frac{\omega_{12}}{1+\frac{q_1}{q_2}}\right)\left(1+\frac{q_2 x_2}{q_1 x_1}\right)^{-2}.$$

(7)

There are two obstacles when using the MVL model in the above equations. First, the model uses two empirical parameters for each binary system (q_1/q_2 and ω_{12}). This makes it difficult to regress experimental solid-liquid equilibrium data, which generally consist of a single point (i.e., solubility) at a given temperature. Second, the model implicitly relies upon a restrictive relationship between ratios of q's in multicomponent systems. As an example,

10

ternaries must obey the relationship $(q_3/q_2) = (q_3/q_1) \times (q_1/q_2)$ for the model to

maintain mathematical consistency. This limitation, first discussed by Wohl

(1946), is undesirable because some systems may not satisfy the relationship. A

way to address both concerns is to replace q ratios with ratios of actual volumes.

Two candidates are liquid volume ratios (Hildebrand & Scott, 1950) and critical

volume ratios (Peng, 2010). During the course of regressing data as described in

Section 3, it was found that best-fit q ratios are similar to critical volume ratios,

but smaller than liquid volume ratios, as illustrated in Fig. 1. Thus, I recommend

that critical volume ratios be used, which implies that critical volumes be

substituted for effective volumes in the model. However, caution should be

exercised if the critical volumes of two components differ by more than a factor

of ~3, or if one of the components is polar (e.g., Poling et al., 2001).

Next, solid-liquid equilibrium can be characterized by equating fugacities

in the solid and liquid phases

$$\left(\gamma_k x_k f_k^0 \right)^{sol} = \left(\gamma_k x_k f_k^0 \right)^{liq}. \tag{8}$$

Equation (8) can be used to calculate the solubilities of solids in liquids on Titan.

A common simplification is to assume that the solid of interest is pure (e.g.,

Preston & Prausnitz, 1970), so that both γ_k^{sol} and x_k^{sol} can be set to unity. This

does not mean that solids must occur as pure deposits on Titan; instead, the

requirement is purity on the scale of crystals. Of course, nothing is presently

known about the nature of solids on Titan at this scale, and it is doubtful that such information will be obtained in the near-future. On the other hand, it is arguable that solid solution formation may be inhibited on Titan owing to low surface temperatures, which should make processes of mixing molecules in crystal lattices less thermodynamically favorable. As a starting point for modeling, I assume that solids on Titan's surface are pure phases.

Standard state fugacities of solids and supercooled liquids are now needed, and here the focus is C_2H_2 as an example. Fugacities are assumed to be equal to their respective vapor pressures, which is a reasonable approximation at temperatures below the triple point, where pressures are low (<1 bar). Vapor pressures above solid C_2H_2 were taken from Tickner & Lossing (1951) and Ambrose (1956), and are represented by the following equation

$$\log\left(p_{C_2H_2}, \mathrm{bar}\right) = 11.977 - 1333.01 \times T^{-1} - 0.9399 \times \ln(T), \qquad (9)$$

which may be used between ~90 and 192 K (Fig. 2). Close agreement between Eq. (9) and data from Stull (1947) was also found, but vapor pressures reported by Bourbo (1943) are up to two times larger than those from Eq. (9). Thus, vapor pressures from Eq. (9) may be uncertain by a factor of ~2.

What would be the vapor pressure above liquid C_2H_2 if C_2H_2 could exist as a supercooled liquid? This question can be addressed using the Ambrose-Walton corresponding-states method (Poling et al., 2001). This correlation relates vapor pressures of fluids to critical properties, and works well for nonpolar fluids.

12

Critical properties of C_2H_2 were taken from Ambrose & Townsend (1964). As shown in Fig. 2, the correlation reproduces experimental vapor pressures of liquid C_2H_2 well (to within ~0.3%) between the triple (193 K) and critical (308 K) points. In addition, vapor pressures of liquid C_3H_8 from the correlation were compared with those from REFPROP to determine whether the correlation is reliable at lower temperatures. Results agreed to within ~3% at temperatures from 86-370 K (C_3H_8 was chosen as a test substance because it is a nonpolar compound with a wide temperature range of liquidity).

The solubility of a solid in a liquid depends on the ratio of standard state fugacities (equivalent to the equilibrium constant generally used in geochemical studies), rather than on individual values. For C_2H_2, the fugacity ratio can be represented by

$$\log\left(\frac{f^{sol}}{f^{liq}}\right)^0_{C_2H_2} = 1.6463 - 371.46 \times T^{-1} + 10548 \times T^{-2}, \tag{10}$$

from ~60-192 K. Equation (10) was fit to numerical data generated from Eq. (9), and to results from the corresponding-states method (90-192 K). Graphical analysis (not shown) revealed that the derivative of the logarithm of the fugacity ratio with respect to inverse temperature is approximately linear, so I performed a quadratic extrapolation down to 60 K. Equation (10) has an estimated uncertainty of ~0.5 log units.

It is important to mention that there is an alternative method of calculating standard state fugacity ratios. The key equation is (Preston & Prausnitz, 1970)

$$\ln\left(\frac{f^{sol}}{f^{liq}}\right)^0_{C_2H_2} = \frac{\Delta S^0_{fus}}{R}\left(1-\frac{T_t}{T}\right) - \frac{\Delta C^0_p}{R}\left(1-\frac{T_t}{T}\right) - \frac{\Delta C^0_p}{R}\ln\left(\frac{T_t}{T}\right),$$ (11)

where ΔS^0_{fus} stands for the entropy of fusion at T_t, and ΔC^0_p indicates the difference in isobaric heat capacity between the liquid and solid at the triple-point temperature, T_t. I could not use Eq. (11) for C_2H_2 because I could not find heat capacities of the solid or liquid in the literature. This presents a problem as the heat capacity terms in Eq. (11) assume greater quantitative significance at temperatures further from the triple point, and surface temperatures on Titan are substantially below the triple point of C_2H_2 ($T_t/T \sim 2$). It should be acknowledged, however, that the situation may be the opposite for other compounds, with thermal data being more plentiful or reliable, and vapor pressure data being less available or reliable. In those cases (which may be common), Eq. (11) is preferred.

3. Regression of binary data

Binary phase equilibrium data that can be used to parameterize the MVL model at temperatures bracketing those on Titan (~90-95 K) are summarized in Table 1. Vapor-liquid equilibrium (VLE) data consist of measurements of liquid

phase composition, total pressure, and temperature (the composition of the vapor phase is given in some cases). Solid-liquid equilibrium (SLE) data correspond to solid solubility as a function of temperature. Compositions of immiscible liquids, total pressures, and temperatures are reported in studies of liquid-liquid equilibrium (LLE). In this study, LLE were not considered because it is unlikely that LLE exist on Titan (Thompson, 1985), because the partial pressure of N_2 at Titan's surface (~1.4 bar) is too low to induce phase splitting. Extrapolation of separation pressures for the N_2-C_2H_6 system indicates that two liquid phases should form only if $p_{N_2} > 3.8$ bar at 91 K (Gasem et al., 1981). The N_2-C_3H_8 binary requires similar pressures for phase separation (Schindler et al., 1966). In contrast, N_2 and CH_4 are miscible. The MVL model in this work should not be used whenever LLE are suspected (e.g., C_2H_6- or C_3H_8-rich systems containing N_2 near the saturation pressure of liquid N_2).

Binary VLE data were regressed using Barker's method (Barker, 1953), which is a standard technique for determining parameters in activity coefficient models. Least squares fitting was used to obtain parameters in Eqs. (6) and (7) that minimize differences between calculated and experimental total pressures. The fitting procedure was iterative. I initially let the regression program optimize both ω_{12} and q_1/q_2. However, it became apparent that best-fit q ratios and critical volume ratios are very similar (Fig. 1), so q ratios in Eqs. (6) and (7) were replaced with the respective critical volume ratio (Table 2). This reduces the MVL model to a one-parameter form, which brings benefits as discussed in Section 2, and this simplification does not introduce significant inaccuracies (see

15

below). Binary SLE data were regressed by applying least squares fitting to reported solubilities. While all of the datasets listed in Table 1 were analyzed, only a subset of the data was used in the final regressions. Decisions were made by examining trends in derived values of ω_{12}; values of ω_{12} from mutually consistent data varied smoothly with temperature. The recommendations of Hiza et al. (1979), Miller et al. (1980), and Kidnay et al. (1985) were also given preference. Note that data not used in the final regressions are not necessarily "bad", as they are simply less consistent with other data.

Activity coefficients depend on temperature, pressure, and composition. The MVL model accounts for the composition dependence via mole fraction terms. The temperature dependence is represented by specifying interaction energies as $\omega_{ij} = \omega_0 + \omega_1 T + \omega_2 T \times \ln(T)$, where subscripted parameters denote constants that are determined by regressing experimental data at different temperatures. In some cases, the data do not warrant a value for ω_2. Interaction energies are parameterized over certain temperature intervals, and extrapolations are governed by *caveat emptor*. I do not account for effects of pressure on activity coefficients because pressure effects should be negligible, except at high pressures (>100 bar or >10 km depth on Titan). Binary solutions of nonpolar compounds of interest have small excess volumes of mixing (generally between 0 and -2 cm^3 mol^{-1}; e.g., Hiza et al., 1979; Miller et al., 1980; Kidnay et al., 1985), which means that mixing is nearly ideal with respect to volume. This makes activity coefficients weak functions of pressure. Exceptions are systems close to

16

the critical point of a component. For this reason, data at temperatures >120 K for systems with N_2 (critical temperature, 126.19 K) were not regressed.

Comparisons between model results and experimental data are shown in Figs. 3-10. It is helpful to show these comparisons because they make it possible to assess the strengths and weaknesses of the MVL model. Results for VLE regressions are shown in Figs. 3-8, and those for SLE regressions are shown in Figs. 9-10. Regressed interaction energies are given in Table 3. These parameters can be used to perform calculations for arbitrary compositions.

In general, the MVL model reproduces the experimental data well. The model is most accurate for all of the binaries involving CH_4 (Figs. 3, 4, 6, 9). Computed pressures agree with measured values to within ~1-2% for CH_4-C_2H_6, CH_4-C_3H_8, and CH_4-N_2. Solubilities of solid C_2H_2 in liquid CH_4 are calculated to within ~10% of experimental values (Fig. 9). Such small variations are characteristic of high-quality experimental data. Residuals in total pressure exhibit either no or weak trends with composition or temperature (Figs. 3, 4, 6), providing additional evidence that the model provides a close representation of the data. The MVL model works well for CH_4-C_2H_6, CH_4-C_3H_8, and CH_4-N_2 because these systems exhibit small deviations from ideality. The activity coefficient of the more volatile component is generally less than ~2, which means that not much demand is placed upon the activity coefficient model. A general rule is that systems with greater non-ideality require more complex models with more parameters (Prausnitz et al., 1999). The C_2H_2-CH_4 system seems to provide a contradiction, as $\gamma_{C_2H_2}^{liq}$ reaches values as large as ~1100. The MVL model

presumably works well for this system because solutions are always dilute with respect to C_2H_2 (Fig. 9), which implies that the chemical nature of the solutions is approximately constant (infinite dilution regime). This simplifies the thermodynamic description.

The C_2H_6-C_3H_8 system is assumed to be ideal (i.e., $\omega_{ij} = 0$). An initial attempt was made to derive interaction energies by regressing VLE data. However, derived values were inconsistent, showing no apparent trend with temperature. It appears that errors in the experimental data are larger than the very small deviations from ideality. This idea was tested by assuming ideal behavior in Fig. 5. Total pressures from the ideal solution model agree with measured values to within ~5-10%. Djordjevich & Budenholzer (1970) reported that their experimental pressures have errors of up to 4%, and their composition measurements have an uncertainty of 3 mole %. Thus, C_2H_6-C_3H_8 probably deviates from ideality by ~5%, but the ideal model is sufficient for applications of interest to Titan.

The MVL model reproduces experimental data for the N_2-C_2H_6, N_2-C_3H_8, and C_2H_2-N_2 binaries with respectable accuracy, although there are some issues (Figs. 7, 8, 10). Deviations in total pressure of ~5-10% characterize N_2-C_2H_6 (Fig. 7), while N_2-C_3H_8 features larger deviations of ~10-20% (Fig. 8). However, N_2-C_3H_8 is less crucial because C_3H_8 is probably much less abundant than C_2H_6 on Titan (see Section 5). Solubilities of solid C_2H_2 in liquid N_2 are computed to within ~20% of experimental values (Fig. 10). Residuals in total pressure display trends with composition, becoming larger at smaller mole fractions of N_2 (Figs. 7-

8). This is not surprising since the activity coefficient of N_2 is large in mixtures containing small amounts of N_2 (γ_{N_2} up to ~7 and ~14 for N_2-C_2H_6 and N_2-C_3H_8, respectively). A great demand is placed upon the activity coefficient model to correct for such non-idealities, and trends in residuals imply that my simple model does not capture all of the complexities of these systems. Comparisons of solubilities of solid C_2H_6 and solid C_3H_8 in liquid N_2 were also made (not shown), and it was found that calculated values agree with data reported by Szczepaniec-Cieciak et al. (1980) to within ~15%. Again, some accuracy is sacrificed for the simplicity and generality of the MVL model.

A new correlation is used to estimate interaction energies for C_2H_2-C_2H_6 and C_2H_2-C_3H_8, as SLE data could not be found for these systems at relevant temperatures. The correlation at 90.6941 K is shown in Fig. 11. It can be seen that regressed interaction energies follow linear trends with differences in enthalpies of vaporization between binary components. There are linear relationships for N_2 and CH_4 with C_1-C_3 alkanes, and the lines go through the origin (coefficient of determination, $R^2 > 0.99$). This simple behavior suggests that interaction energies for C_2H_2-C_2H_6 and C_2H_2-C_3H_8 can be estimated by drawing a line between the point for C_2H_2-CH_4 and the origin. I used this "C_2H_2-alkane line" along with enthalpies of vaporization from Table 2 to estimate the interaction energies, which are given in Table 3.

The correlation adopted in this study invites questions, many of which are addressed here. First, I chose a temperature of 90.6941 K (i.e., the triple-point temperature of CH_4; Setzmann & Wagner, 1991), and I advocate that this be

adopted as the reference temperature for studies of Titan's surface geochemistry, because surface temperatures on Titan are within a few Kelvin of this value (Fulchignoni et al., 2005; Jennings et al., 2009), and because it is easy to achieve this temperature in the laboratory using the solid-liquid equilibrium of CH_4 as a cryostat. The situation is similar to terrestrial geochemistry, where 298.15 K is adopted as the reference temperature for convenience (e.g., Garrels & Christ, 1965; Anderson, 2005). Second, it makes sense that interaction energies correlate positively with differences in enthalpies of vaporization. The enthalpy of vaporization provides a measure of the strength of intermolecular forces in a liquid. A larger difference in enthalpies of vaporization means that interactions between molecules in two liquids are less similar, so the mixture should be less ideal and have a larger value of ω_{ij}. This may also explain why the lines in Fig. 11 pass through the origin. Yet, it is unclear why the correlations are apparently linear, as I am not aware of any theory that predicts this. It is possible that this is an artifact from a lack of data, or that the present data occur in a linear regime. For now, the linear relationships should be viewed as empirical phenomena that require further study. Third, there is the question of uncertainties, which is difficult to address. I lack a good understanding of potential errors, as I have not correlated a sufficient amount of data. However, numerical tests indicate that, if C_2H_2 follows a linear correlation but the slope in Fig. 11 is in slight error, predicted solubilities of solid C_2H_2 in liquid C_2H_6 or C_3H_8 may be uncertain by tens of percent. On the other hand, results could be uncertain by a factor of at least several if linear behavior does not hold. Finally, it may be possible to develop

20

completely predictive correlations. This would allow computational exploration of systems that have not been experimentally characterized, such as C_2N_2(cyanogen)-C_2H_6. The requirement is a method of computing slopes of lines in Fig. 11 using only pure-component properties (e.g., critical temperature, acentric factor, polarizability). It is premature to attempt this type of generalization now because only three slopes are available. More regressions of chemically diverse binaries will be needed.

4. Comparing models of ternary systems

Liquids on Titan are expected to be multicomponent mixtures (Lunine et al., 1983; Raulin, 1987; Cordier et al., 2009). Thus, it is vital to test the MVL model using experimental data for systems containing more than two components. However, experimental phase equilibrium data for relevant ternary systems at conditions relevant to Titan's surface are scarce. Almost all of the available data are for temperatures that are too high (e.g., Chang & Lu, 1967; Yu et al., 1969; Wichterle & Kobayashi, 1972; Poon & Lu, 1974; Llave et al., 1987). The notable exception is a Master's thesis (Gabis, 1991) that contains data on the CH_4-C_2H_6-N_2 system at 95 K. CH_4-C_2H_6-N_2 is regarded as the most important ternary on Titan (Lunine et al., 1983), so it represents a crucial test for the MVL model. Ternary VLE data from Gabis (1991) are reprinted in Table 4, as they are useful and from an unpublished source. Gabis (1991) performed experiments inside a vapor recirculation cell, where vapor is pumped through a liquid to facilitate

21

equilibrium. This type of apparatus is commonly used in studies of low-temperature VLE. Pressure was measured using a Bourdon gauge (±0.01 bar), temperature was measured using a resistance thermometer (±0.2 K), and composition was determined using gas chromatography (±0.003 mole fraction) (Gabis, 1991). Note that VLE data for N_2-CH_4 from Gabis (1991) are consistent with N_2-CH_4 data from McClure et al. (1976) and Parrish & Hiza (1974) to within a few percent (Fig. 6). CH_4-C_2H_6-N_2 data from Gabis (1991) are used in the present study to determine how well the MVL model and others extrapolate to the ternary system.

Various models of VLE in the CH_4-C_2H_6-N_2 ternary at 95 K are compared in Fig. 12. Raoult's law provides the simplest description, by assuming that the mixture is ideal. It can be seen that Raoult's law is the least accurate model, and always underestimates the total pressure. In other words, N_2 gas is predicted to be too soluble in the liquid phase. Raoult's law performs worse in more C_2H_6-rich systems. Evidently, interactions between N_2 and C_2H_6 molecules exhibit large departures from ideal behavior. Raoult's law is an insufficient model for this ternary, and provides crude approximations at best.

The model of Heintz & Bich (2009) was developed with Titan in mind. Activity coefficients are calculated with a one-parameter Margules equation. Results from the Heintz & Bich (2009) model resemble those from Raoult's law, but the Heintz & Bich (2009) model provides minor improvements over Raoult's law by predicting slightly higher pressures (Fig. 12). However, the model also gives results that are quite inaccurate for C_2H_6-rich systems. This may be

22

surprising as a one-parameter Margules equation is expected to provide greater improvement over Raoult's law. I checked references in Heintz & Bich (2009), and could not find any on VLE in the N_2-C_2H_6 system. Hence, it is unclear how Heintz & Bich (2009) determined their Margules parameter for N_2-C_2H_6, which seems to be too small.

The model of Preston & Prausnitz (1970) is based on Scatchard-Hildebrand regular solution theory, with one empirical parameter per binary. This model is popular in the Titan literature (e.g., Dubouloz et al., 1989; Cordier et al., 2009), so it is important to assess its accuracy. Figure 12 shows that the model provides a close representation of CH_4-rich systems (to within ~15%), but the model predicts total pressures that are too high by about a factor of two for systems enriched in C_2H_6. There is a systematic trend in the results (Fig. 12), which suggests that there is a problem with the representation of the N_2-C_2H_6 binary in the Preston & Prausnitz (1970) model; N_2 gas should be more soluble in liquid C_2H_6. It appears that the binary parameter for N_2-C_2H_6 should be more negative than the value given by Preston & Prausnitz (1970). It is recommended that users of this model re-evaluate the parameter using references in Table 1. Cordier et al. (2012) attempted to estimate uncertainties in their regular-solution calculations by performing Monte Carlo simulations. However, a more direct approach would be more informative, and a suggestion is to make comparisons between predictions from the model and experimental phase equilibrium data.

The model of Thompson (1985) has also been used in studies of Titan (e.g., Raulin, 1987; McKay et al., 1993). Activity coefficients are computed using

23

one-parameter Margules equations, with empirically determined exponents of one or two in the activity coefficient equations. Thus, the Thompson (1985) model was formulated similarly to that of Heintz & Bich (2009), but the latter model uses a fixed exponent of two for binaries. I find that Thompson's model is fairly consistent with the experimental ternary data, and it performs significantly better than the Heintz & Bich (2009) model (Fig. 12). The largest discrepancies in total pressure ($\sim$20-30%) occur where CH_4 and C_2H_6 are approximately equimolar, suggesting that three-body interactions are largely responsible for the discrepancies (the model features binary terms only). A key concern is that the Thompson (1985) model is not thermodynamically consistent, as it does not satisfy the Gibbs-Duhem equation. Modifying activity coefficient equations empirically led to this inconsistency. This problem can be prevented if empirical modifications are made to the equation for the excess Gibbs energy of mixing instead (Prausnitz et al., 1999). Thompson recognized this in later works on the N_2-CH_4 binary (Thompson et al., 1990, 1992), but he did not revisit more complex mixtures. However, the issue may be more academic than practically important, as Thompson's (1985) model gives reasonably accurate predictions for the ternary.

The Groupe Europeen de Recherches Gazieres (GERG) model is the most sophisticated model that was tested (Kunz et al., 2007). I used this model as part of the NIST REFPROP software package (Lemmon et al., 2010). The model was developed for technical applications in the natural gas industry. It is an equation of state that is explicit in the Helmholtz energy, and the model is valid over wide

ranges of density, temperature, and composition. Thermodynamic properties of mixtures are computed using departure functions that were fit to binary data. These functions account for non-ideal behavior, and they contain four empirical parameters per binary. The GERG model is the most accurate one in Fig. 12, and reproduces experimental pressures to within ~15%, with deviations that are weakly systematic at most. In terms of accuracy, the GERG model is impressive. The version in REFPROP is also easy-to-use, featuring a graphical user interface. But, the GERG model has disadvantages with respect to Titan applications. A complex mathematical structure (see Kunz et al., 2007) makes the model difficult to modify or expand, and obtaining parameters for the model requires complex, non-linear regression algorithms. A more serious shortcoming is that the model cannot be applied to equilibria involving solids, rendering it inapplicable to solving many geochemical problems.

The MVL model ranks second place; it is slightly more accurate than Thompson's model, but slightly less accurate than the GERG model (Fig. 12). Here, slightly means a few percent or so. The overall agreement with experimental data is encouraging (within ~20%), and suggests that Eq. (3) may provide reasonable representations of other multicomponent systems. Like in the model of Thompson (1985), the deviations in the MVL model are greatest where CH_4 and C_2H_6 are about equally abundant. As mentioned above, this appears to be a ternary effect, which should be strongest at the midpoint in Fig. 12. This effect can be accounted for by adding a ternary term to the model, leading to the general equation for activity coefficients from the MVL model (see Appendix A)

25

$$RT \times \ln\left(\gamma_k^{liq}\right) = -\sum_{i=1}^{n-1}\sum_{j>i}^{n} \frac{\omega_{ij}\lambda_i\lambda_j q_k}{q_i + q_j} + \sum_{a=1}^{n-2}\sum_{b>a}^{n-1}\sum_{c>b}^{n} \frac{\omega_{abc}\delta_a\delta_b\delta_c q_k}{4\left(q_a + q_b + q_c\right)}, \tag{12}$$

where ω_{abc} represents the interaction energy for ternary a-b-c, and auxiliary function δ is given in terms of effective volume fraction by $\delta_i = 1-2z_i$ when $i = k$, and $\delta_i = -2z_i$ when $i \neq k$. I applied Eq. (12) to the Gabis (1991) dataset in Table 4, and derived an interaction energy for CH_4-C_2H_6-N_2 of 2604 J mol^{-1} at 95 K. Interestingly, this value is somewhat close to the arithmetic mean of the constituent binaries (2256 J mol^{-1}). This could be a coincidence, or a hint of a predictive scheme. Additional experimental data for ternary systems will need to be obtained and regressed to determine which.

Figure 13 shows that adding a ternary term to the MVL model (MVL+T) increases the accuracy of the model by ~5-10%. Furthermore, the new model is, on average, a couple percent more accurate than the GERG model. The improvements highlight the flexible architecture of the MVL model. It was also found that computed vapor compositions compare favorably to those in Table 4 (p_{N_2} within ~2%, p_{CH_4} within ~20%). This can be taken as evidence for the thermodynamic consistency of the experimental data. The ternary term shifts the MVL line segment in Fig. 13 upward, with the largest shifts occurring around the CH_4-C_2H_6 midpoint. The maximum absolute deviation in total pressure is now 18% (previously 27%), and corresponds to the most C_2H_6-rich composition. This discrepancy most likely reflects deficiencies in the simplistic description of the

26

N_2-C_2H_6 system (see Section 3), but the magnitude of the discrepancy is probably tolerable for Titan applications.

How important are ternary interactions to solution thermodynamics in non-polar liquids? Figure 14 shows that ternary interactions between CH_4, C_2H_6, and N_2 are of minor quantitative significance, yet they are not completely negligible. Evidently, non-ideal behavior is mostly controlled by binary interactions, and forces between three different molecules fine-tune the system. Based on this inference, I favor a hybrid of Eqs. (3) and (12) for geochemical modeling. Equation (12) is the more general expression, and ternary terms should be included whenever high-quality experimental data exist. If such data are unavailable, ternary interaction energies in Eq. (12) may be set to zero (*à la* Eq. 3), which may lead to errors on the order of tens of percent (Fig. 12). For complex mixtures on Titan, it can be imagined that some ternary terms will be evaluated, while most will be neglected. This will depend on the experimental data and the desired accuracy. My recommendation is to use Eq. (12), but make appropriate simplifications. For now, all ternary terms must be excluded (due to lack of ternary data), with the exception of that for CH_4-C_2H_6-N_2 (I am assuming that the interaction energy for this ternary at 95 K will be appropriate for nearby Titan temperatures).

A summary of the aforementioned models is provided in Fig. 15. It can be seen that Raoult's law, and the models of Heintz & Bich (2009) and Preston & Prausnitz (1970) deviate most from the experimental ternary data. Therefore, these models should not be used to represent equilibria involving CH_4, C_2H_6, and

N_2 on Titan. Thompson's (1985) model provides adequate agreement, but I believe that this model is inferior to the MVL model. The MVL model possesses comparable simplicity but yields more accurate results than those from the Thompson (1985) model (Figs. 12, 15), and the MVL model maintains thermodynamic consistency. The GERG and MVL+T models perform best. Choosing between them is not a clear-cut decision; the choice depends on the specific application. If the user is interested in VLE only (e.g., clouds) and wants user-friendly software that is relatively inexpensive (http://www.nist.gov/srd/nist23.cfm), then the GERG model would be an excellent choice. The MVL+T model would be preferred if the application of interest involves the coupled geochemistry of fluids and solids on Titan's surface, or if the user wants full control over the model (e.g., so they can add new components to the model).

Comparing models to experiments for ternary systems containing solid C_2H_2 would be useful, as this would provide indications of how well current models can predict solid solubility in mixed solvents, like those expected on Titan. However, I could not find solubility data for solid C_2H_2 in liquid mixtures of the components in the MVL model (there are data for C_2H_2 in CH_4-C_2H_4; Neumann & Mann, 1969; and those data will be analyzed once ethylene is added to the MVL model). As a result, it was decided that the next best strategy was to check the consistency of models, as this provides information about uncertainties. The N_2-CH_4-C_2H_2 and CH_4-C_2H_6-C_2H_2 ternaries were adopted as bases for model comparisons. To the best of my knowledge, only the MVL model and the model

of Preston & Prausnitz (1970) can be used to compute the solubility of solid C_2H_2 in these systems at Titan surface temperatures. The latter model has been used extensively to estimate the concentration of C_2H_2 in lakes and hypothetical oceans on Titan (Raulin, 1987; Dubouloz et al., 1989; Cordier et al., 2009).

Calculated solubilities of solid C_2H_2 in liquid mixtures of N_2 and CH_4 at 90.6941 K are shown in Fig. 16. There is reasonable agreement between the MVL and Preston & Prausnitz (1970) models. Both predict that C_2H_2 is slightly more soluble in CH_4 than in N_2. The models agree to within ~30% for N_2-rich compositions, but they deviate by as much as a factor of ~2 for CH_4-rich compositions. The former value may lie within experimental uncertainties, but the latter value implies that one of the models provides an inaccurate representation of the C_2H_2-CH_4 binary (the same solubility data were regressed). Preston & Prausnitz (1970) assumed that the empirical parameter in their model is independent of temperature, whereas the interaction energy in the MVL model varies linearly with temperature (Table 3). This difference is likely to be responsible for the discrepancy, although a factor of ~2 may not be geochemically significant in terms of mineral solubility.

It is also informative to compare results from the MVL model with those from Henry's law, the simplest form of which can be written as (Prausnitz et al., 1999)

$$\log\left(x_3^{sat}\right)_{\text{in mixture}} = \left(\frac{x_1}{x_1 + x_2}\right) \times \log\left(x_3^{sat}\right)_{\text{in pure 1}} + \left(\frac{x_2}{x_1 + x_2}\right) \times \log\left(x_3^{sat}\right)_{\text{in pure 2}}, \quad (13)$$

for the saturation mole fraction of solute 3 in a mixture of cosolvents 1 and 2. Examination of this equation reveals why the "Henry plot" in Fig. 16 is linear. In contrast, the MVL model generates a curve in Fig. 16. Curvature is a general phenomenon in experimental ternary systems (e.g., Tiffin et al., 1979). In this ternary, the curvature results in a solubility enhancement of up to ~35% relative to Henry's law. Numerical analysis of derivatives reveals that there are two reasons for curvature in general. The dominant factor in this case is non-ideal mixing between the cosolvents (the interaction energy for N_2-CH_4 has a non-zero value). The solute plays no role in creating most of the curvature. The second, minor factor here is differences in the effective volumes (i.e., sizes and shapes) of components. This is relatively minor for N_2-CH_4-C_2H_2 because the components have similar critical volumes (Table 2).

Results from models of the CH_4-C_2H_6-C_2H_2 ternary at 90.6941 K are shown in Fig. 17. There are large differences between the MVL and Preston & Prausnitz (1970) models at the C_2H_6 end of the composition scale. The MVL model predicts that C_2H_2 has a mole-fraction solubility of 1.8×10^{-2} in C_2H_6 (approaching the ideal solubility of 6.8×10^{-2}), while the Preston & Prausnitz (1970) model predicts a solubility of 2.4×10^{-4}. At least one of the models must be incorrect! Insight can be gained by comparing these solubilities with those in liquid CH_4. Preston & Prausnitz's model predicts that the solubility increases by a factor of ~3 going from CH_4 to C_2H_6, while the MVL model predicts an enhancement factor of ~390. The enhancement factor for CH_4-C_2H_4-C_2H_2

extrapolates to ~300 at 90.6941 K (Neumann & Mann, 1969), and the estimated

enthalpy of vaporization of C_2H_2 is more similar to that of C_2H_6 (Table 2) than to

that of C_2H_4 (16389 J mol^{-1}; Smukala et al., 2000). Thus, an enhancement factor

>300 seems likely for CH_4-C_2H_6-C_2H_2; so it appears that the MVL model is the

more correct model, although uncertainties remain. Most likely, the problem with

the Preston & Prausnitz (1970) model is that the empirical parameter for C_2H_2-

C_2H_6 cannot be assumed to be constant over a wide temperature range (regressed

data were for 150-170 K). This practice was followed in previous Titan studies

and should be discontinued. The solubility function from the MVL model displays

pronounced curvature (Fig. 17), but here differences in critical volumes (Table 2)

are largely responsible for the curvature. Overall, inconsistencies between models

stress the need for experimental solubilities of solid C_2H_2 in liquid C_2H_6 and in

CH_4-C_2H_6 mixtures at Titan surface temperatures.

5. Titan geochemistry examples

The thermodynamic model outlined above can be used to explore

possibilities for Titan's cryogenic geochemistry. The focus in this section is

examples of solvent composition and mineral solubility that illustrate how

equilibrium calculations can provide insights into the geological behavior and

occurrence of materials on Titan. As on Earth, the geochemistry of materials can

be expected to be linked to geological processes. Analogies to processes on Earth

are made in the following discussion to aid understanding. Examples are chosen

31

to elucidate principles using reasonable values for unknown parameters. Future work will need to devote greater attention to the parameter space of temperature, pressure, and composition on Titan.

The situation of interest is a system consisting of a CH_4-C_2H_6-C_3H_8 liquid that is in equilibrium with atmospheric N_2 and CH_4, and solid C_2H_2 (e.g., Lunine et al., 1983). I adopt reference values for temperature and pressure of 90.6941 K and 1.467 bar, respectively. The temperature is a little lower than that (93.65±0.25 K; Fulchignoni et al., 2005) measured at the equatorial (11°S) landing site of the Huygens probe, but it is similar to surface brightness temperatures in the polar regions (~90-92 K; Jennings et al., 2009). The pressure is the surface pressure on Titan (Fulchignoni et al., 2005). This system can be taken as a model of a polar lake or sea (Stofan et al., 2007; Turtle et al., 2009) that is in contact with C_2H_2-bearing sediments. A thermodynamic description of this system requires five equations for the five components. Equation (2) is used for N_2 and CH_4, with standard state fugacities and fugacity coefficients that were parameterized to REFPROP data (Lemmon et al., 2010) [log($f_{N_2}^{0,liq}$,bar) = 3.493-268.655/T(K), log($f_{CH_4}^{0,liq}$,bar) = 4.045-451.463/T(K); ϕ_{N_2} = 1.063-9.17/T(K), ϕ_{CH_4} = 1.2-26.09/T(K)]. These equations are accurate to within ~1% for 85-105 K, 1.467 bar, and a mole fraction of CH_4 gas between 0-10% (the mole fraction or mixing ratio of a gas is the partial pressure of the gas divided by the total pressure). Some standard state fugacities are also given in Table 2. Titan air in equilibrium with liquids is assumed to be a mixture of N_2 and CH_4 only (Niemann et al., 2010). Equilibrium between solid and dissolved C_2H_2 is represented by Eq. (8). I adopt a

C_2H_6/C_3H_8 mole ratio of 10 in the liquid phase, as predicted by the recent photochemical model of Lavvas et al. (2008a, 2008b). The final constraint is mass balance, where $\sum x_i = 1$. The five equations are solved iteratively until convergence is reached. The easiest way to do this is to assume initially that all activity coefficients are unity, so that liquid-phase mole fractions can be computed readily. Subsequently, Eq. (12) is used to calculate new activity coefficients, which are used to solve for new mole fractions. For the system of interest, activity coefficient expressions from the MVL model contain 11 terms (10 binary terms and a term for CH_4-C_2H_6-N_2; 9 ternary terms are omitted because interaction energies are unavailable). Note that, in general, the number of binary ($j = 2$) or ternary ($j = 3$) terms for an n-component system will be

$$C = \frac{n!}{j!(n-j)!}. \tag{14}$$

Mole fractions of CH_4, C_2H_6, C_3H_8, and N_2 in the model liquid are shown in Fig. 18. It can be seen that either CH_4 or C_2H_6 is the dominant constituent. The crossover point occurs at a mixing ratio of atmospheric CH_4 of 4.5% (this will depend on temperature). At higher mixing ratios, the liquid is dominated by CH_4, while C_2H_6 dominates at lower ratios. The concentration of N_2 in the liquid is sensitive to the CH_4/C_2H_6 mole ratio of the liquid. Atmospheric N_2 is predicted to be more soluble in liquids that are richer in CH_4, and the equilibrium mole fraction of N_2 in the liquid varies between 0.048 and 0.226 (Fig. 18) (based on

discussions in Sections 3 and 4, calculated mole fractions of N_2 and CH_4 have

maximum potential errors of ~20% and ~5%, respectively). The greater solubility

in CH_4 occurs because N_2 behaves more ideally in solutions with CH_4 than in

those with C_2H_6. For comparison, the solubility of atmospheric N_2 on Earth is

~5×10^{-4} molal or ~9×10^{-6} mole fraction at 298.15 K (Shock et al., 1989). Thus, N_2

has a much greater thermodynamic propensity to dissolve in liquids on Titan's

surface than in surface waters on Earth. Reasons for this include the lower

temperature, higher partial pressure of N_2, and the nonpolar solvent on Titan. The

high solubility of N_2 gas in CH_4-rich liquids may have geological consequences,

by altering physical (e.g., density, viscosity, heat capacity) and chemical (e.g.,

energy of solvation) properties of liquids on Titan. CH_4-rich liquids could also

sequester significant amounts of N_2 from the atmosphere (especially if extensive

"aquifers" exist; Hayes et al., 2008), which has implications for the evolution of

Titan's atmosphere (e.g., Glein et al., 2009). C_3H_8 is predicted to be a less

abundant constituent of surface liquids on Titan, with a maximum concentration

of 8.5% mole fraction (Fig. 18). This value may seem small, but this

concentration is considerably higher than that of NaCl in seawater (~0.8% mole

fraction; Eby, 2004). Even a brine that is saturated with respect to the mineral

halite at 298.15 K contains only ~9.9% mole fraction of NaCl (Marion & Kargel,

2008). These comparisons draw attention to a fundamental difference between

Titan and Earth. The solvent, or major composition of liquids, on Titan is

expected to be more complex than that on Earth, which is basically pure water.

There will be mixed solvents on and near Titan's surface containing CH_4, C_2H_6,

C_3H_8, and N_2, whose proportions are controlled by local physiochemical conditions (e.g., the relative "humidity" of CH_4).

Possible compositions of surface liquids in Titan's polar regions can be explored by comparing the results described above with determinations of mixing ratios of CH_4 gas at the surface. The Huygens GC-MS measured a mixing ratio of $(5.65\pm0.18)\times10^{-2}$ for CH_4 at the probe's equatorial landing site (Niemann et al., 2010). Penteado & Griffith (2010) used a radiative transfer model to derive near-surface mixing ratios from ground-based infrared spectra, and found that CH_4 gas abundances at low and mid-latitudes are consistent with the Huygens value to within ~10-20%. If CH_4 gas is well-mixed at all latitudes, polar lakes and seas would have equilibrium compositions on the mole fraction scale similar to 62.4% CH_4, 22.9% C_2H_6, 12.4% N_2, and 2.3% C_3H_8 (Fig. 18). In this case, surface liquids would be dominated by CH_4. However, mixing ratios of CH_4 gas near Titan's poles may be different from those at lower latitudes, like on Earth, where water vapor in the lower troposphere is not uniformly mixed. This seems likely because the ubiquity of lakes in Titan's polar regions, and their apparent absence elsewhere (Aharonson et al., 2009) (although, see Griffith et al., 2012), indicate that the polar climate is wettest, as predicted by the recent general circulation model of Schneider et al. (2012). Different climate implies different mixing ratio of CH_4 gas. If the CH_4 content of Titan's atmosphere is buffered by high-latitude lakes (Mitri et al., 2007), then the average mixing ratio of CH_4 in the polar atmosphere should be greater than the Huygens value, as polar air would be closer to the CH_4 source than equatorial air would be. Net evaporation of CH_4 must also

occur for lakes to buffer atmospheric CH_4 against photochemical destruction, which means that lakes must be in a state of disequilibrium with respect to polar air (i.e., actual mixing ratio of CH_4 gas < equilibrium mixing ratio). Overall, the buffer model suggests that Titan's lakes and seas may be CH_4-rich (~63-77% mole fraction; Fig. 18).

While spectral features consistent with the presence of liquid C_2H_6 were detected in Ontario Lacus (a south polar lake), the relative abundance of C_2H_6 in the lake is not known (Brown et al., 2008), so this observation cannot be used as a quantitative constraint. Observed shrinkage of Ontario Lacus would imply that the lake contains appreciable CH_4 if evaporation is responsible for the shrinkage, because C_2H_6 is not volatile enough to yield sufficient rates of evaporation (Hayes et al., 2011). Yet, infiltration of liquid into the subsurface could also be responsible for loss of liquid from Ontario Lacus, and there is insufficient information at present on the relative roles of these loss processes.

On the other hand, modeling of infrared data from the Voyager 1 spacecraft suggests that mixing ratios of CH_4 gas become lower at higher latitudes (~6 to ~2% from 0 to ±60°; Samuelson et al., 1997). If this model is correct, polar lakes may be rich in C_2H_6 (containing perhaps ~70% mole fraction; Fig. 18), unless liquids are severely out of equilibrium with the near-surface atmosphere. A highly dynamic polar environment (e.g., Tokano, 2009) could maintain a small actual mixing ratio of CH_4 gas and a large equilibrium mixing ratio. Prevention of equilibrium between air and liquids would require advection of evaporated CH_4 away from polar regions and compensating input of rain to maintain a non-

equilibrium steady state (evaporation and rainfall need not occur in the same place on a local scale; e.g., lakes versus highlands). A greater understanding of the relationships between the compositions of surface liquids and climate can be achieved by obtaining more information about latitudinal variations in the CH_4 gas mixing ratio (especially near the poles). It should be emphasized that thermodynamic models are not restricted to systems at equilibrium. As shown here, comparisons between the real system and its equilibrium state can lead to insights into processes that create disequilibrium.

Equilibrium compositions of surface liquids from several models in the Titan literature are compared in Table 5 (Lunine, 1985; Thompson, 1985; Dubouloz et al., 1989; Cordier et al., 2009). The comparisons are not strictly parallel because there are slight differences in temperature between the models (higher temperatures cause liquids to lose CH_4 and N_2, and gain C_2H_6). The models also have different numbers of components, so some caution is in order. In general, there is fair agreement among the models in terms of concentrations of CH_4, C_2H_6, and N_2. Lower-temperature models generally predict that surface liquids contain more CH_4 and N_2, and less C_2H_6, as expected. Close agreement between the MVL and GERG models suggests that predictions from these models may be accurate. The anomaly is the model of Cordier et al. (2009), which predicts far less CH_4 and N_2 than do the others (Table 5). There are four possible reasons for the discrepancy: (1) Cordier et al. used inaccurate thermodynamic data; (2) they solved the equations of phase equilibrium incorrectly; (3) their model parameters are not consistent with their thermodynamic data; or (4) minor

37

components in their model have very large effects on the activity coefficients of major components.

Because Cordier et al. (2009) did not publish their thermodynamic data or model parameters, I cannot assess these possibilities quantitatively. However, it is useful to discuss the last two possibilities. Cordier et al. (2009) followed Dubouloz et al. (1989) in using the model of Preston & Prausnitz (1970), but Cordier et al. (2009) used updated thermodynamic data from the NIST database. This may have generated inconsistencies because binary parameters in Preston & Prausnitz (1970) were fit to experimental data using older thermodynamic data. There may not be internal consistency between older binary parameters and newer thermodynamic data. This could be checked by comparing model predictions with experimental phase equilibrium data (e.g., Table 1). In addition, the model of Cordier et al. (2009) contains 9 more components than the MVL model in this section. If these extra components have large non-ideal interactions with liquid CH_4 and N_2, atmospheric CH_4 and N_2 would be predicted to have decreased solubilities in liquids on Titan's surface. It seems unlikely that dissolved species with abundances on the order of 1% mole fraction (Cordier et al., 2009) can have such profound effects, given that the vast majority of intermolecular interactions in solution will not involve these molecules. As an example, minor components would need to cause the activity coefficient of N_2 to increase by about an order-of-magnitude, which seems unrealistic. For comparison, the activity of H_2O in a halite-saturated solution at 298.15 K differs from that in pure water by only ~25% (Marion & Kargel, 2008). A problem may be that Cordier et al. (2009) included

hydrogen cyanide (HCN) in their regular-solution calculations, and regular

solution theory is not appropriate for hydrogen-bonding components (Prausnitz et

al., 1999). The sensible conclusion is that there are legitimate reasons to be

skeptical of the Cordier et al. (2009) model (see also Cordier et al., 2012).

Now, I consider the solubility of solid C_2H_2 (acetylite?) in surface liquids

on Titan. Model results are shown in Fig. 19, where it can be seen that C_2H_2

solubility is predicted to be a strong function of the mixing ratio of atmospheric

CH_4. This is because solid C_2H_2 is likely to be much more soluble in liquid C_2H_6

than in liquid CH_4 (Fig. 17), so the computed solubility of C_2H_2 is responding to

changes in the composition of the solvent (Fig. 18). This is another example of

how Titan's complex solvent can influence geochemistry. One potential

consequence is that, by analogy to the formation of ore deposits on Earth, mixing

of liquids with different compositions could lead to the formation of concentrated

deposits of solid C_2H_2, as well as other organic minerals on Titan. Imagine a

C_2H_6-rich subsurface fluid (whose original CH_4 and N_2 were mostly driven off by

mild heating) migrating through C_2H_2-bearing sediments. This fluid might contain

~10^4 ppm C_2H_2 (Fig. 19). Mixing of this fluid with fresh meteoric fluid (e.g., 77%

CH_4, 23% N_2; Fig. 18) may cause solid C_2H_2 to precipitate in the mixing zone.

The amount of solid formed would depend on the proportions and compositions

of the two fluids, and could be modeled. Many terrestrial minerals, such as

carbonates and silicates, have solubilities that are also sensitive to liquid

composition. However, the activity of H^+ (i.e., pH) is usually the most important

compositional variable in aqueous geochemistry on Earth, whereas the presence

of cosolvents appears to heavily influence mineral solubilities on Titan. C_2H_6 in liquid hydrocarbons on Titan seems like the geochemical equivalent of acid in aqueous solutions on Earth, since both substances increase the solubilities of minerals in their respective environments.

Further insights into the geochemistry of C_2H_2 on Titan can be gained by making comparisons with the solubilities of common minerals in water on Earth (Fig. 19). Halite is NaCl, gypsum is $CaSO_4 \cdot 2H_2O$, and calcite is a polymorph of $CaCO_3$. The solubility of calcite in water depends on the partial pressure of CO_2. The two cases considered here are 3.9×10^{-4} bar (i.e., the contemporary terrestrial atmosphere), and 10^{-2} bar (a representative value for groundwaters in limestone aquifers; Garrels & Christ, 1965; Drever, 1997). Solubilities of terrestrial minerals in pure water at 298.15 K and 1 bar are calculated using the FREZCHEM model (Marion & Kargel, 2008).

Solid C_2H_2 in CH_4-N_2 meteoric fluid on Titan is about as soluble as calcite in water on Earth's surface (Fig. 19). The solubility of C_2H_2 in liquid hydrocarbons on Titan is predicted to rival that of calcite in subsurface waters on Earth if the meteoric fluid on Titan picks up small amounts of C_2H_6 and C_3H_8 (~10% mole fraction) during fluid transport. This could have significant geomorphological implications. For example, Mitchell & Malaska (2011) reported that landforms consistent with karst topography, such as steep-rimmed depressions, are present in Titan's "Arctic Lake District". On Earth, karst typically develops as groundwater dissolves calcite and other carbonate minerals in limestone (Summerfield, 1991). By analogy, my calculations suggest that

dissolution of solid C_2H_2 by CH_4-rich weathering fluids could produce sinkholes or other karstic features on Titan. Of course, this will depend on many unknowns, such as the existence of thick deposits of C_2H_2-rich rock, the mechanical strength of the rock, and whether there is sufficient flow of weathering fluid through the rock. While these are difficult issues to address at present, the computed solubilities may serve as a starting point for models of solution erosion on Titan (e.g., Lorenz & Lunine, 1996; Mitchell et al., 2008; Malaska et al., 2011).

Another application of the MVL model is assessing the geochemistry of evaporite minerals on Titan. Recently, Barnes et al. (2011) discovered a 5-μm bright unit in what appear to be dry lakebeds near Titan's north pole, and proposed that the unit is composed of organic evaporites. Observations of decreasing depths and shoreline recessions of lakes with time are consistent with evaporation or infiltration of liquid from lakes (Hayes et al., 2011; Turtle et al., 2011b). Evaporation may be an agent of geochemical change on Titan (Mitri et al., 2007), as it is on Earth and Mars (e.g., Tosca & McLennan, 2006). Evaporation of volatile species from lakes, seas, or pore fluids will concentrate residual liquids in non-volatile, soluble species. If the liquids become sufficiently concentrated, minerals will precipitate. An obvious difference between Earth and Titan is that evaporitic sediments are inorganic on Earth, while they should be predominately organic on Titan. Another difference is that evaporation will markedly change the composition of the solvent on Titan, since C_2H_6 and C_3H_8 are much less volatile than CH_4 (Table 2); the proportions of C_2H_6 and C_3H_8 will increase during net evaporation of CH_4. The difference is due to the fact that

aqueous solutions on Earth do not contain appreciable amounts of non-volatile liquids that are miscible with water. A dramatic change in solvent composition will affect evaporite geochemistry because mineral solubilities are expected to differ greatly between CH_4-rich and C_2H_6-rich liquids (see Fig. 19; Tiffin et al., 1979). This type of behavior is unfamiliar in terrestrial saline lakes; for instance, gypsum is only ~3.4 times more soluble in a 5 molal NaCl solution than in pure water at ambient conditions (Marion & Kargel, 2008). It seems possible that some minerals on Titan could precipitate during an early stage of evaporation, but that they may stop forming during later stages of evaporation after the C_2H_6 concentration has built up sufficiently. Details of how this might work probably depend on the solute of interest, its initial concentration, and the starting composition of the solvent. This strange precipitation behavior may be useful for future exploration, as the process may create gaps in the sedimentary record on Titan, which may help future workers in interpreting stratigraphies.

Returning to the specific case of C_2H_2, Fig. 19 shows that solid C_2H_2 should have a solubility in C_2H_6-dominated saline fluids ($\sim 10^3$-10^4 ppm) that is roughly comparable to that of gypsum in surface waters on Earth. Thus, C_2H_2 looks like it can be an evaporite mineral on Titan, so C_2H_2 is a reasonable substance to look for in putative evaporite deposits (e.g., Moriconi et al., 2010). The evaporitic character of C_2H_2 may explain why C_2H_2 has not been detected by remote sensing on the surface (Clark et al., 2010). Fluvial modification of Titan's surface may cause dissolution of solid C_2H_2, and weathering fluids may ferry C_2H_2 into the subsurface. One possible outcome is that subsurface evaporation of

CH$_4$ may lead to precipitation of solid C$_2$H$_2$ in pore spaces of sediments, forming duricrusts by cementing sediment particles. Calcrete (calcite) and gypcrete (gypsum) duricrusts are common in deserts on Earth (Goudie, 1983; Watson, 1983), and similar predicted solubilities of C$_2$H$_2$ (Fig. 19) suggest that C$_2$H$_2$ could be a duricrust-former in arid regions on Titan (e.g., Lorenz et al., 2006). Note, however, that there are alternative explanations for the apparent lack of widespread C$_2$H$_2$ on Titan's surface, such as polymerization and cyclization reactions that consume C$_2$H$_2$ (Matteson, 1984; Zhou et al., 2010). This complex issue cannot be settled here, but the geochemical model has demonstrated its usefulness by suggesting a testable hypothesis. If C$_2$H$_2$-cemented duricrusts (acetylcretes?) are present on Titan, a future robotic digger may encounter a hardened soil layer that is rich in sedimentary C$_2$H$_2$.

In closing this discussion, I would like to address a few lingering issues. Will liquid solutions be at equilibrium with solids on Titan's surface? It is plausible that they may be at least close to equilibrium because small energy changes are involved when nonpolar solids dissolve or precipitate. This should make it easier for molecules with even small amounts of kinetic energy to surmount activation barriers. Contrast this with minerals on Earth, where most lattices are held together by strong ionic bonds, which result in large kinetic barriers for dissolution and growth processes in many cases (quartz is a notorious example). Next, calculated solubilities of solid C$_2$H$_2$ in C$_2$H$_6$-rich liquids should be regarded as provisional because the interaction energy for C$_2$H$_2$-C$_2$H$_6$ was estimated using a correlation whose accuracy is poorly understood (see Section

3). However, the predicted trend of increasing solubility with decreasing mixing

ratio of CH_4 gas (Fig. 19) is sound, as a greater proportion of C_2H_6 (Fig. 18) is

expected to increase the solubility of solid C_2H_2 (see Section 4). Above, I

emphasized that Titan's solvent is more complex than Earth's, which gives rise to

unique geochemical features. I should also point out that Earth's solute

geochemistry is immensely richer than Titan's. On Titan, a molecule can occur in

different phases, but it is still the same molecule. In contrast, ions in waters on

Earth can combine in myriad ways to produce diverse secondary minerals (e.g.,

salts, clay minerals). This combinatorial chemistry is possible because the

building blocks of ionic minerals are more elementary than the formula units of

minerals. For molecular minerals, such as those presumably on Titan, the two are

the same. This means that the classic geochemical concepts of incongruent

dissolution and chemical divides (Drever, 1997) will not apply to the

geochemistry of liquid hydrocarbons on Titan.

6. Concluding remarks

To summarize, I presented a generalized thermodynamic framework for

quantifying phase equilibria between solids, liquids, and gases in the CH_4-C_2H_6-

C_3H_8-N_2-C_2H_2 system at Titan surface conditions. The modified van Laar (MVL)

model was developed to account for non-ideal behavior in liquid mixtures by

calculation of activity coefficients of mixture components. Interaction energy

parameters were derived by critically evaluating experimental phase equilibrium

data, and then regressing internally consistent data. The model provides an excellent fit to most of the data, and fits the rest of the data sufficiently well for applications to Titan. It was found that interaction energies at the triple-point temperature of CH_4 correlate linearly with differences in enthalpies of vaporization between binary components, and this knowledge was used to estimate interaction energies for the experimentally uncharacterized binaries C_2H_2-C_2H_6 and C_2H_2-C_3H_8. Close agreement between model predictions and experimental results for the CH_4-C_2H_6-N_2 ternary shows that the model can provide reasonable descriptions of non-idealities in multicomponent solutions. It was also shown that ternary data can be used to improve the model by inclusion of a ternary parameter, and that the model compares favorably to alternatives. The MVL model was applied to Titan, providing quantitative information on possible compositions of surface liquids in Titan's polar regions. Comparisons between the solubility of solid C_2H_2 in liquid hydrocarbons on Titan and the aqueous solubilities of some sedimentary salts on Earth yielded insights into the geochemistry of C_2H_2 in weathering and arid environments, with potential geological consequences of karst and evaporite formation, respectively. Overall, substantiation and demonstration of the MVL model show that the model can be used to explore Titan's strange yet familiar geochemistry, which will allow more learning about how geochemical processes can produce or modify geological features on this extraordinary world.

There are many theoretical and experimental studies, remote observations, and *in situ* measurements that can lead to a better understanding of fluvial geochemistry on Titan:

1) Additional binary systems at phase equilibrium could be characterized, by regressing existing literature data (e.g., Hiza et al., 1982), and by obtaining new experimental data. Expanding the number of components in the MVL model will allow more complete models of geochemical processes on Titan. Such developments will also allow tests of assumptions and correlations used in this study, leading perhaps to the development of improved predictive methods. Of special interest are binaries with CH_4 or C_2H_6, and compounds that have been detected in Titan's atmosphere (e.g., HCN; Magee et al., 2009; Coustenis et al., 2010); and compounds that may be present on the surface (e.g., benzene; Clark et al., 2010; Niemann et al., 2010). Models could be enhanced further by considering organic products from atmospheric chemistry models (e.g., Lavvas et al., 2008a, 2008b) and experiments (e.g., Thompson et al., 1991), as well as cosmochemically abundant ices and noble gases. A speculative class of surface materials would be organometallic compounds (e.g., iron pentacarbonyl), which could form from delivery of metals by comets or interplanetary dust. It is also recommended that compounds with diverse structural or electronic properties be studied to obtain fundamental information about non-ideal behavior in cryogenic solutions.

2) Phase equilibrium experiments with ternary mixtures at Titan surface

conditions would provide data that could be used to test the MVL model more

thoroughly and refine the model, or call for new approaches. Of greatest relevance

to Titan are ternaries with liquid CH_4 and C_2H_6.

3) Determining whether relevant organic solids can form appreciable solid

solutions at Titan surface conditions will affect the thermodynamic treatment

adopted here (see Eq. 8). It might be expected that substances can form a solid

solution if they have identical crystal structures, and similar critical volumes and

chemical characteristics.

4) Extension of the MVL model to higher temperatures and pressures will permit

computational studies of thermally-driven geochemical processes in Titan's

subsurface. This could lead to insights into possible diagenetic mechanisms for

producing sedimentary rocks (e.g., sandstones), such as precipitation of cements

during cooling of fluids that are saturated with respect to organic minerals. Also,

higher-temperature organic precipitates could serve as spectral markers that may

help in identifying current or past regions of elevated thermal activity using

remote sensing.

5) More comprehensive modeling of phase equilibria would lead to a better

understanding of how Titan's cryogenic geochemistry might respond to different

geochemical variables. The bioenergetics of speculative life in liquid

47

hydrocarbons (McKay & Smith, 2005) could also be explored using standard Gibbs energies of formation (Table 2) in conjunction with the MVL model.

6) I am inspired by the success of the geochemistry program SUPCRT92 (Johnson et al., 1992), which can be attributed to internally consistent, critically evaluated thermodynamic data and (primarily) ease of use. Long-term plans call for development of a similar program called CRYTIG (Cryogenic Titan Geochemistry), which will be a web-based tool that facilitates thermodynamic calculations using the MVL model.

7) Laboratory studies of kinetic phenomena, such as rates of evaporation of CH_4 and dissolution of relevant organic solids, will help in clarifying the appropriateness of the equilibrium assumption under various conditions. Experiments could also examine equilibrium and kinetic isotopic fractionations. As an example, there may be a meteoric methane line on Titan that is analogous to the meteoric water line on Earth (Craig, 1961), so experiments could provide lessons on how the isotopic composition of CH_4 evolves in response to non-equilibrium processes. Precipitation of minerals may also fractionate isotopes appreciably, implying that the isotopic composition of minerals may constitute a record of geochemical conditions in Titan's past.

8) The ability to simulate actual geochemical processes on Titan is hampered by limited knowledge of the composition of Titan's surface. Unambiguous

identification of surface materials will most likely require *in situ* measurements. Desirable pieces of information are the compositions, proportions, and distributions of liquids and solids, as functions of local climate and geology. As on Earth, a great deal could be learned about how liquids evolve geochemically by comparing the molecular and isotopic compositions of Titan's air, rain, rivers, lakes, seas, and subsurface fluids.

9) Finally, further exploration of Titan's CH_4-based volatile cycle (at present and in the past) is called for to enable better assessments of its potential for supporting diverse types of geochemistry. Continued geomorphological studies of fluvial landforms and associated features, observations of seasonal changes in tropospheric clouds and liquid bodies such as lakes, and models of climate and the carbon cycle will all be helpful.

Table 1. Experimental phase equilibrium data for some binary mixtures at cryogenic temperatures (Abbreviations: VLE, vapor-liquid equilibrium; SLE, solid-liquid equilibrium; LLE, liquid-liquid equilibrium).

Reference	Type of Data	Temperature Range (K)	Used in this work?
CH_4-C_2H_6			
Gomes de Azevedo & Calado (1989)	VLE	90.69-103.99	Yes
Miller & Staveley (1976)	VLE	115.77	Yes
Wilson (1975)	VLE	110.93	No
CH_4-C_3H_8			
Calado et al. (1974)	VLE	115.77-134.83	Yes
Cheung & Wang (1964)	VLE	91.7-128.4	No
Cutler & Morrison (1965)	VLE	90-110	No
Poon & Lu (1974)	VLE	114.1-122.2	No
Stoeckli & Staveley (1970)	VLE	90.68	Yes
Wilson (1975)	VLE	110.93	No
C_2H_6-C_3H_8			
Djordjevich & Budenholzer (1970)	VLE	127.59-255.37	Yes (127.59-172.04 K)
N_2-CH_4			
Cheung & Wang (1964)	VLE	91.6-124.1	No
Fuks & Bellemans (1967)	VLE	84.15-90.84	No
Gabis (1991)	VLE	84.84-94.04	Yes
McClure et al. (1976)	VLE	90.68	Yes
Omar et al. (1962)	VLE, SLE	~58-98	No
Parrish & Hiza (1974)	VLE	95-120	Yes (95-110 K)
Sprow & Prausnitz (1966)	VLE	90.67	No
Stryjek et al. (1974)	VLE	113.71-183.15	No
Wilson (1975)	VLE	110.93	No
N_2-C_2H_6			
Cheung & Wang (1964)	VLE	92.8	No
Ellington et al. (1959)	VLE, LLE	99.82-299.82	Yes (99.82-110.93)
Guedes et al. (2002)	VLE, LLE	90.69	No
Kremer & Knapp (1983)	VLE, LLE	120-133.15	Yes (120 K)
Llave et al. (1985)	VLE, LLE	118-132.38	Yes (118-120 K)
Szczepaniec-Cieciak et al. (1980)	SLE	69.5-85.5	Yes
Wilson (1975)	VLE, LLE	110.93	Yes
Yu et al. (1969)	VLE, LLE	113.71-133.26	Yes (113.71-119.26 K)
N_2-C_3H_8			
Cheung & Wang (1964)	VLE	91.9-128.4	Yes (91.9-110.2 K)
Houssin-Agbomson et al. (2010)	VLE	109.98-125.63	Yes (109.98-119.75 K)
Kremer & Knapp (1983)	VLE, LLE	120-127	Yes (120 K)
Llave et al. (1985)	VLE, LLE	117-126.62	No
Poon & Lu (1974)	VLE	114.1-122.2	No
Schindler et al. (1966)	VLE, LLE	103.15-353.15	Yes (103.15 K)
Szczepaniec-Cieciak et al. (1980)	SLE	64.8-101	Yes (64.8-85 K)
C_2H_2-CH_4			
Neumann & Mann (1969)	SLE	93.3-143.1	Yes
C_2H_2-N_2			

| Fedorova (1940) | SLE | 65-95 | Yes |
| Ishkin & Burbo (1939) | SLE | 77.4 | Yes |

Table 2. Physical and thermodynamic properties of some compounds on Titan (P_{ref} = 1.467 bar, T_{ref} = 90.6941 K).

Compound	Critical Volume (cm^3 mol^{-1})	Volume at P_{ref} and T_{ref} (cm^3 mol^{-1})	Enthalpy of Vaporization at T_{ref} (J mol^{-1})	Fugacity at P_{ref} and T_{ref} (bar)	ΔG_f^0 (kJ mol^{-1})
CH$_4$	98.6291 [a]	35.5342 (liq.) [a]	8731 [a]	0.1168 (liq.) [a]	-64.744 (gas) [h] -66.363 (liq.) [i]
C$_2$H$_6$	145.8388 [a]	46.1732 (liq.) [a]	17873 [a]	1.255×10^{-5} (liq.) [a]	-63.827 (gas) [j] -72.337 (liq.) [i]
C$_3$H$_8$	200 [a]	60.5882 (liq.) [a]	24587 [a]	1.261×10^{-8} (liq.) [a]	-73.394 (gas) [j] -87.11 (liq.) [i]
N$_2$	89.4142 [a]	37.8343 (liq.) [a]	5023 [a]	3.408 (liq.) [a]	0 (gas) [h] 0.9246 (liq.) [i]
C$_2$H$_2$	112.2 [b]	35 (liq.) [c] 33.4 (sol.) [d]	20648 [e]	1.63×10^{-6} (liq.) [f] 1.1×10^{-7} (sol.) [g]	221.584 (gas) [h] 211.535 (liq.) [i] 209.502 (sol.) [i]

[a], Lemmon et al. (2010); [b], Poling et al. (2001); [c], Estimated by scaling a volume near the triple point (McIntosh, 1907) with the Rackett equation (Poling et al., 2001); [d], Lunine et al. (1983); [e], Estimated by scaling the enthalpy of vaporization at the triple point (Ambrose, 1956) with the Watson relation (Poling et al., 2001); [f], Estimated using the Ambrose-Walton corresponding-states method (Poling et al., 2001); [g], Computed using Eq. (9); [h], Chase (1998); [i], Derived from the standard Gibbs energy of formation (ΔG_f^0) of the gas from constituent elements, and from the fugacity of the condensed phase; [j], Chao et al. (1973).

Table 3. Interaction energy parameters for the modified van Laar model (T_{ref} = 90.6941 K).

System	$\omega_{ij} = \omega_0 + \omega_1 T + \omega_2 T \times \ln(T)$			Temperature Range (K)	ω_{ij} at T_{ref} (J mol^{-1})
	ω_0	ω_1	ω_2		
CH_4-C_2H_6	1366	-36.68	7.143	90.69-115.77	959
CH_4-C_3H_8	2412	-58.11	11.279	90.68-134.83	1753
C_2H_6-C_3H_8 [a]	0	0	0	127.59-172.04	~0
N_2-CH_4	2443	-75.16	14	84.84-110	1350
N_2-C_2H_6	1797	27.79	0	69.5-120	4317
N_2-C_3H_8	2099	50.05	0	64.8-120	6638
C_2H_2-CH_4	14940	-50.34	0	93.3-143.1	~10374
C_2H_2-C_2H_6	2416 [b]	0	0	90.6941	~2416
C_2H_2-C_3H_8	3429 [b]	0	0	90.6941	~3429
C_2H_2-N_2	6886	51.92	0	65-95	11595
CH_4-C_2H_6-N_2	2604	0	0	95	~2604

[a], This system is approximately ideal at low temperatures (see Fig. 5); [b], Estimated using the correlation for C_2H_2 in Fig. 11.

Table 4. Experimental vapor-liquid equilibrium data for the CH_4-C_2H_6-N_2 system at 95 K (Gabis, 1991). Mole fractions are in the liquid phase, except for values in parentheses, which are in the vapor phase.

Mole Fraction of CH_4	Mole Fraction of C_2H_6	Mole Fraction of N_2	Total Pressure (bar)
0.7955	0.0612	0.1432	1.523
0.8220	0.0850	0.0929	1.218
0.6612 (0.0905)	0.1895	0.1493 (0.9095)	1.885
0.6842	0.2140	0.1018	1.468
0.7180 (0.1160)	0.2205	0.0615 (0.8840)	1.077
0.6793	0.2844	0.0362	0.842
0.5309	0.4305	0.0386	1.124
0.3442	0.6036	0.0522	1.610
0.2426	0.6911	0.0663	2.023
0.2534	0.7002	0.0463	1.357
0.2434	0.7176	0.0389	1.194
0.1699	0.7768	0.0533	1.750
0.0779	0.8813	0.0407	1.756

Table 5. Comparisons between various equilibrium composition models of multicomponent liquids on Titan's surface for a CH_4 gas mixing ratio (or mole fraction) of 6% at the base of the atmosphere (i.e., similar to the Huygens value; Niemann et al., 2010). GERG refers to the GERG model (Kunz et al., 2007), and MVL refers to the modified van Laar model (Eq. 12).

Variable	Lunine (1985)	Thompson (1985)	Dubouloz et al. (1989)	Cordier et al. (2009)	GERG	MVL
Surface temperature (K)	94	94	92.5	93.65	90.6941	90.6941
Surface pressure (bar)	1.5	1.5	1.52	1.46	1.467	1.467
Mole percent CH_4 in liquid	~50 [b]	50.1	~55 [b]	~7.3 [b]	68.1	68.1
Mole percent C_2H_6 in liquid	~41.2 [b]	41.3	~35 [b]	~78.3 [b]	15	15.5
Mole percent C_3H_8 in liquid	-	-	-	~7.6 [b]	1.5	1.55
Mole percent N_2 in liquid	~8.8 [b]	8.6	~10 [b]	~0.32 [b]	15.4	14.8
Mole percent C_2H_2 in liquid	≤0.031	-	~0.02 [b]	~1.18 [b]	-	0.022
Mole percent others in liquid [a]	-	-	<0.01	~5.3 [b]	-	-

[a], "Others" correspond to various hydrocarbons, nitriles, and inorganic compounds; [b], Values are approximate because they were obtained by interpolating results from published figures.

Fig. 1. Comparison of best-fit q ratios to critical and liquid volume ratios. The

blue line designates a 1:1 correspondence. Best-fit q ratios were obtained from

regressions of vapor-liquid equilibrium data along isotherms; each point

represents an isotherm. Only binaries involving CH_4 are shown because data for

the other binaries in Table 1 do not cover sufficient compositional space for

accurate determination of best-fit q ratios.
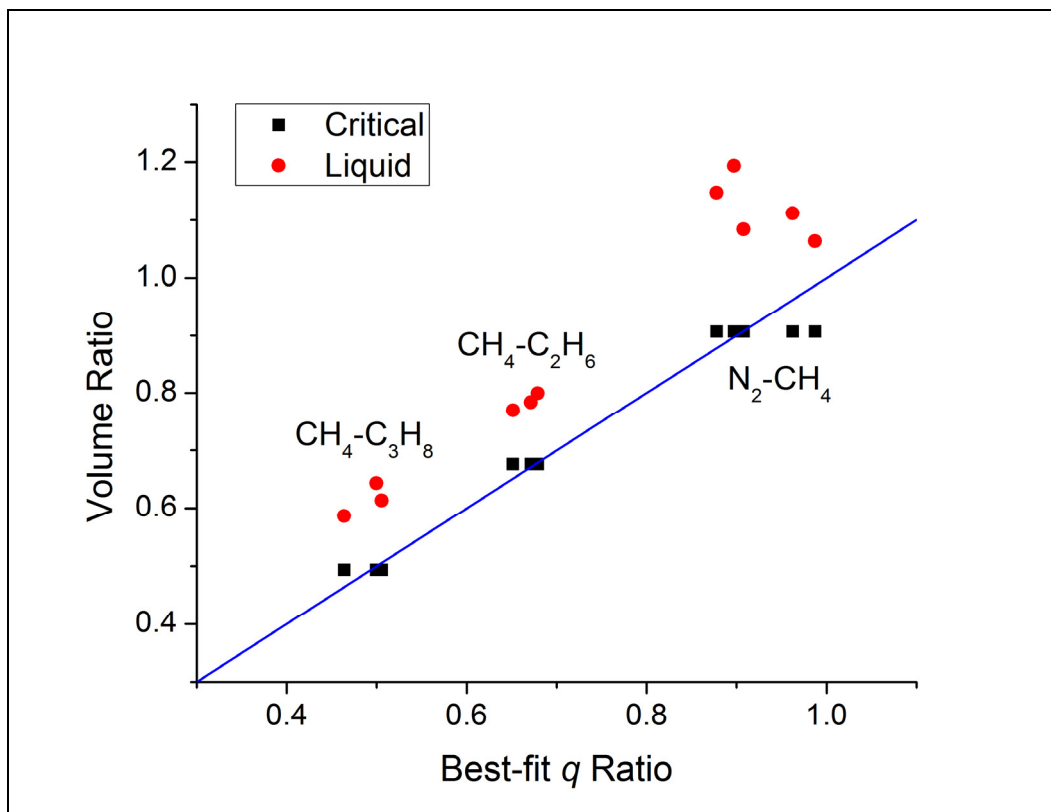
Fig. 2. Comparison of calculated and experimental vapor pressures of C_2H_2 as functions of inverse temperature. The green curve corresponds to vapor pressures of liquid C_2H_2 from the Ambrose-Walton corresponding-states (C.S.) method, and the curve extends into the supercooled region. The black curve designates vapor pressures of solid C_2H_2 from Eq. (9). The curves intersect at the triple point (192.6 K, 1.282 bar; Ambrose, 1956). Symbols represent vapor pressures from experiments. Abbreviations: A&T, Ambrose & Townsend (1964); Amb., Ambrose (1956); T&L, Tickner & Lossing (1951).
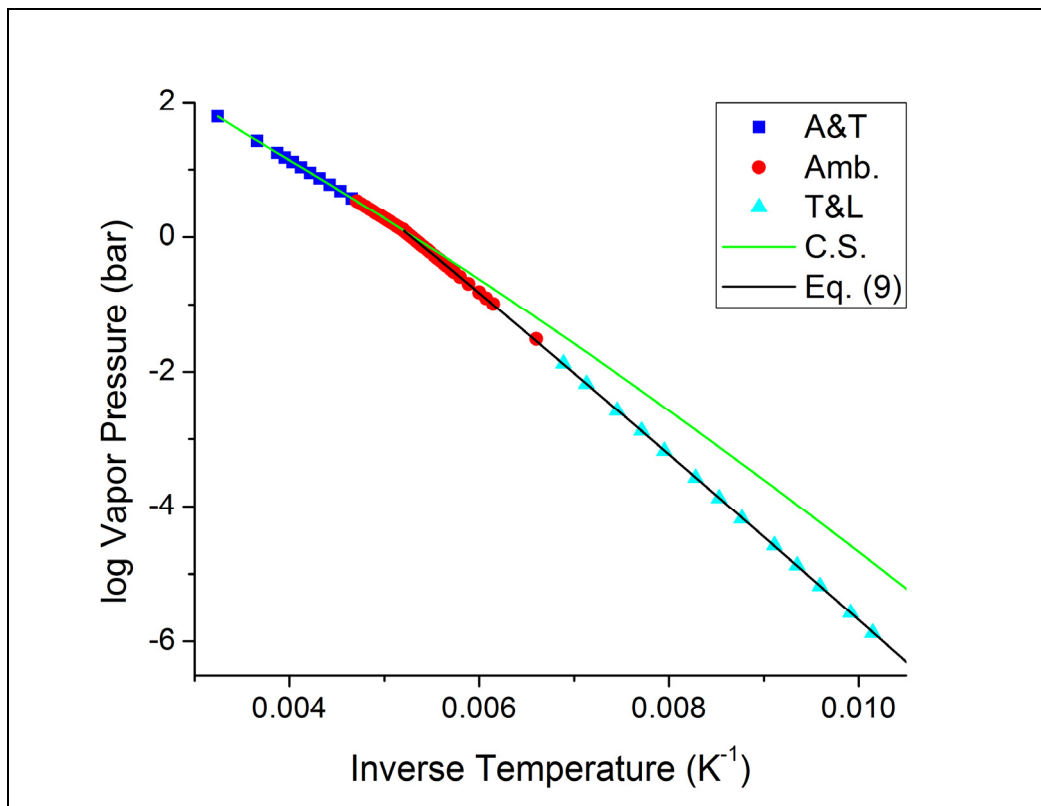
Fig. 3. Comparison of total pressures from the modified van Laar model to those from experiments for the CH_4-C_2H_6 binary. Symbols represent percent differences between computed and measured pressures (i.e., residuals), as a function of liquid-phase composition and temperature. Experimental data are from Gomes de Azevedo & Calado (1989) [91 K, 104 K], and Miller & Staveley (1976) [116 K].
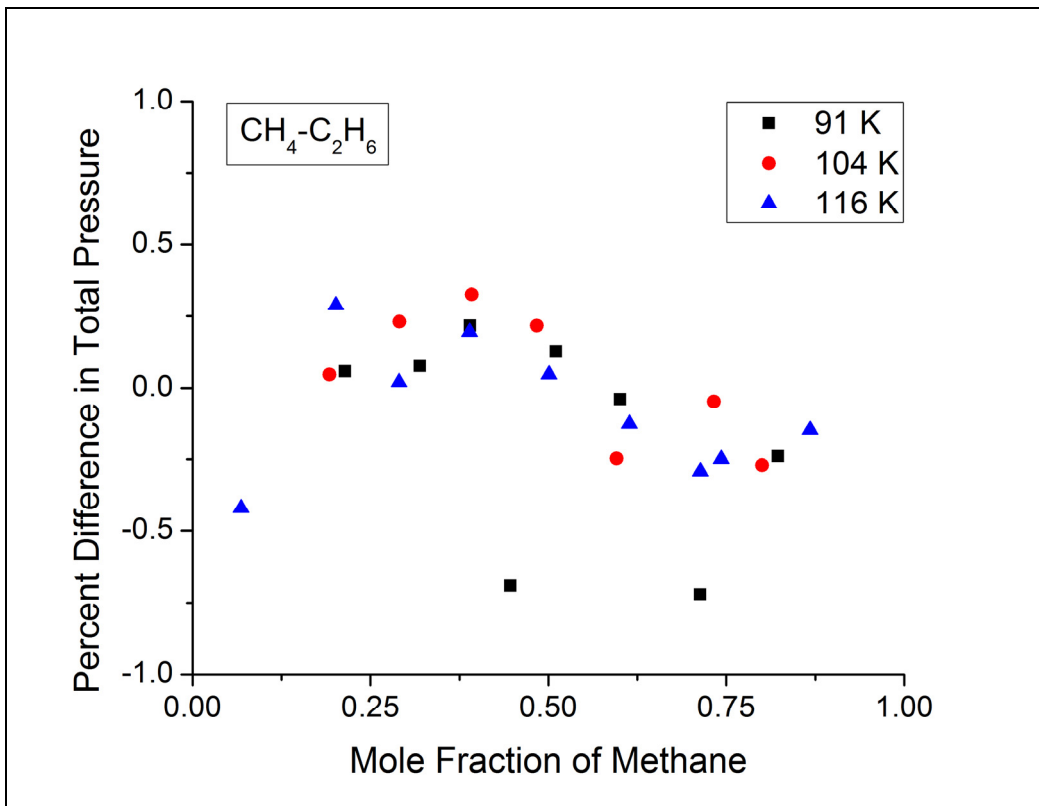
Fig. 4. Comparison of total pressures from the modified van Laar model to those from experiments for the CH_4-C_3H_8 binary. Symbols represent percent differences between computed and measured pressures (i.e., residuals), as a function of liquid-phase composition and temperature. Experimental data are from Stoeckli & Staveley (1970) [91 K], and Calado et al. (1974) [116 K, 135 K].
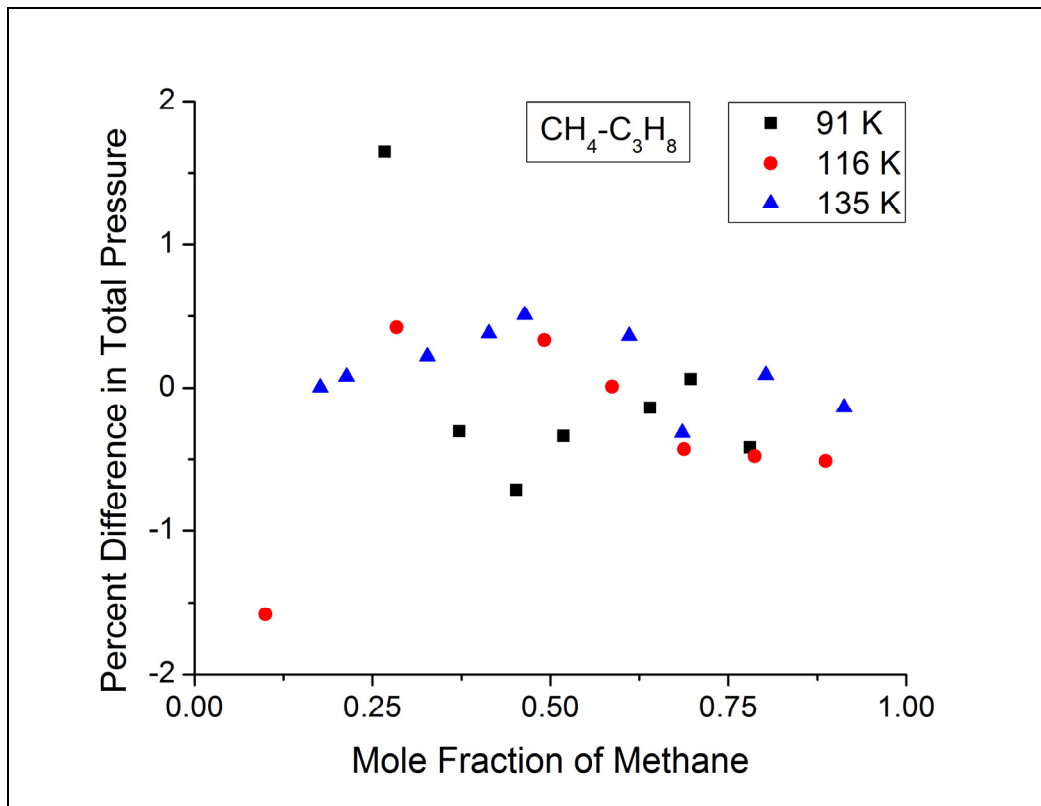
Fig. 5. Comparison of total pressures from the ideal solution model to those from experiments for the C_2H_6-C_3H_8 binary. Symbols represent percent differences between computed and measured pressures (i.e., residuals), as a function of liquid-phase composition and temperature. All experimental data are from Djordjevich & Budenholzer (1970).
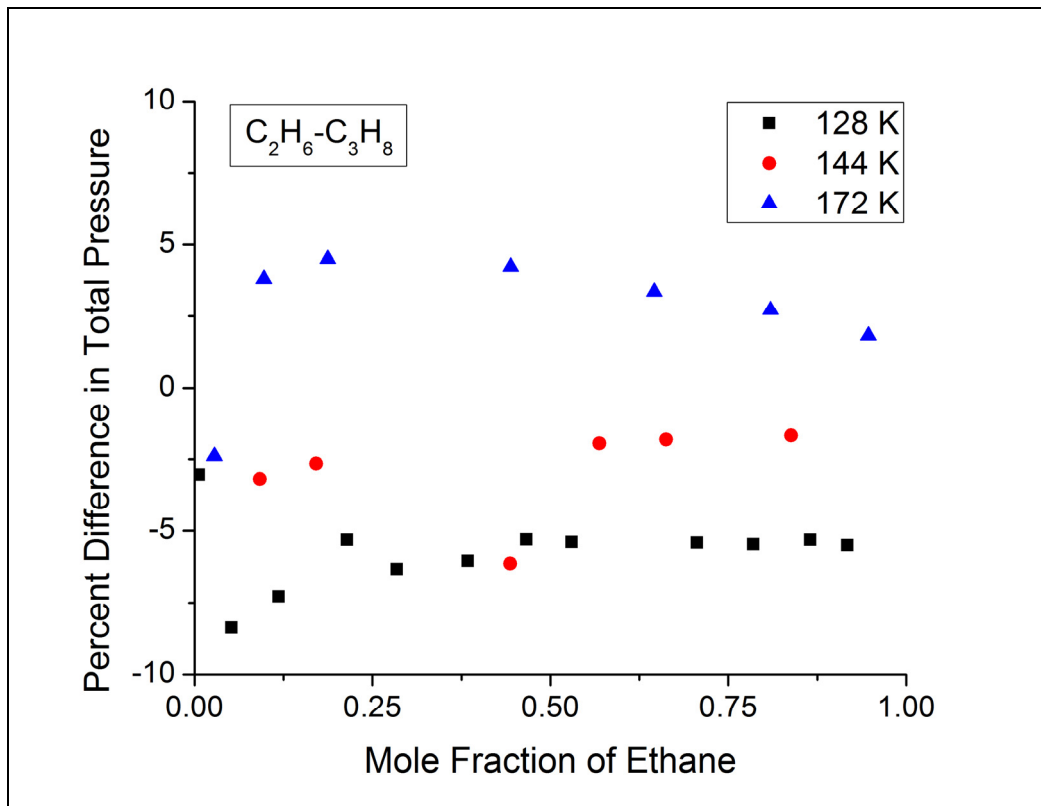
Fig. 6. Comparison of total pressures from the modified van Laar model to those from experiments for the N_2-CH_4 binary. Symbols represent percent differences between computed and measured pressures (i.e., residuals), as a function of liquid-phase composition and temperature. Experimental data are from Gabis (1991) [85-90 K, 94 K], McClure et al. (1976) [91 K], and Parrish & Hiza (1974) [95-110 K].
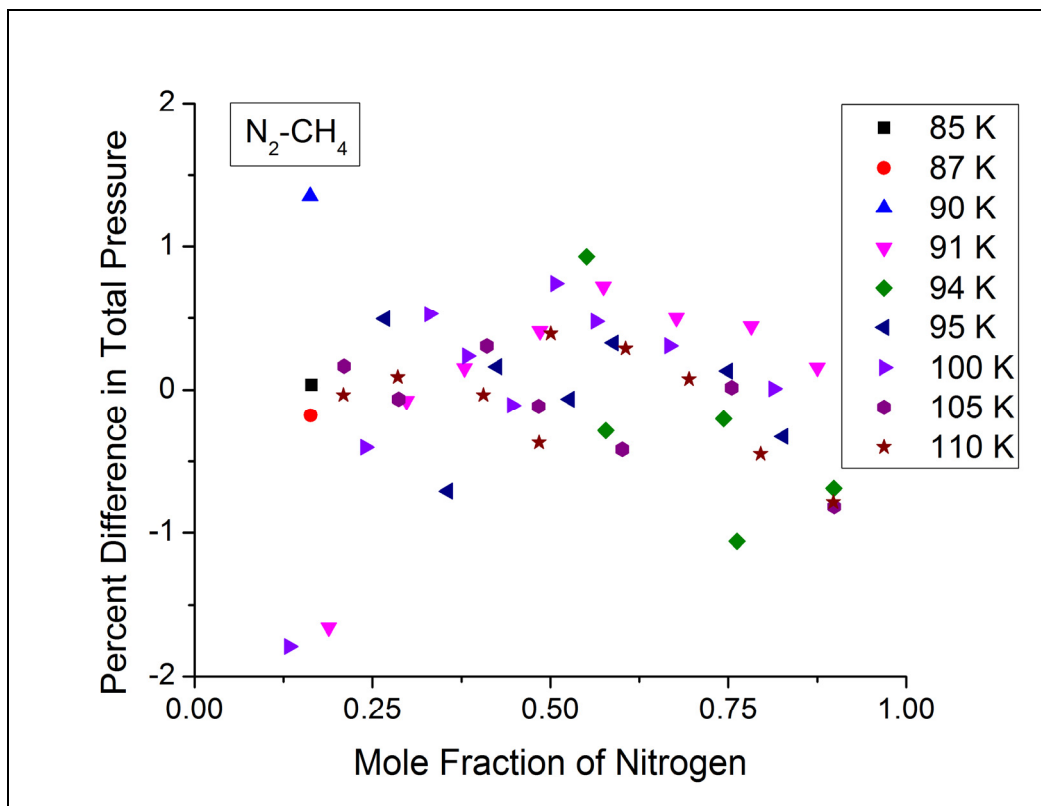
Fig. 7. Comparison of total pressures from the modified van Laar model to those from experiments for the N_2-C_2H_6 binary. Symbols represent percent differences between computed and measured pressures (i.e., residuals), as a function of liquid-phase composition and temperature. Experimental data are from Ellington et al. (1959) [100 K, 111 K (E59)], Wilson (1975) [111 K (W75)], Yu et al. (1969) [114-116 K], Kremer & Knapp (1983) [120 K (K83)], and Llave et al. (1985) [120 K (L85)]. Data do not cover the entire compositional range because this system has a miscibility gap, where intermediate compositions are less stable than two liquid phases.
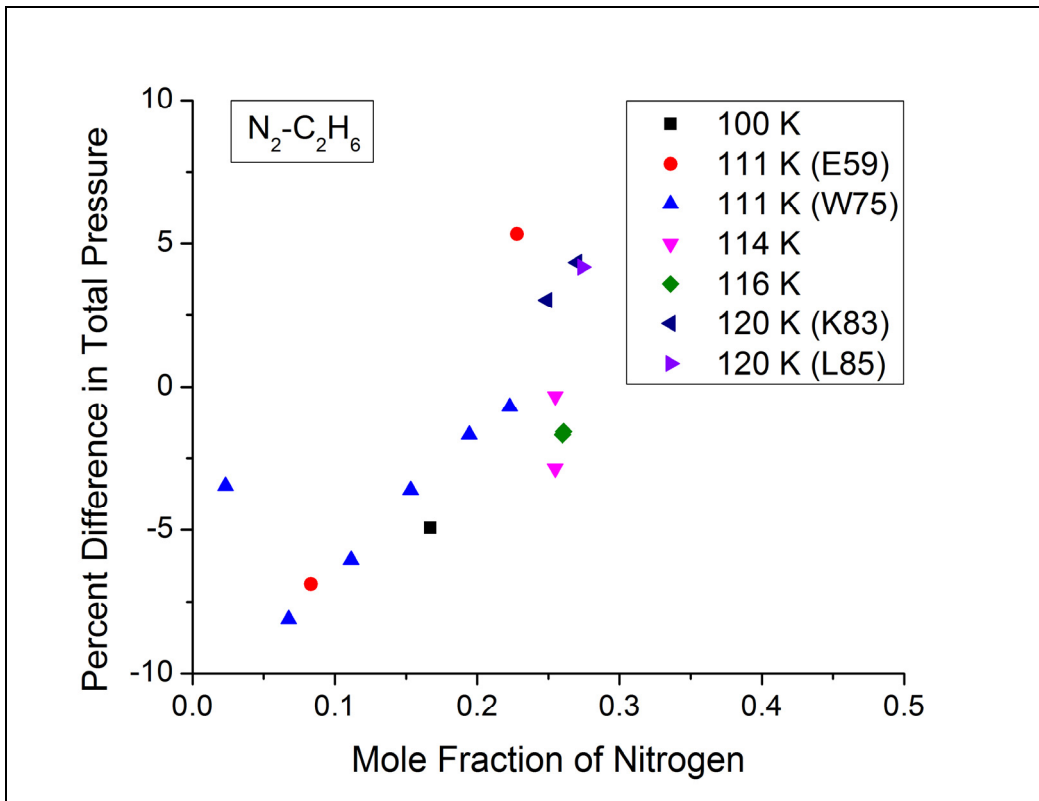
Fig. 8. Comparison of total pressures from the modified van Laar model to those from experiments for the N_2-C_3H_8 binary. Symbols represent percent differences between computed and measured pressures (i.e., residuals), as a function of liquid-phase composition and temperature. Experimental data are from Cheung & Wang (1964) [92-97 K], Schindler et al. (1966) [103 K], Houssin-Agbomson et al. (2010) [110-114 K], and Kremer & Knapp (1983) [120 K]. Data do not cover the entire compositional range because this system has a miscibility gap, where intermediate compositions are less stable than two liquid phases.
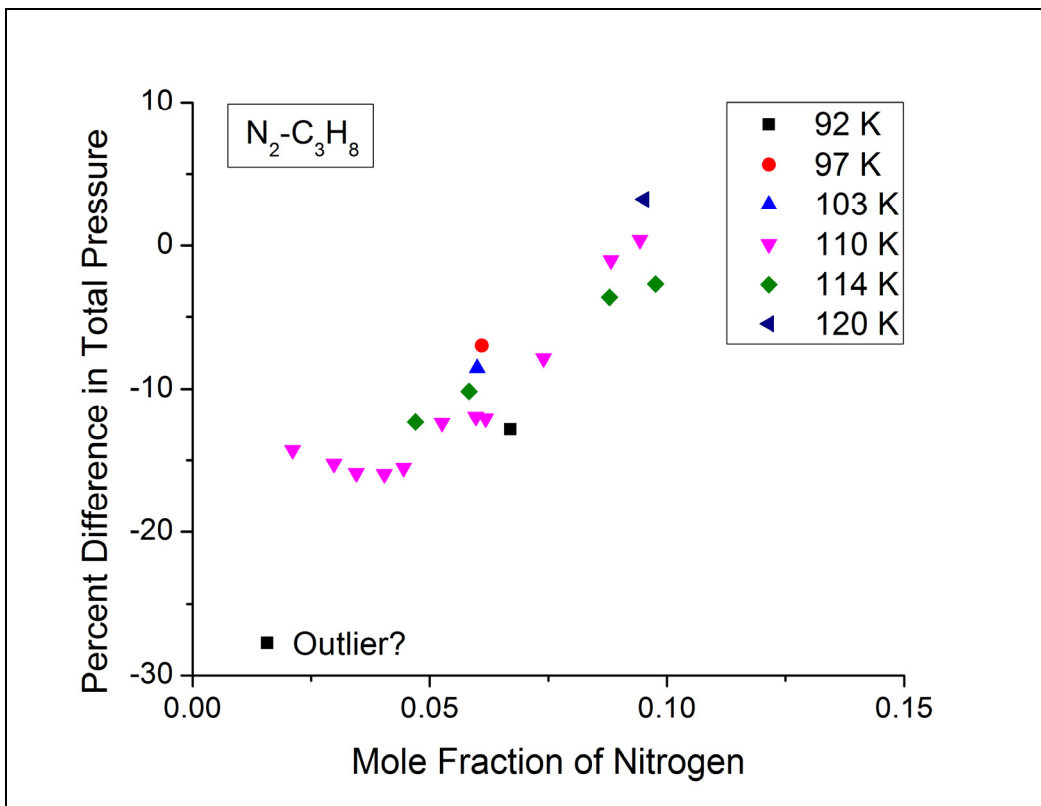
Fig. 9. Solubility of solid C_2H_2 in liquid CH_4 as a function of inverse temperature at the saturation pressure of liquid CH_4. Symbols denote experimental data from Neumann & Mann (1969), and the red curve represents predicted solubilities from the modified van Laar model.
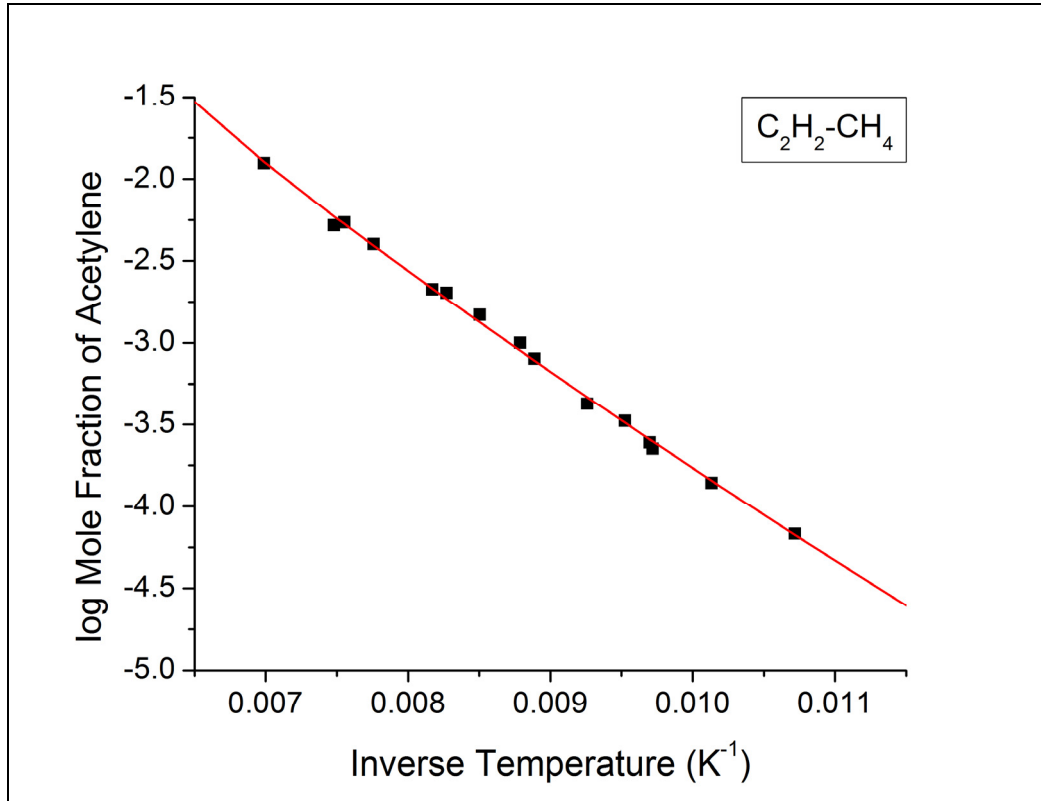
Fig. 10. Solubility of solid C_2H_2 in liquid N_2 as a function of inverse temperature at the saturation pressure of liquid N_2. Symbols denote experimental data from Fedorova (1940) [abbr. Fed.], and Ishkin & Burbo (1939) [abbr. I&B]. The red curve represents predicted solubilities from the modified van Laar model.
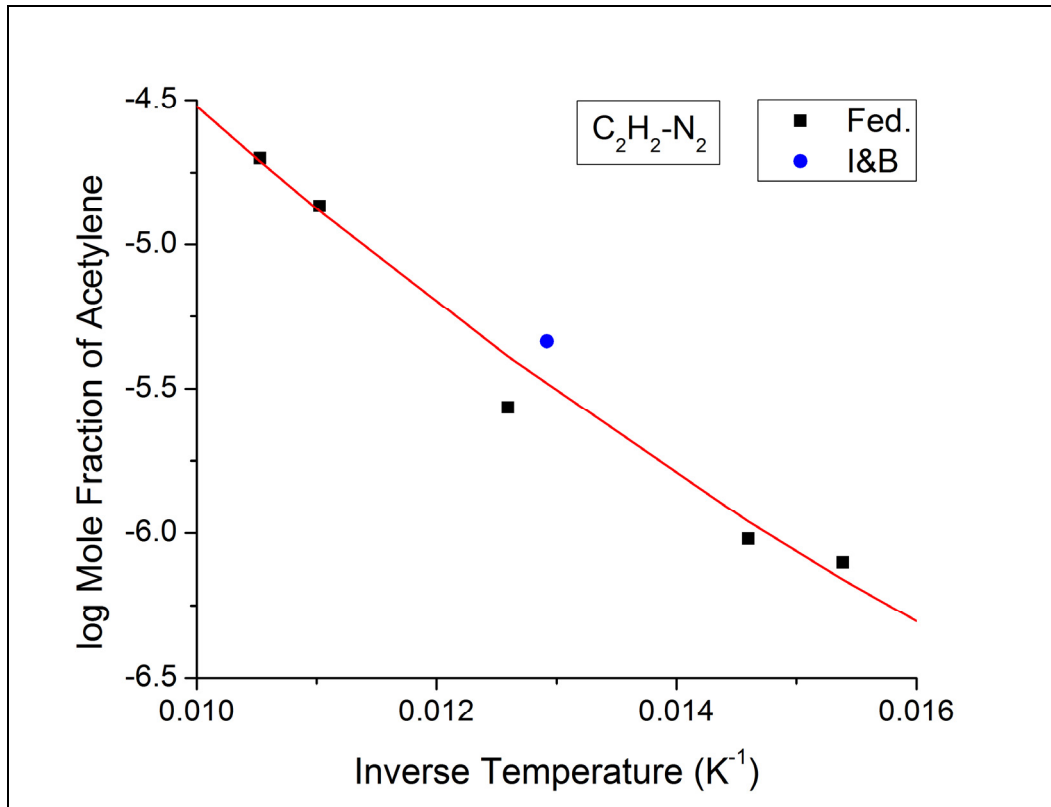
Fig. 11. Linear correlations between binary interaction energies and differences in enthalpies of vaporization at 90.6941 K. Symbols correspond to absolute differences in enthalpies of vaporization from Table 2, and interaction energies for binary systems from Table 3. Lines represent correlations for species in liquid alkanes, converging at the origin; and the slopes of the lines for CH_4, N_2, and C_2H_2 are 0.1091, 0.3389, and 0.8705, respectively.
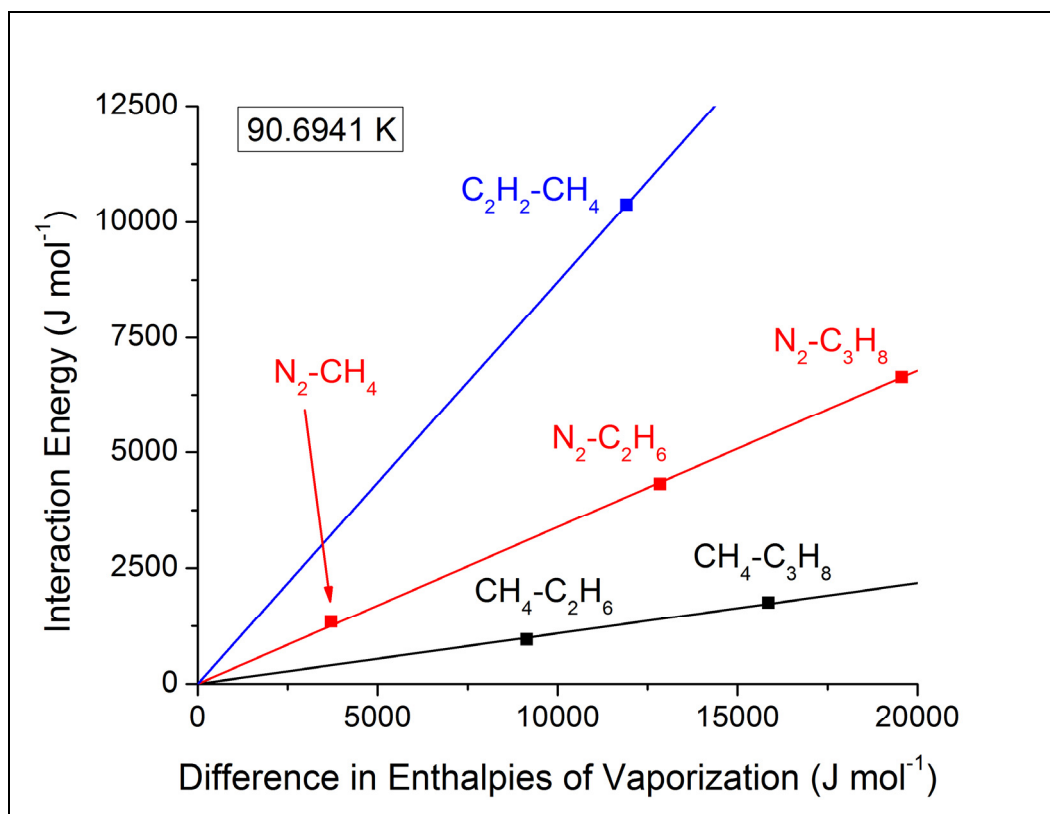
Fig. 12. Comparisons between models of the CH_4-C_2H_6-N_2 ternary at 95 K. Symbols show differences between common logarithms of total pressures from models and experiments (Table 4), as a function of the relative amounts of CH_4 and C_2H_6 in the liquid. Points are connected by lines to highlight trends. The dashed black line corresponds to perfect agreement between model and experiment. Raoult refers to Raoult's law, and GERG refers to the GERG model (Kunz et al., 2007). Abbreviations: Tmp., Thompson (1985); H&B, Heintz & Bich (2009); P&P, Preston & Prausnitz (1970); MVL, modified van Laar (Eq. 3).
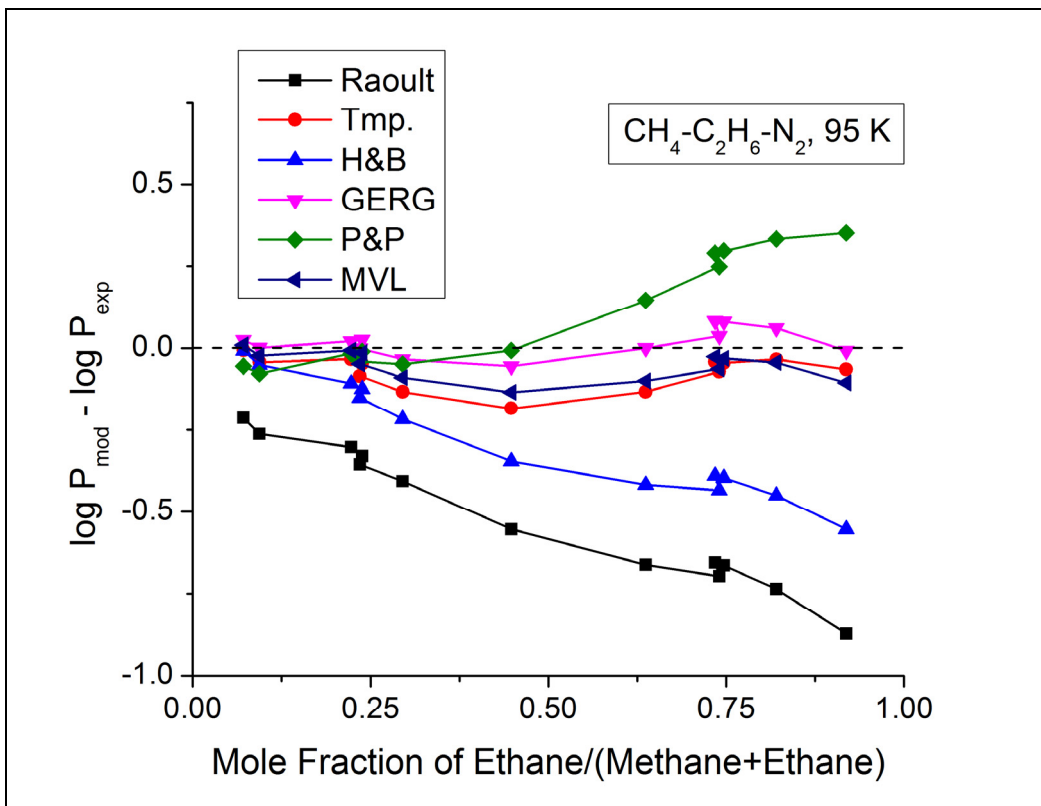
Fig. 13. Improvements to the modified van Laar model by inclusion of a ternary parameter for CH_4-C_2H_6-N_2 at 95 K. Symbols show differences between common logarithms of total pressures from models and experiments (Table 4), as a function of the relative amounts of CH_4 and C_2H_6 in the liquid. Points are connected by lines to highlight trends. The dashed black line corresponds to perfect agreement between model and experiment. GERG refers to the GERG model (Kunz et al., 2007); MVL, modified van Laar model (Eq. 3); and MVL+T, modified van Laar model with a ternary parameter (Eq. 12).
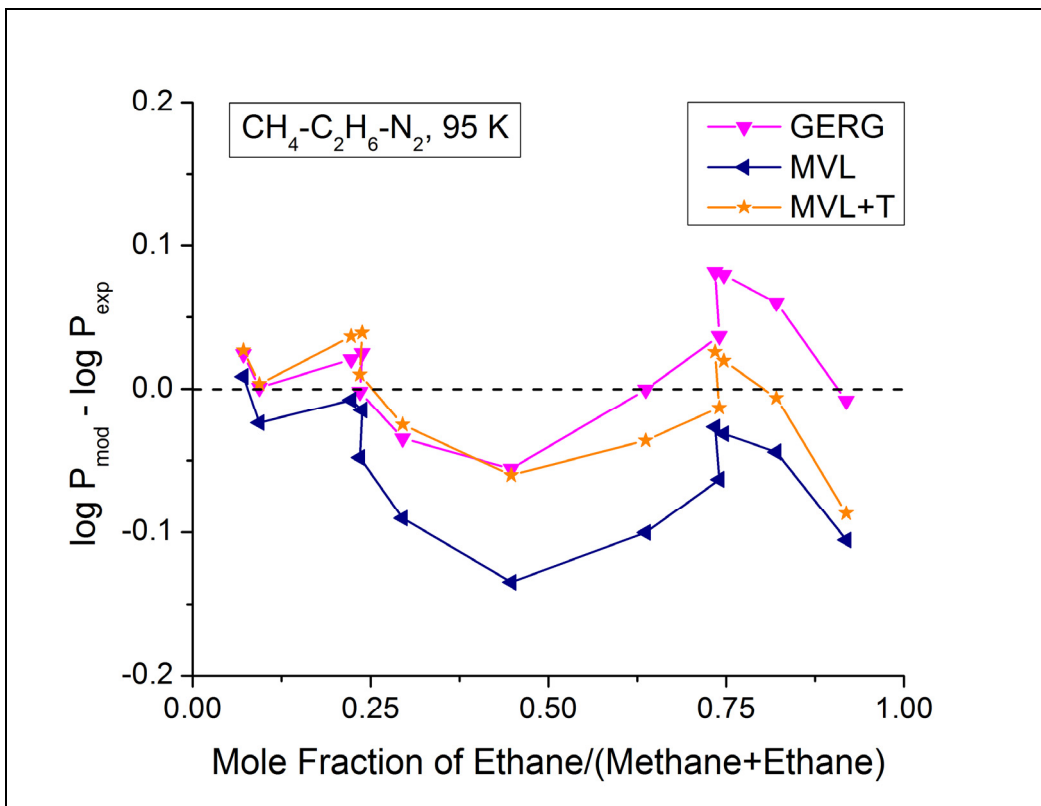
Fig. 14. Magnitudes of terms in the improved modified van Laar model (Eq. 12) contributing to the natural logarithm of the activity coefficient of N_2 in liquids containing CH_4, C_2H_6, and N_2 at 95 K (Table 4), as a function of the relative amounts of CH_4 and C_2H_6 in the liquid. Symbols denote contributions from the labeled binary or ternary term in the model, and are connected by lines to highlight trends. Summing the terms yields the natural logarithm of the activity coefficient of N_2 in the liquid mixture.
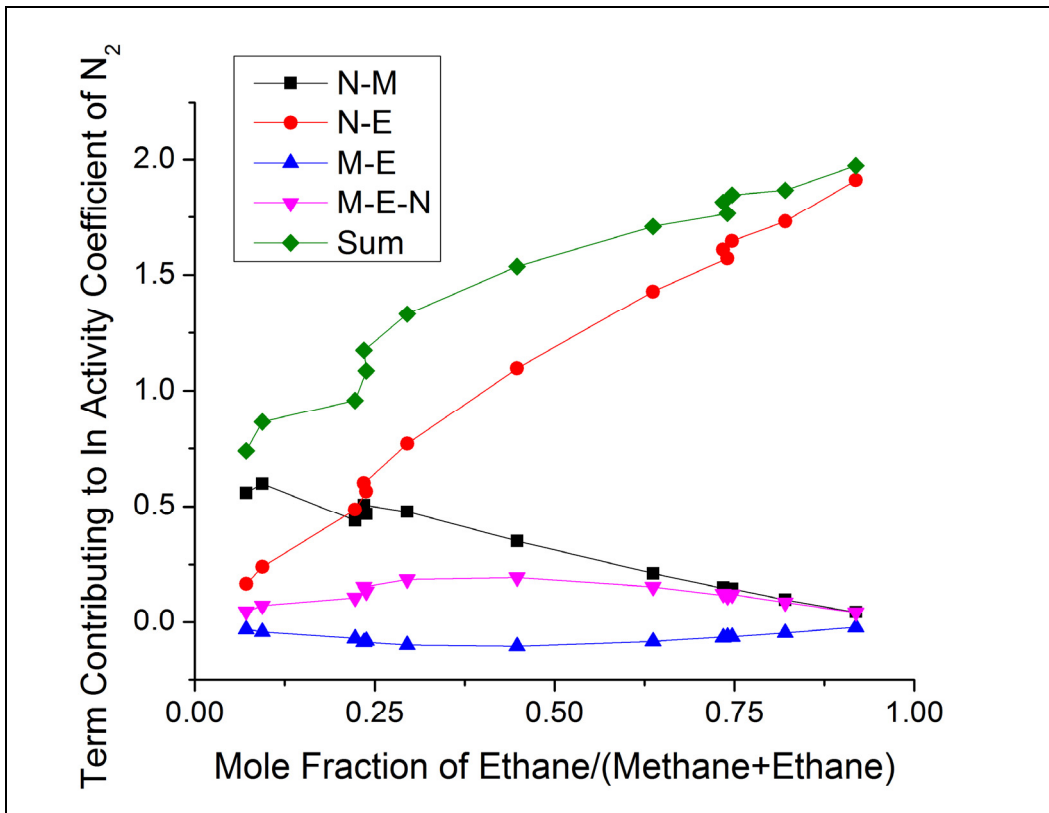
Fig. 15. Summary of models of the CH$_4$-C$_2$H$_6$-N$_2$ ternary at 95 K. Columns show averages of absolute deviations in common logarithms of total pressures from models and experiments (Table 4). Error bars denote one standard deviation (color has no meaning), and the error bar for Raoult's law goes off scale. Raoult refers to Raoult's law, and GERG refers to the GERG model (Kunz et al., 2007). Abbreviations: Tmp., Thompson (1985); H&B, Heintz & Bich (2009); P&P, Preston & Prausnitz (1970); MVL, modified van Laar (Eq. 3); MVL+T, modified van Laar with a ternary parameter (Eq. 12).
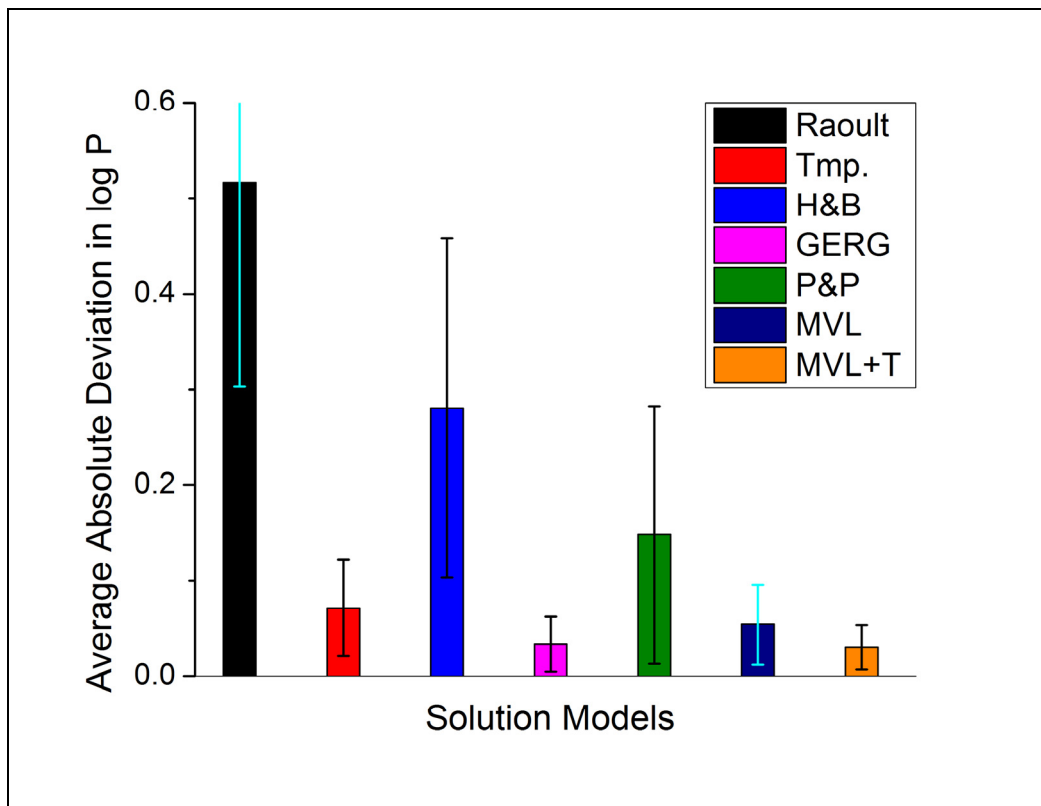
Fig. 16. Comparisons between models of the N_2-CH_4-C_2H_2 ternary at 90.6941 K.

Curves show predicted solubilities of solid C_2H_2 in liquids with varying

proportions of N_2 and CH_4. Henry refers to the simplest form of Henry's law (Eq.

13). Abbreviations: P&P, Preston & Prausnitz (1970); MVL, modified van Laar

(Eq. 3).
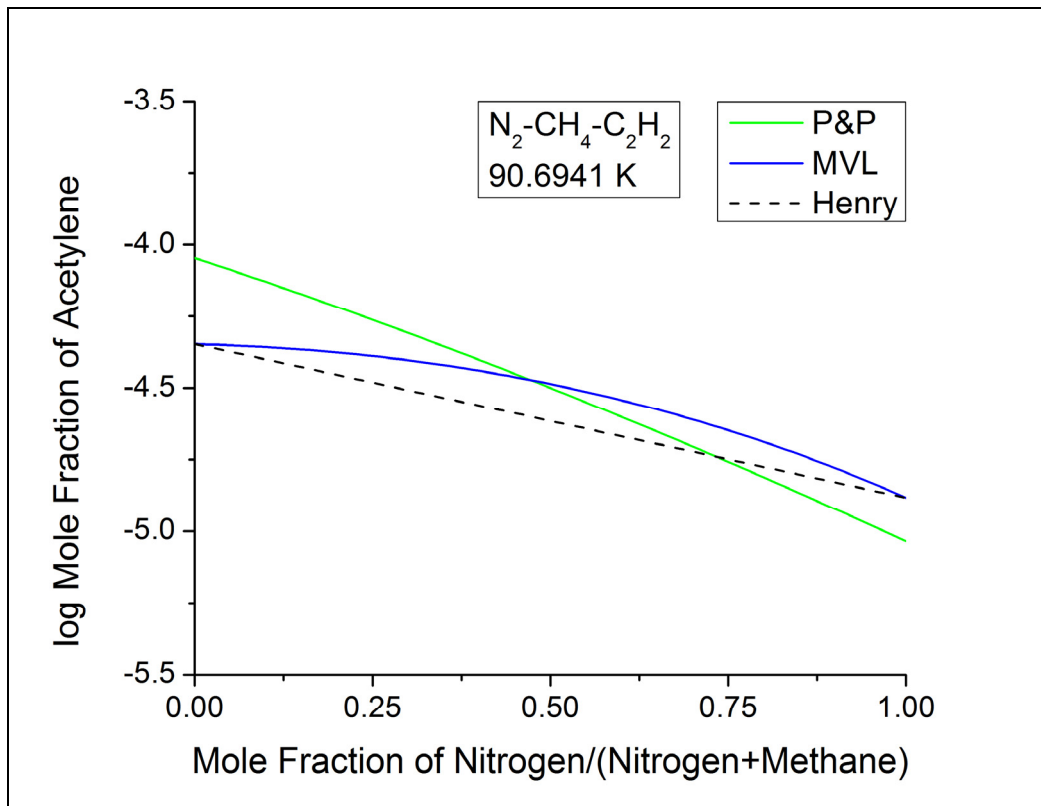
Fig. 17. Comparisons between models of the CH_4-C_2H_6-C_2H_2 ternary at 90.6941 K. Curves show predicted solubilities of solid C_2H_2 in liquids with varying proportions of CH_4 and C_2H_6. Raoult refers to Raoult's law ($\gamma^{liq}_{C_2H_2} = 1$), and Henry refers to the simplest form of Henry's law (Eq. 13). Abbreviations: P&P, Preston & Prausnitz (1970); MVL, modified van Laar (Eq. 3).
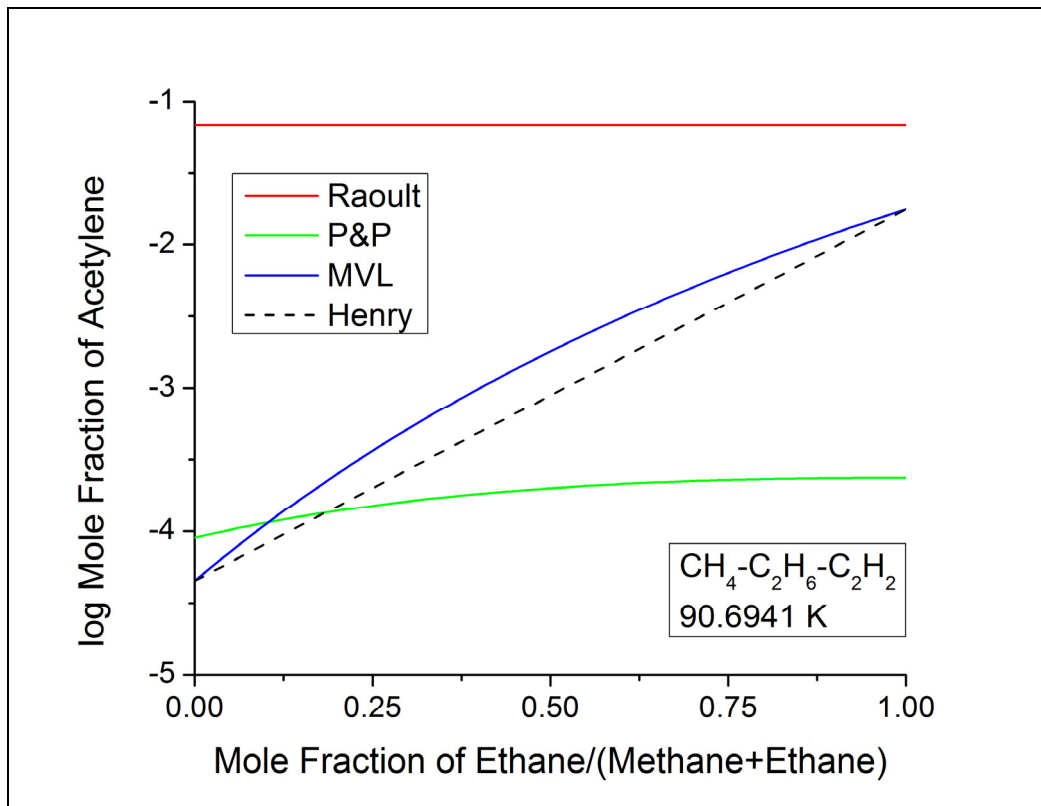
Fig. 18. Predicted equilibrium composition of major components in liquids on Titan's surface, as a function of the mixing ratio (or mole fraction) of CH_4 in the near-surface atmosphere at 90.6941 K and 1.467 bar. Calculations are based on the assumptions that CH_4 and N_2 are at vapor-liquid equilibrium, liquids are saturated with respect to solid C_2H_2, and the liquid-phase mole ratio of C_2H_6/C_3H_8 is 10. The dashed magenta line indicates the near-surface mixing ratio of CH_4 gas measured by the Gas Chromatograph-Mass Spectrometer onboard the Huygens probe (Niemann et al., 2010), and the dashed black line indicates the upper limit mixing ratio of CH_4 gas for vapor-liquid equilibrium to be possible (i.e., the dew point of the N_2-CH_4 binary at these conditions).
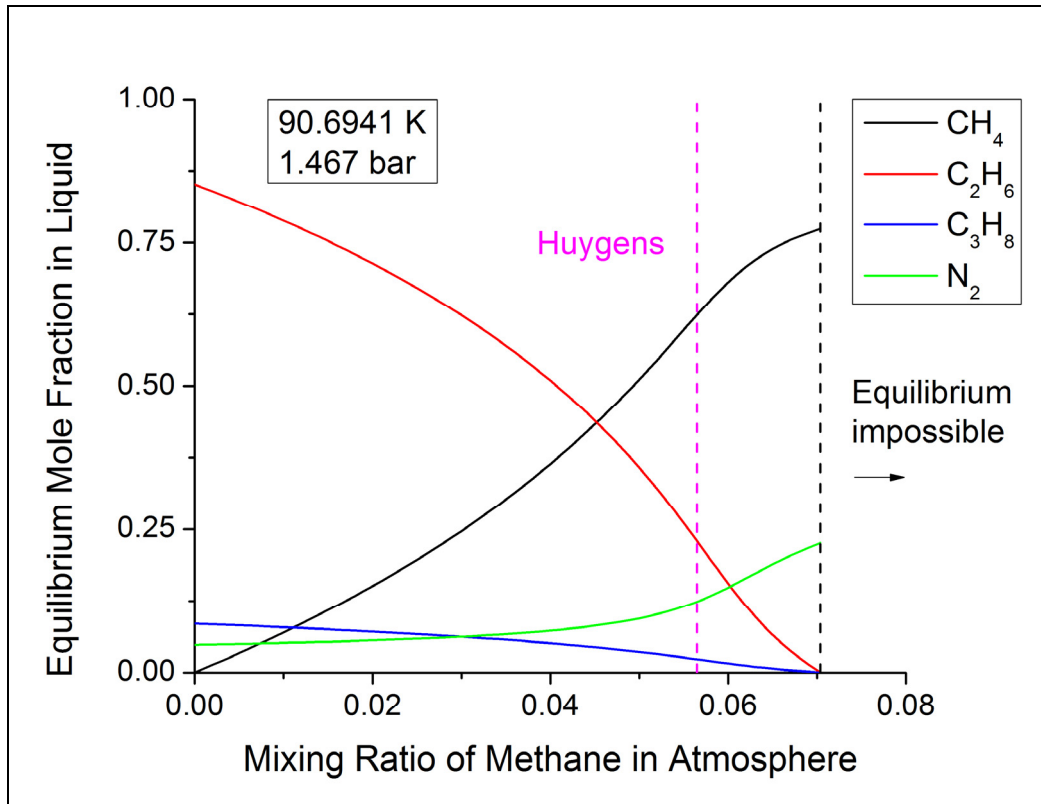
Fig. 19. Predicted solubility of solid C_2H_2 (black curve) in liquids on Titan's surface, as a function of the mixing ratio (or mole fraction) of CH_4 in the near-surface atmosphere at 90.6941 K and 1.467 bar. The composition of the corresponding solvent is shown in Fig. 18. Colored horizontal lines designate solubilities of salts in pure water at Earth reference conditions (298.15 K, 1 bar). Surface calcite refers to the solubility of calcite in water at a fixed partial pressure of CO_2 of 3.9×10^{-4} bar, and subsurface calcite corresponds to a fixed partial pressure of CO_2 of 10^{-2} bar. The dashed magenta line indicates the near-surface mixing ratio of CH_4 gas measured by the Gas Chromatograph-Mass Spectrometer onboard the Huygens probe (Niemann et al., 2010), and the dashed black line indicates the upper limit mixing ratio of CH_4 gas for vapor-liquid equilibrium to be possible (i.e., the dew point of the N_2-CH_4 binary at these conditions). The ppm scale was selected to facilitate comparisons between Titan and Earth.
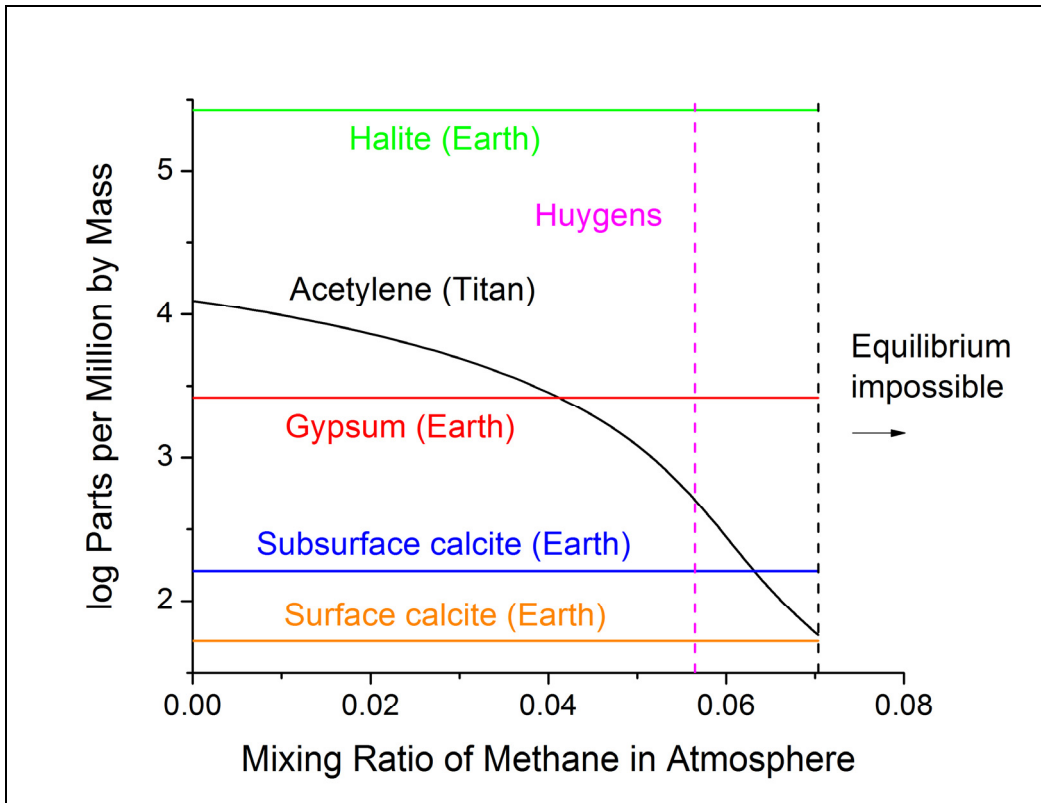
Chapter 2

MECHANISMS OF DECARBOXYLATION OF PHENYLACETIC ACIDS

AND THEIR SODIUM SALTS IN WATER AT HIGH TEMPERATURE AND

PRESSURE

1. Introduction

Carboxylic acids are organic compounds that contain the carboxyl

functional group (CO_2H). They are typically weak acids that can dissociate into

carboxylate anions in aqueous solution depending on pH, temperature, and

pressure. The carboxyl group is present in many biological molecules, such as

fatty and amino acids. Natural waters contain numerous carboxylic acids or

carboxylates that were originally derived from biological material (Thurman,

1985). Some of these compounds may serve as food for microorganisms; may

lower solution pH, facilitating mineral dissolution and increasing rock porosity; or

may mobilize insoluble metals in weathering and ore-forming solutions (see

reviews in Pittman & Lewan, 1994). Carboxylic acids can have an important

influence on geochemical processes.

The geochemistry of deep sedimentary systems is likely to be especially

influenced by carboxylic acids, given the widespread occurrence of carboxylic

acids in oil-field brines (Willey et al., 1975; Fisher, 1987; MacGowan & Surdam,

1990; Barth, 1991; Lundegard & Kharaka, 1994). Within sediments at depth,

carboxylic acids can undergo chemical transformations that are promoted by

76

higher temperatures (diagenesis). One common abiotic reaction of carboxylic acids is decarboxylation

$$RCO_2H \text{ (Carboxylic acid)} \rightarrow RH \text{ (Alkane)} + CO_2, \hspace{2cm} (1)$$

where R denotes an arbitrary organic group. Decarboxylations can turn substances of little economic value into ones of much greater value. For example, alkanes produced by decarboxylation reactions may contribute to petroleum or natural gas deposits (Shimoyama & Johns, 1971; Carothers & Kharaka, 1978; Tissot & Welte, 1984). Alternatively, oxidative decarboxylation may occur under suitable geochemical conditions (Shock, 1988; 1994), generating CO_2 and more oxidized organic compounds such as alkenes (McCollom & Seewald, 2003). Subsequent reactions of decarboxylation products in the presence of water and minerals may produce new, shorter carboxylic acids (Seewald, 2001). Carboxylic acids appear to be key intermediaries in the abiotic degradation of organic matter in deeply buried sediments (e.g., Helgeson et al., 1993). Thus, a detailed understanding of their chemical reactivity may illuminate aspects of the deep carbon cycle.

The decarboxylation reaction is well-known in the field of organic chemistry (e.g., Smith & March, 2007), and there is much information about the reaction (see reviews by Brown, 1951; Clark, 1969; Richardson & O'Neal, 1972; Bell & Palmer, 1994). However, comparably less attention has been given to decarboxylation in water at elevated temperatures and pressures, which is of great importance to geochemists. Carboxylic acids studied previously in hydrothermal

fluids include: formic (McCollom & Seewald, 2003), acetic (Kharaka et al., 1983; Palmer & Drummond, 1986; Bell et al., 1994; McCollom & Seewald, 2003), acetic acid derivatives with electron-withdrawing groups (Belsky et al., 1999), butyric (Palmer & Drummond, 1986), valeric (McCollom & Seewald, 2003), palmitic (Fu et al., 2010), stearic (Watanabe et al., 2006), benzoic (Katritzky et al., 1990a), OH-substituted benzoic acids (Li & Brill, 2003), phenylacetic (Katritzky et al., 1990b), mandelic (Katritzky et al., 1990c), oxalic (Crossey, 1991), and malonic acid (Maiella & Brill, 1996). These studies significantly improved knowledge of decarboxylation rates under hydrothermal conditions, and factors affecting decarboxylation rates (e.g., mineral catalysts). However, the sequence of molecular events, or reaction mechanism, by which decarboxylation occurs in hydrothermal systems remains unknown (Bell & Palmer, 1994). How are chemical bonds broken and formed during the reaction? Mechanisms in water at high temperatures and pressures could be different from mechanisms at ambient conditions, as the physical and chemical properties of water (e.g., dielectric and dissociation constants) change with temperature and pressure (e.g., Johnson & Norton, 1991). Mechanistic information at geochemically relevant conditions is needed to develop generalized kinetic models that may eventually allow accurate predictions of rates of decarboxylation for a diversity of organic structures, as functions of environmental conditions. This would lead to a better quantitative understanding of the geochemical evolution of subsurface sedimentary systems. This work seeks to take a step in that direction by obtaining

information about a mechanistically-revealing decarboxylation reaction in aqueous solution at high temperature and pressure.

Unambiguous evidence of organic reaction mechanisms is rare in the geochemical literature. In general, experimental geochemists report equilibrium or rate constants, inferred reaction pathways, isotope effects, and/or heterogeneous phenomena. Many systems of geochemical interest are too complicated to characterize mechanistically. In some cases, mechanisms are discussed, but proposed mechanisms are usually based on analogies to well-known mechanisms in the organic chemical literature, rather than on experimental data that permit the investigator to distinguish between possible mechanisms. This is a key shortcoming of previous work because reaction mechanisms in hydrothermal fluids could be different from those in ambient laboratory solvents or in the gas phase. To address this point, I performed experimental kinetic studies using the model compound phenylacetic acid (PAA), which can provide crucial mechanistic information. PAA is preferable to simpler, more geochemically relevant compounds like acetic acid, as changes in the electronic properties of the aromatic ring lead to predictable thermodynamic and kinetic consequences that reflect the underlying mechanism (Anslyn & Dougherty, 2006). Thus, a valuable mechanistic constraint can be obtained by studying decarboxylation of ring-substituted PAAs, and determining how substituents on the benzene ring affect the rate of decarboxylation. Structures, names, and abbreviations of PAAs studied here are shown in Table 1. Sodium phenylacetate is abbreviated as Na-PA.

79

Other favorable characteristics of PAA are: (1) the carbon atom bonded to the carboxyl group in PAA is adjacent to an aromatic system (i.e., it is a benzyllic carbon), which can stabilize ionic and radical reaction intermediates by resonance, leading to relatively rapid rates that can be quantified over a convenient timescale; (2) PAA and its decarboxylation product, toluene, have low volatility and can be extracted easily into organic solvents for subsequent quantitative analysis; (3) reactions other than decarboxylation are eliminated/minimized because the majority of the PAA structure is an inert benzene ring (McCollom et al., 2001); (4) PAA is non-toxic; and (5) decarboxylation of PAA has been studied under different experimental conditions (Back & Sehon, 1960; Epling & Lopes, 1977; Katritzky et al., 1990b), permitting comparisons.

The present communication has three objectives: (1) to show how experimental tools from the subdiscipline of physical organic chemistry can be used to test candidate mechanisms for a type of organic reaction of geochemical importance; (2) to determine how the rate and mechanism of decarboxylation are influenced by speciation between phenylacetic and phenylacetate species; and (3) to deduce mechanisms of decarboxylation for phenylacetic acid and sodium phenylacetate in high temperature-pressure water. This project represents a continuation of mechanistic studies of functional group chemistry in aqueous systems at high temperature and pressure (Shipp et al., submitted; Yang et al., submitted).

2. Procedure

80

Hydrothermal experiments were performed in gold (Au) capsules (5 mm outer diameter × 0.127 mm wall thickness × 37.5 mm length, Au tubing from Depths of the Earth Co.). The quoted purity of the Au tubing was 99.99%, with impurities of Cu, Fe, or Ag of ≤50 ppm. Au was used because previous work demonstrated that Au is among the weakest known heterogeneous catalysts for acetic acid decarboxylation (Palmer and Drummond, 1986), and the flexibility of Au allows reaction vessels to be pressurized significantly above the saturation pressure of water, eliminating the possibility of producing a vapor phase (if a vapor phase were present, there would be ambiguity as to whether decarboxylation occurred in the aqueous or vapor phase). Prior to use, precut Au tubes were cleaned by refluxing in 12 M HCl for 30 min, rinsed three times with high-purity water (18.2 MΩ-cm), then annealed by baking at 600°C for 12 h. Afterward, one end of each tube was sealed by arc-welding, and starting material (200 μmol) and Ar-sparged, high-purity water (200 μL) were loaded into each tube. Reagents were of the highest purity available, and used without further purification. A high concentration of starting material (ca. 1 molal) was used to minimize errors in weighing and loading small quantities of solid. Nevertheless, PAA should have an aqueous solubility of at least 1 m at high temperatures, given that its solubility is 0.130 m at 25°C and 0.686 m at 86.7°C (Morrison, 1944); and given the fact that organic compounds are much more soluble in high-temperature water (e.g., Price, 1981; Neely et al., 2008) because water becomes a less polar solvent (i.e., lower dielectric constant) at higher temperatures. The substituted

81

PAAs are sufficiently similar to the parent that their aqueous solubilities should not be dramatically different from that of PAA. The headspace of Au capsules was gently purged with ultra-high purity (99.999%) Ar for 2 min to minimize the amount of air in capsules. Capsules were arc-welded without evaporative loss of water by submerging the previously welded end of the capsules in an H_2O-CH_3OH cold bath that had been chilled to the eutectic point using liquid N_2. All sealed capsules were tested for leaks prior to use by placing them in an oven at 105°C for 10 min, then checking for mass loss.

Au capsules containing a PAA and water were put into a stainless steel cold-seal vessel (Williams et al., 2001). The vessel was pressurized with distilled water, and heated by placement in a preheated furnace. Owing to the large heat capacity of the vessel, 2-3 h of heating was required to reach the experimental temperature of 300°C. To avoid a temperature effect from slow heating on subsequent kinetic analyses, $t = 0$ was defined as 2 h after the vessel was placed in the furnace. This means that there may be some product present at $t = 0$, because time here refers to time at ca. 300°C rather than time since heating was initiated. The vessel was heated isobarically at 1034 bar (15,000 psi), which is similar to pressures under several kilometers of sediment in sedimentary basins. Temperature was measured using a corrosion-resistant thermocouple, and pressure was measured using a Bourdon gauge. Estimated uncertainties are <5°C in temperature, and ±50 bar in pressure (Williams et al., 2001). Reactions were performed at 300°C to expedite reaction rates; yet it is understood that diagenetic reactions of organic compounds generally occur at lower temperatures over longer

durations. Here, I assume that thermal energy is a reasonable substitute for time (e.g., McCollom & Seewald, 2003).

Experiments were performed at 300°C and 1034 bar for different durations. Once the desired duration was reached, the experiment was quickly quenched by placing the steel vessel into a room-temperature water bath. Au capsules were weighed to confirm that no leaks occurred during the experiment. Leak-free capsules were rinsed with methylene chloride (CH_2Cl_2), then placed in 4 mL glass vials containing 3.00 mL of a solution of gas chromatography (GC) internal standards: n-decane (0.10% by vol.) and an appropriate PAA (30 mM) in CH_2Cl_2. An appropriate PAA is one that cannot be produced in the experiment of interest, such as p-F-PAA in p-Me-PAA experiments. Capsules were opened by puncturing them several times with a hobby knife. A stoichiometric excess of aqueous HCl was added to vials to ensure that only the carboxylic acid form of the starting material was present, as the carboxylate cannot be extracted into CH_2Cl_2. Vials were capped and shaken repeatedly to extract organics into the CH_2Cl_2 phase. Organic reactants and products are sufficiently hydrophobic that they could be extracted without prior derivatization (e.g., esterification).

Quantitative analysis was performed using a Varian CP-3800 gas chromatograph. Organics were separated using a poly(5% diphenyl/95% dimethylsiloxane) capillary column (Equity-5, Supelco), and were detected using a flame ionization detector. Organic products were identified using authentic standards, and amounts of organics were determined using linear calibration curves that were referenced to internal standards. Triplicate autosampler (Varian

CP-8400) injections were performed to verify reproducibility. Mass balance was computed by comparing the number of benzene rings in the reactant and products. The assumption of conservation of benzene rings is supported by experiments demonstrating the inertness of the benzene ring under hydrothermal conditions (McCollom et al., 2001). When needed, gas chromatography-mass spectrometry (GC-MS) analyses were performed by the High Resolution Mass Spectrometry Laboratory at Arizona State University.

Materials: phenylacetic acid (Aldrich, 99%), p-methylphenylacetic acid (Alfa Aesar, 99%), m-methylphenylacetic acid (Alfa Aesar, 99%), o-methylphenylacetic acid (Aldrich, 99%), p-fluorophenylacetic acid (Alfa Aesar, 98%), m-fluorophenylacetic acid (Alfa Aesar, 98%), o-fluorophenylacetic acid (Alfa Aesar, >98%), methylene chloride (Fisher Scientific, 99.9%), n-decane (≥99%, Sigma-Aldrich), hydrochloric acid (36% w/w aq. soln., Alfa Aesar), sodium hydroxide (98%, Alfa Aesar), deuterium oxide (99.9 atom % D, Aldrich). Sodium phenylacetates were prepared by neutralizing the appropriate PAA with aqueous NaOH. The purity of all starting materials was verified by GC. Standards for organic products (substituted toluenes, cresols, and benzene) were purchased from Sigma-Aldrich or Alfa Aesar. HCl solutions were standardized by pH titration. High-purity water (18.2 MΩ-cm) was obtained from a Barnstead NANOpure DIamond water purification system.

3. Results

Analytical data from hydrothermal experiments with phenylacetic acid or sodium phenylacetate are given in Table 2, and results for methyl- and fluoro-substituted phenylacetic acids or sodium phenylacetates are given in Tables 3 and 4, respectively. These experiments were performed to determine how changes in pH, solvent isotopic composition, equilibrium speciation, and ring substitution affect rates of decarboxylation. Only CH_3 and F substituents were used because many of the classic substituents (e.g., Anslyn & Dougherty, 2006) were found to be incompatible with high-temperature water – high temperature may lead to homolysis of the carbon-substituent bond, or nucleophilic attack by water may destroy the substituent (e.g., OCH_3, CN).

In all experiments, disappearance of PAAs or Na-PAs was observed, a toluene ($PhCH_3$; Ph standards for the phenyl group, C_6H_5) was the dominant/only detected organic product, and mass balance was satisfactory (almost always >90%). The major/only reaction involved cleavage of the bond between the benzyl and carboxyl carbons in the starting material. In experiments with PAAs, Au capsules were inflated after the experiment, and bubbling was observed after capsules were punctured. This shows that a gas was produced. Taken together, these observations imply that PAAs reacted by decarboxylation

$$PhCH_2CO_2H \rightarrow PhCH_3 + CO_2. \qquad\qquad (2)$$

In experiments with Na-PAs, Au capsules were not inflated after the experiment, and bubbling was not observed after capsules were punctured. However, bubbles

formed after aqueous HCl was added to capsules during the extraction procedure. The most reasonable explanation for this is that the capsules contained HCO_3^-, which reacted with H^+, forming $CO_2 + H_2O$. The presence of a toluene and bicarbonate inside capsules is indicative of the following net reaction

$$PhCH_2CO_2Na + H_2O \rightarrow PhCH_3 + NaHCO_3. \tag{3}$$

The form of carbon in the second product is different in Eqs. (2) and (3) because the systems have different bulk compositions, causing Na-PA systems to have a higher pH than PAA systems (see Section 4.3).

Minor organic products were also detected in some experiments. Trace amounts of benzene (C_6H_6) were produced in PAA + HCl experiments (Table 2). C_6H_6 may have also formed in PAA + H_2O experiments, but C_6H_6 appeared to be at the threshold of detectability, so this identification should be regarded as tentative. The formation of C_6H_6 indicates that another type of carbon-carbon bond can be broken at the experimental conditions, albeit at a rate that is much slower than that of decarboxylation. Enhanced production of C_6H_6 in HCl-rich systems suggests that C_6H_6 formation may be acid-catalyzed. The precursor of benzene is presumably phenylacetic acid or toluene, but experiments are needed to determine whether benzene can be made from toluene alone under acidic hydrothermal conditions.

Small quantities of cresols (methylphenols) were detected in experiments with F-PAAs and Na-F-PAs (Table 4). This provides evidence for the following type of reaction.

$$\text{F}-\langle\text{C}_6\text{H}_4\rangle-\text{R} \;+\; H_2O \;\longrightarrow\; \text{HO}-\langle\text{C}_6\text{H}_4\rangle-\text{R} \;+\; HF$$
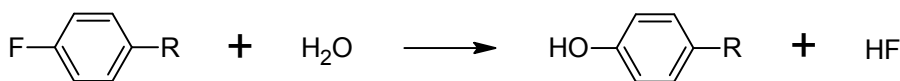
Here, R represents CH_2CO_2H or CH_3. If the former, cresols are produced by hydrolysis of F-PAA, followed by decarboxylation of hydroxyphenylacetic acid; and if the latter, cresols are produced by decarboxylation of F-PAA, followed by hydrolysis of fluorotoluene. Insufficient information is available at present to distinguish between these possibilities. Hydroxyphenylacetic acids were not detected in the F-PAA or Na-F-PA experiments, but these compounds may elude the detection method, as it was determined that p-hydroxyphenylacetic acid is poorly soluble in CH_2Cl_2. Relatively high mass balances (Table 4) demonstrate that hydroxyphenylacetic acids cannot be abundant. However, hydroxyphenylacetic acids need not build up to high concentrations to be intermediates in cresol formation if their rate of decarboxylation is faster than the hydrolysis rate of F-PAA. It is notable that the rate of cresol formation was greater in experiments with Na-F-PAs than in those with F-PAAs (Table 4). This indicates that the rate of cresol formation is sensitive to pH, and suggests that substitution of OH for F occurs by a nucleophilic aromatic substitution mechanism (Anslyn & Dougherty, 2006), with OH⁻ acting as the nucleophile and

F⁻ as the leaving group. A more detailed understanding of cresol formation will require separate experiments with fluorotoluenes and hydroxyphenylacetic acids to disentangle the hydrolysis and decarboxylation reactions.

There may be small amounts (<10-20 μmol) of undetected products (except for CO_2 or HCO_3^-, which must be major products owing to the stoichiometry of Eqs. 2 and 3). To escape detection, sufficient quantities of a compound must not be extracted into CH_2Cl_2 during sample workup, which could occur if the compound is a gas, highly soluble in water, or if the compound has a large molar mass. Examples include H_2, CH_4, acetic acid, and large polymers. Unidentified products are probably responsible for mass balance deficits in experiments where the mass balance decreases systematically with time (e.g., p-F-PAA, o-F-PAA; Table 4). This should be more pronounced in longer-duration experiments, where extra time may allow synthesis of secondary and tertiary products, such as polymers. For this reason, it is possible that unidentified polymers formed in the p-F-PAA and o-F-PAA experiments. Random fluctuations in mass balance with time may be attributed to standard errors in laboratory work, such as loss of sample during capsule opening or extraction problems. It is notable that experiments with Na-o-F-PA have mass balances that are slightly lower than those of other experiments (as low as 87%; Table 4). This may be due to the formation of o-hydroxyphenylacetic acid, which may not partition into CH_2Cl_2. Impure starting material cannot be a factor that results in decreased mass balance, as GC analysis of acidified Na-o-F-PA revealed that the starting material has a purity of 101±1%.

A potential issue is reactor wall catalysis. The goal here is to study mechanisms of decarboxylation reactions in homogeneous water at high temperature and pressure, but surfaces of Au capsules could catalyze decarboxylation. To help address this possibility, I performed experiments where cut pieces of Au tubing were added to capsules containing PAA or Na-PA, and these experiments were run alongside controls. After 23 h at 301°C and 1034 bar in H_2O, the reaction progress of PAA was 66±1%, and that of PAA + Au was 66±1% (Table 2). After 6 h at 301°C and 1034 bar in H_2O, the reaction progress of Na-PA was 55±1%, and that of Na-PA + Au was 53±1% (Table 2). Because results from + Au experiments are essentially identical to those from controls, it appears that Au does not catalyze decarboxylation of PAA or Na-PA under the experimental conditions. Of course, these limited experiments do not rule out Au catalysis for all kinetic scenarios imaginable, but they cast doubt on the possibility, consistent with everyday experience of the inertness of Au. However, more extensive experiments on Au catalysis of hydrothermal organic reactions are being performed by a member of the hydrothermal organic geochemistry group at Arizona State University.

Replicates were performed to check the reproducibility of experiments. Triplicates were performed for PAA and Na-PA, and duplicates were performed for Na-PA + NaOH, p-Me-PAA, Na-p-Me-PA, o-Me-PAA, p-F-PAA, and Na-o-F-PA (Tables 2-4). In terms of reaction progress, some replicates were consistent to within a few percent, while others exhibited discrepancies of 5-10%. The average standard deviation for replicates in the entire dataset is 3%. Possible

89

reasons for why some replicates were more discrepant than others include: (1) Au capsules that were placed at different locations inside the pressure vessel may have been at slightly different temperatures as a result of small temperature gradients in the vessel; (2) possible changes in temperature during overnight experiments, when temperature could not be monitored; and (3) overall improvement in the ability of the investigator to perform and analyze experiments through the course of this project. In general, the reproducibility of the experiments was satisfactory, although minor variabilities will lead to corresponding uncertainties in derived rate constants.

The kinetics of disappearance of PAAs and Na-PAs can be characterized by plotting percent yields of remaining starting material, and organic products as functions of time (Figs. 1-18). Reactions were run to high conversion (>70%) to obtain tighter constraints on kinetic models. There was no evidence of an approach to a measureable equilibrium between the reactant and products, as some reactants (m-Me-PAA, Na-m-F-PA, Na-o-F-PA) became undetectable after a sufficient amount of time (Tables 3-4). Evidently, decarboxylation of PAAs and Na-PAs is irreversible and under kinetic control, consistent with prior thermodynamic evaluations (Shock, 1988; 1994). This distinguishes decarboxylation from functional group transformations that do not involve the breaking of carbon-carbon bonds (e.g., alkane-alkene interconversion), which can be under thermodynamic control in hydrothermal systems (Seewald, 1994; Shipp et al., submitted). Homolytic dissociation of dibenzyl ketone, another reaction

studied by this research group, also appears to be irreversible under similar

hydrothermal conditions (Yang et al., submitted).

Yield is defined as moles of organic compound divided by moles of

starting material (conservation of benzene rings), and yields were calculated using

data from Tables 2-4. Yield is preferable to concentration as a kinetic variable in

the present experimental system because the concentration of starting material

varies slightly between experiments (Tables 2-4), and yield normalizes the data. I

attempted to fit the kinetic data using zero-, first-, and second-order integrated

rate equations (e.g., Atkins, 1998), and determined that first-order kinetics

reproduces the data well with an acceptable amount of scatter. The other kinetic

models performed worse as indicated by non-random deviations. This is not

surprising as an uncatalyzed decomposition reaction in solution should follow

first-order kinetics. The first-order equations can be written as

$$\left[\sum \mathrm{PA}\right] = \left[\sum \mathrm{PA}\right]_{t=0} e^{-k_{app}t} , \tag{4}$$

and

$$\left[\mathrm{Org.\ Prod.}\right] = \left[\mathrm{Org.\ Prod.}\right]_{t=0} + \left[\sum \mathrm{PA}\right]_{t=0} \left(1 - e^{-k_{app}t}\right) , \tag{5}$$

where [∑PA] stands for the concentration of all species containing phenylacetate

(all PA species are converted to the acid form during sample preparation prior to

GC analysis, so the analytical method quantifies the total amount of PA species), [Org. Prod.] represents the concentration of all organic products bearing a benzene ring, k_{app} designates the apparent rate constant for disappearance of the starting material, and t corresponds to duration at ca. 300°C. These equations are written in terms of concentrations for the sake of familiarity, yet yields can be substituted for concentrations without changing the mathematical relationships. A regression program was used to obtain best-fit values of the parameters: $[\sum PA]_{t=0}$, [Org. Prod.]$_{t=0}$ (actually, percent yields at $t = 0$), and k_{app}. Model curves are drawn in Figs. 1-18, and apparent rate constants are given in the figure captions.

Rate constants for decarboxylation (k_{decarb}) corresponding to Eq. (2) or (3) are required to learn mechanistic details of decarboxylation. These can be derived from apparent rate constants for disappearance of the starting material by considering product distributions. For systems with a toluene as the only organic product and a high mass balance, $k_{app} = k_{decarb}$. These criteria are satisfied by the parent and methyl-substituted systems (Tables 2-3) (yields of benzene in PAA + HCl experiments are too small to upset the equality). The fluoro-substituted systems are more complicated because cresols are produced (Table 4). F-PAAs and Na-F-PAs could react by hydrolysis in addition to decarboxylation. In this case, $k_{app} = k_{decarb} + k_{hydro}$, where k_{hydro} signifies the rate constant for hydrolysis of the fluorinated acid or salt. Alternatively, if cresols are produced solely by hydrolysis of fluorotoluenes, $k_{app} = k_{decarb}$. Because it is not known which pathway is responsible for cresol formation, a conservative assumption is that both pathways are responsible (i.e., $k_{decarb} = k_{app} - 0.5k_{hydro}$). Ratio k_{hydro}/k_{decarb} can be

estimated by numerically evaluating the initial derivative of yield of cresol with respect to yield of fluorotoluene. This analysis indicates that k_{decarb} has similar values to k_{app} (within ca. 10-20%), especially in light of experimental uncertainties in determining k_{app}. Hence, ambiguity in the pathway of cresol formation is unlikely to introduce uncertainties to k_{decarb} that are larger than those inherent to the experimental data. Similarly, small discrepancies in mass balance may be neglected. Values of k_{decarb} are given in Table 5.

4. Discussion

Rate constants for decarboxylation provide key information about how decarboxylation occurs. One mechanistic clue is relative rates of decarboxylation of PAAs and Na-PAs. Surprisingly, the ratio of rate constants k_{salt}/k_{acid} varies considerably (by about a factor of 10^3), and can be larger or smaller than unity, depending on the identity and position of the substituent (Table 5). For the unsubstituted parent, the salt decarboxylates somewhat faster than the acid. In contrast, the salt decarboxylates slower than the acid for m-Me, whereas o-F causes a large effect in the opposite direction. These results may seem perplexing at first because systematic behavior may be expected – the salts should all react faster than the acids if the carboxylate anion is the species that undergoes decarboxylation, and the opposite should be true if the carboxylic acid is the reactive species. This is because Na-PAs will dissociate more than PAAs, which are only weakly acidic (Dippy & Williams, 1934). There will be more carboxylate

93

anion in experiments with Na-PAs, and more carboxylic acid in experiments with PAAs. The most reasonable resolution to this paradox of non-systematic behavior is that there are different mechanisms of decarboxylation for PAAs and Na-PAs. This means that not all Na-PAs should be expected to decarboxylate faster than their respective PAAs, and vice versa; the relative reactivities of the salt and acid will depend on how well the structure of interest satisfies the energetic requirements of the different mechanisms.

4.1. Overview of decarboxylation mechanisms

Some possible mechanisms for decarboxylation of PAA are shown in Fig. 19. This is not an exhaustive list of possibilities, but a manageable list highlighting mechanisms that seem plausible based on a review of the decarboxylation literature, background knowledge of organic chemistry, and chemical intuition. The mechanisms depict changes in chemical bonding that may occur as PAA is converted to toluene and CO_2. In all of the mechanisms, it is assumed that carbon-carbon bond fragmentation is irreversible at the present experimental conditions.

In Mechanism A, decarboxylation is caused by homolytic dissociation of the bond between the benzyl and carboxyl carbons in PAA. Back & Sehon (1960) proposed that this mechanism occurs in the gas phase at temperatures above 587°C; detection of bibenzyl showed that benzyl radicals ($PhCH_2^{\bullet}$) are reaction intermediates. The benzyl radical is a resonance-stabilized radical with

delocalized electrons. Deuterium labeling experiments demonstrated that the benzyl radical is also an intermediate in photodecarboxylation of PAA (Epling & Lopes, 1977). Thus, Mechanism A can occur under some conditions. Furthermore, Yang et al. (submitted) performed cross-over experiments that showed that benzyl radicals can form under hydrothermal conditions, at least from decomposition of dibenzyl ketone. In the present experimental system, the benzyl radical could convert to toluene by abstracting a hydrogen atom from water or from another source, and the carboxyl radical ($^\bullet CO_2H$) could decompose into CO_2 and a hydrogen atom.

Carboxylic acids with strong electron-withdrawing groups attached to the carbon atom adjacent to a carboxyl group are thought to decarboxylate by heterolytic fission per Mechanism B (Brown, 1951; Segura et al., 1985). Trihalogenic and nitroacetic acids are prominent examples. Electron-withdrawing groups facilitate decarboxylation by increasing the dissociation constant of the acid, and by stabilizing the intermediate carbanion. The phenyl group appears to be weakly electron-withdrawing, as PAA has a pK_a that is only 0.45 units less than that of acetic acid at ambient conditions (Dippy & Williams, 1934). More significantly, the phenyl group stablizes carbanions by resonance. Yet, the benzyl anion ($PhCH_2^-$) is still strongly basic (pK_a of toluene, ca. 40; Streitwieser & Ni, 1985), and water will quickly protonate it (the extrapolated lifetime of the benzyl anion in water at 24°C is ca. 0.3 ns; Bockrath & Dorfman, 1974). Note that Katritzky et al. (1990b) proposed that PAA reacted via Mechanism B in their hydrothermal experiments.

Mechanisms C through E (Fig. 19) are related. All feature protonation of the benzene ring, and formation of an isotoluene (para or ortho) as an intermediate. Differences between Mechanisms C and D are that PAA is protonated, and protonated CO_2 is cleaved off in C; while PA⁻ is protonated, and neutral CO_2 is cleaved off in D. Mechanism E is subtly different from D, in that ring protonation and decarboxylation occur in the same step. Studies of hydrogen isotope exchange show that aromatic rings can be protonated (Ingold, 1969; Cox, 1991), but protonation is difficult at ambient conditions because the protonated species (arenium ions) have very negative pK_a's (e.g., Nagaoka et al., 1990; Lawlor et al., 2008) as a result of loss of aromaticity. Yet, it must be remembered that the present reactions were run at 300°C, so high-energy intermediates may be accessible. Isotoluenes are not unreasonable intermediates as they are stable enough to be prepared (e.g., Gajewski & Gortva, 1982). Isotoluenes may tautomerize to toluene by an acid-catalyzed mechanism, such as that shown below.
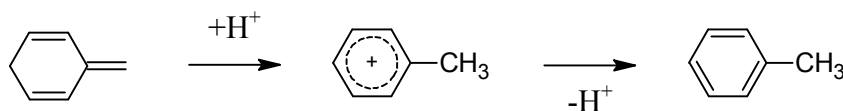
Many aromatic acids are thought to decarboxylate by mechanisms that involve ring protonation (Taylor, 1972b; Willi, 1977). These reactions are acid-catalyzed, and electron-donating substituents (e.g., OCH_3) increase reaction rates by stabilizing the arenium ion. It is thought that pyridylacetic acids, which are

nitrogen heterocyclic analogues of PAA, decarboxylate by a mechanism that is analogous to Mechanism D (Stermitz & Huang, 1971; Taylor, 1972a; Button & Taylor, 1973), where carbon-carbon bond heterolysis occurs in the zwitterion.

A handful of possible mechanisms for decarboxylation of Na-PAs are shown in Fig. 20. Mechanism F is similar to A in that homolytic fission generates the benzyl radical. In this case, there may be two routes to toluene: (1) hydrogen atom transfer to the benzyl radical; or (2) reduction of the benzyl radical to the benzyl anion by carbon dioxide radical anion ($^{\bullet}CO_2^-$), followed by protonation of the benzyl anion by water. I am not aware of any reports of this mechanism in the literature, but bond homolysis should always be considered at high temperatures. Mechanism G is basically the same as D in Fig. 19, except that the free carboxylate is produced by dissociation of the salt, rather than that of the acid. Nevertheless, these mechanisms will exhibit different kinetics in PAA and Na-PA systems because the compositions of the systems are different. Mechanisms H through J are carbanion mechanisms (e.g., Callahan & Wolfenden, 2004) that are close relatives of B in Fig. 19. In H, Na(PA) ion pair is the reactive species, while PA$^-$ is the species that undergoes decarboxylation in I. Complete dissociation of Na(PA) cannot be assumed given that dissociation of metal-organic complexes becomes less thermodynamically favorable at higher temperatures (e.g., Shock & Koretsky, 1993). Thus, an appreciable concentration of Na(PA) could allow the ion pair to decarboxylate at a significant rate, provided that this species can decarboxylate. Like Mechanism B, H and I feature the benzyl anion as the key intermediate. Buncel et al. (1984) demonstrated spectroscopically that benzyl

97

anions are produced by decarboxylation of potassium phenylacetates bearing NO_2 substituents in polar aprotic solvents. In constrast, the benzyl anion would not be an intermediate of decarboxylation in water if decarboxylation and protonation of the benzyl carbon are concerted (i.e., occur simultaneously), as depicted in Mechanism J.

4.2. Analysis of substituent effects

The mechanisms in Figs. 19 and 20 can be tested using the experimental results in this study. The first test is the relative kinetics of ring-substituted PAAs and Na-PAs (substituent effects), which are analyzed using the Hammett equation (Johnson, 1973)

$$\log(k) = \rho\sigma + b, \tag{6}$$

where k represents the rate constant; ρ denotes the reaction constant (i.e., it is constant for the mechanism of interest); σ refers to the substituent parameter, which depends on the identity and position of the substituent on the benzene ring; and b stands for a constant that is determined by linear regression. Note that the Hammett equation only applies to compounds with a benzene ring. The reference reaction for the Hammett equation is acid dissociation of substituted benzoic acids in water at 25°C and 1 bar. Accordingly, electron-withdrawing substituents have a positive σ, and electron-donating substituents have a negative σ. There are many

different types of σ in the literature. The most common are σ_m (meta) and σ_p (para), which are obtained by correlating pK_a's of benzoic acids. Ortho is excluded because steric effects caused by electron repulsion between neighboring groups cannot be generalized for a broad range of reactions (Gould, 1959). Two specialized substituent parameters are σ^+ and σ^-, which account for conjugative interaction (resonance) between the substituent and a positively or negatively charged carbon atom, respectively. The Hammett equation successfully correlates equilibrium and rate constants for a wide variety of organic reactions (e.g., Jaffe, 1953). The power of the equation for deciphering mechanisms comes from ρ. The reaction constant indicates how sensitive rates of a reaction are to substituents, and the sign and magnitude of ρ generally reflect changes in charge in or near the benzene ring during the portion of the mechanism that controls kinetics.

Understandably, it is easiest to rationalize the sign of ρ – simple rules are $\rho > 0$ means that negative charge is building (or positive charge is diminishing), and $\rho < 0$ means that positive charge is building during the reaction (Anslyn & Dougherty, 2006). Using these rules, the sign of ρ for the candidate mechanisms (Figs. 19 and 20) can be predicted. A negative ρ is predicted for mechanisms where the benzene ring is protonated, while a positive ρ is predicted for mechanisms that produce the benzyl anion or a transition state with benzyl anion character. Because ρ is an empirical quantity, its magnitude is generally impossible to predict *ab initio*, especially for multi-step mechanisms with charged intermediates in polar solvents. Simple homolytic dissociation mechanisms such as A (Fig. 19) and F (Fig. 20) may be exceptions, as the thermochemistry of

radical reactions is not sensitive to solvent effects (Kanabus-Kaminska et al., 1989). In organic solvents near ambient temperature, ρ for reactions that generate the benzyl radical ranges from -1 to -2, and becomes less negative at higher temperatures (Bartlett & Ruchardt, 1960; Pearson & Martin, 1963). Thus, a small negative ρ seems appropriate for Mechanisms A and F, and it is suggested that a reasonable value is -1 at 300°C. The magnitude of ρ for mechanisms with ionic carbon intermediates in Figs. 19 and 20 is expected to be larger than this, as electrons from substituents will respond more strongly to the presence of electric charge in the molecule. Here, I assume that $|\rho| \geq 3$ for the ionic mechanisms (Table 6), but this could be an underestimate in some cases. This possibility will be revisited in Section 4.5.

Hammett plots are constructed to determine experimental values of ρ for decarboxylation of PAAs and Na-PAs in water at 300°C and 1034 bar. Because there are different σ scales, the recommended procedure is to make a plot for each scale, and see which scale gives the best linear plot. Hammett plots were made using substituent parameters from Hansch et al. (1991) and rate constants for decarboxylation from Table 5. I found that plots with the classic σ scale exhibit poorer correlations than do plots with the σ^+ or σ^- scales (not shown). This indicates that resonance effects are important in the mechanisms of decarboxylation of PAAs and Na-PAs. Specifically, logarithms of rate constants for decarboxylation of PAAs were found to correlate best with σ^+ (Fig. 21); while those of Na-PAs correlate best with σ^-, excluding the ortho-substituted salts (Fig. 22). Values of σ that were used to make the Hammett plots are given in Table 5.

Values of σ_p^+ were used for meta-substituted PAAs because protonation of the para or ortho carbons (Fig. 19) creates positive charge on the meta carbons, as illustrated by the resonance structures in the example below.
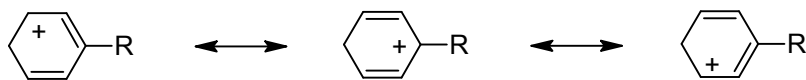
The reference reaction for the σ^+ scale is ionization of cumyl chlorides, which proceeds via the following carbocation intermediate.
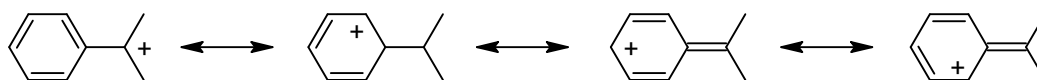
In this case, the para carbon bears positive charge, hence the designation σ_p^+. Irrespective of the naming convention, σ_p^+ should be used for substituents on ring carbons developing positive charge in resonance-dominated systems, as those carbon atoms can interact conjugatively with the substituent. An analogous argument applies to σ_p^-. For ring carbons that do not develop a formal charge, σ_m values should be used to account for the ability of the substituent to donate or withdraw electrons by polarizing covalent bonds (inductive effects).

Linear regression of the Hammett plots reveals that the ρ's for decarboxylation of PAAs and Na-PAs are ca. -3 and 3, respectively (Figs. 21 and 22). Fits to the data are reasonable considering the limited number of substituents

and the relatively narrow range in k_{decarb} here, although there are some outliers that will be commented on in Section 4.5. The opposite signs of the ρ values for PAAs and Na-PAs provide additional evidence that the two types of starting material decarboxylate by different mechanisms, as the systems respond kinetically to substituents in an opposite manner. The negative ρ shows that electron donation increases the rate of decarboxylation of PAAs, while the positive ρ indicates that electron withdrawal facilitates decarboxylation of Na-PAs (the similar magnitude of ρ for the two systems is probably coincidental). The predicted signs of ρ for Mechanisms B and G are opposite to the observations (Table 6). The observed magnitude of ρ is moderate for both PAAs and Na-PAs, contrary to the small ρ expected for Mechanisms A and F (Table 6). Therefore, Mechanisms A, B, F, and G are unfavorable models for the decarboxylation reactions. In contrast, the other mechanisms in Figs. 19 and 20 seem sufficiently consistent with the observed ρ values (Table 6). The medium negative value of ρ for PAAs suggests that protonation of a benzene ring occurs during decarboxylation of PAAs, and the medium positive value of ρ for Na-PAs suggests that the benzyl anion or a transition state with benzyl anion character forms during decarboxylation of Na-PAs.

To summarize, my interpretation is that Mechanisms C, D, and E pass the Hammett test for phenylacetic acid (Fig. 19), while A and B fail the test. For sodium phenylacetate (Fig. 20), Mechanisms H, I, and J pass the Hammett test, while F and G fail the test.

4.3. Analysis of HCl or NaOH effects

The next mechanistic test is the kinetic effect of adding aqueous acid to

PAA, or base to Na-PA. Adding a large amount of HCl or NaOH could cause a

significant effect if decarboxylation is acid- or base-catalyzed. The challenge is to

predict how the candidate mechanisms should respond kinetically to a high

concentration of strong acid or base. To address this, rate equations for the

mechanisms (Figs. 19 and 20) are written in Table 6. It can be seen that the rates

of decarboxylation for several mechanisms depend upon the concentration of H^+,

while those for others do not; thus the effect of pH may help in discriminating

between some of the mechanisms. The rate equations also show that the

speciation of the system is important. Adding 1 m HCl or NaOH to the system

will perturb the speciation, but thermochemical calculations must be performed to

determine the extent of perturbation. Thermochemical properties of aqueous

phenylacetate species at high temperatures and pressures have not been

characterized, but there are relevant data for aqueous acetate species (Shock &

Koretsky, 1993; Shock, 1995). The acetate system is probably a suitable proxy for

the phenylacetate system because the carboxyl group is most important for

equilibria between phenylacetate species. As an example, Na^+ can be expected to

interact with phenylacetate and acetate anions similarly because Na^+ will be most

attracted to the negatively charged carboxyl group, which is identical in both

anions. Of course, the systems are not indistinguishable as phenylacetic and acetic

acids have pK_a's differing by about half a unit at room temperature (Dippy &

Williams, 1934) (the benzene ring in PAA thus has a subtle influence).

Nevertheless, the systems are likely to speciate similarly.

Speciation calculations for 1 m acetic acid (HAc) and sodium acetate (Na-Ac) systems in water at high temperature and pressure are performed using the GEOCHEQ code (Zolotov et al., 2006; Mironenko et al., 2008). The code computes standard state Gibbs energies of formation of aqueous species in these systems using equation-of-state parameters from Shock & Koretsky (1993), Shock (1995), and Shock et al. (1997). Activity coefficients of ions are computed using the B-dot equation (Helgeson, 1969), which is applicable for ionic strengths up to 0.3-1 molal (Bethke, 2008). GEOCHEQ calculates thermodynamic equilibrium by minimizing the Gibbs energy of the system.

Results of speciation calculations are shown in Table 7, and are briefly summarized here. HAc completely dominates the speciation of acetate in HAc systems. Addition of 1 m HCl to the calculation causes the concentration of H^+ to increase dramatically, while that of Ac^- decreases. These changes make sense as HCl is a much stronger acid than HAc. The speciation of acetate in Na-Ac systems is more complex, with $Na(Ac)_2^-$, $Na(Ac)$, and Ac^- all having appreciable concentrations (Table 7). Addition of 1 m NaOH to the calculation shifts acetate speciation towards $Na(Ac)$ due to the extra Na, although the speciation responds rather insensitively. In contrast, the concentration of OH^- increases considerably, whereas those of HAc and H^+ decrease in response to the added NaOH. As expected, the calculations show that addition of 1 m HCl or NaOH leads to a large

104

increase in ionic strength (Table 7). High ionic strength in the case of NaAc +

NaOH implies that the computed speciation could have inaccuracies.

Estimates of the kinetic effect of adding HCl to PAA or NaOH to Na-PA

can be made by inputting the speciation data into the rate equations for the

different mechanisms. The estimates rely upon two assumptions: (1) the

speciation of phenylacetate systems is similar to that of acetate systems; and (2)

the rate constants in Table 6 do not depend on ionic strength. As discussed above,

the former assumption seems like a good approximation. Because most of the

candidate mechanisms involve charged structures, rate constants should generally

depend on ionic strength, contrary to the latter assumption. According to

transition state theory, rate constants are proportional to an activity coefficient

quotient (e.g., Lasaga, 1998)

$$k = \frac{\prod \gamma_r}{\gamma_\dagger} k_0 \,, \tag{7}$$

where k designates the rate constant in a solution of arbitrary ionic strength, $\prod \gamma_r$

denotes the product of the activity coefficients of the reactants in the elementary

step of interest, $\gamma_\dagger$ represents the activity coefficient of the transition state, and k_0

corresponds to the rate constant at zero ionic strength. It is impossible to evaluate

Eq. (7) without knowing the structure of the transition state. Nevertheless, the

activity coefficient quotient may not differ much from unity in the present

experimental systems, as GEOCHEQ results indicate that the activity coefficients

of monovalent ions in the HCl and NaOH systems have values around 0.5. If organic ions in the mechanisms being evaluated exhibit somewhat similar non-ideal behavior, consideration of the mechanisms in light of this discussion (i.e., Eq. 7) suggests that neglect of ionic strength could lead to rate constant estimates that are incorrect by perhaps a factor of 2-4.

Predicted HCl and NaOH effects for the candidate mechanisms are shown in Table 6. The experimental effects are generally small, as 1 m HCl increases the rate of decarboxylation of PAA by ca. 60%, and 1 m NaOH may have a slight negative effect on the rate of decarboxylation of Na-PA (Table 6). Thus, decarboxylation in these systems is neither acid- nor base-catalyzed, as equilibrium calculations indicate that adding 1 m HCl to PAA should increase the concentration of H^+ by more than two orders-of-magnitude, and adding 1 m NaOH to Na-PA should increase the concentration of OH^- by a similarly large factor (Table 7). Immediately, it can be seen that Mechanisms B, C, and G are inconsistent with the observed HCl or NaOH effects, so much so that modest uncertainties in the predicted effects are of no consequence to the interpretation. Mechanism A also appears to be unfavorable as it predicts no HCl effect, at odds with the small rate enhancement that was observed experimentally. It seems unlikely that account of ionic strength would lead to a revised effect for Mechanism A that is large enough to be consistent with observation. This is because the rate-limiting bond fission in A only involves neutral species (Fig. 19), and activity coefficients of neutrals do not appear to have the required sensitivity to ionic strength (Barrett et al., 1988).

106

Mechanisms D and E (Fig. 19) are interesting cases. Both mechanisms feature protonation of the benzene ring, so acid catalysis might be expected. Indeed, the concentration of H^+ appears in the rate equations (Table 6). However, these mechanisms are not acid-catalyzed because the carboxylate anion is protonated. This paradoxical behavior can be rationalized by rewriting the rate equation for Mechanism D as an example

$$\text{rate} = \frac{k_{D1}k_{D2}\left[H^+\right]\left[PA^-\right]}{k_{-D1}+k_{D2}} = \frac{\gamma_{PAA}}{\gamma_{PA^-}\gamma_{H^+}}\frac{k_{D1}k_{D2}K_a\left[PAA\right]}{k_{-D1}+k_{D2}}. \tag{8}$$

Notice that the dependence on H^+ concentration vanishes. Changes in the concentrations of H^+ and PA^- tend to cancel, making the product of the two concentrations largely independent of added HCl. HCl addition can weakly affect the rate of decarboxylation of PAA by altering the activity coefficient quotient on the right-hand side of Eq. (8), as a result of increased ionic strength from ionization of HCl. This causes the HCl effect for Mechanisms D and E in Table 6. While the predicted effects for D and E do not match the observation completely (Table 6), the discrepancy is small enough that it can be reasonably attributed to inadequacies in the two assumptions that were used to make the predictions, rather than deficiencies in the mechanisms themselves. Perhaps the most important result is that the predicted HCl effects for these mechanisms are modest, and they are in the same direction as the experimental effect. Thus, it seems likely that Mechanisms D and E pass the HCl test.

107

The NaOH test is not very helpful in discriminating between Mechanisms F, H, I, and J (Fig. 20). All of these mechanisms predict small kinetic effects, and experimentally I found that adding 1 m NaOH to Na-PA may cause a small reduction in the rate constant (Table 6). All of the predicted effects are minor because addition of 1 m NaOH should not change the speciation of phenylacetate significantly (Table 7). Mechanism H appears to be less consistent with observation than are the others, as this mechanism predicts an effect that is in the wrong direction (Table 6). However, care must be taken in dismissing Mechanism H given that there is ambiguity here. Experimentally, there may not even be an NaOH effect when uncertainties are considered (Table 6). In addition, the NaOH speciation calculation in Table 7 may have questionable accuracy because it yields a fairly high ionic strength that may be beyond the capability of the B-dot equation. High ionic strength could also cause slight changes in rate constants (Eq. 7), which may be significant because the observed NaOH effect is so small.

Previous studies of decarboxylation suggest that I am on the right track in disfavoring Mechanism H. Pedersen (1949) found that aqueous nitroacetic acid decarboxylates more slowly in the presence of metal ions, which was attributed to the formation of unreactive metal-nitroacetate complexes. Kemp & Paul (1975) also proposed that ion pairing decreases the rate of decarboxylation of a benzisoxazole-3-carboxylate in polar aprotic solvents. Hunter et al. (1978) found that a crown ether facilitates decarboxylation of various sodium carboxylates in tetrahydrofuran, suggesting that decarboxylation is catalyzed by removal of Na^+ from the ion pair. Results from these studies imply that the free carboxylate

undergoes decarboxylation. Thus, evidence from the literature provides an argument against the viability of Mechanism H.

To summarize, my interpretation is that Mechanisms D and E pass the HCl test for phenylacetic acid (Fig. 19), while A (probably), B, and C fail the test. For sodium phenylacetate (Fig. 20), Mechanisms F, I, and J pass the NaOH test, while G and H (probably) fail the test.

4.4. Analysis of effects from deuterated water

The final mechanistic test is the effect of substituting D_2O for H_2O on the rate of decarboxylation of PAA or Na-PA. This is referred to as the solvent kinetic isotope effect (SKIE), which can be useful for constraining mechanisms of organic reactions (e.g., Laughton & Robertson, 1969; Willi, 1977). Several of the mechanisms in Figs. 19 and 20 feature protonation or deprotonation steps, so these mechanisms could lead to a hydrogen isotopic effect because bonds to hydrogen atoms are changing. Acid-base chemistry in D_2O is noticeably different from that in H_2O, even at high temperatures (e.g., Mesmer & Herting, 1978). In general, all acids are stronger (dissociate more) in H_2O than in D_2O because H_3O^+ (in H_2O) is a weaker acid than D_3O^+ (in D_2O) (Swain & Bader, 1960). Because of this, the reverse reaction, protonation of a species by lyonium ion (i.e., H_3O^+ or D_3O^+), is more thermodynamically favorable in D_2O than in H_2O. For the most part, replacing H_2O with D_2O should affect rates of decarboxylation by (1) shifting acid-base equilibria; or (2) increasing the activation energy for rate-

109

limiting proton transfer (primary kinetic isotope effect). Primary kinetic isotope effects are caused by a difference in zero-point energy between bonds to H and bonds to D, and generally give slower rates with deuterium (Anslyn & Dougherty, 2006). A bond to D can be regarded as stronger than the same bond to H. The magnitude of the isotope effect will depend on the extent of hydrogen transfer in the transition state. Here, I do not quantify secondary kinetic isotope effects, which are caused by isotopic substitution at a bond that is not broken during the rate-limiting step. However, typical secondary effects are small (10-20%; Anslyn & Dougherty, 2006), and they should decrease with temperature. Differences in solvation between H_2O and D_2O are also likely to be minor especially at higher temperatures, as evidenced by very similar solubilities of salts in H_2O and D_2O (e.g., Eddy & Menzies, 1940).

Before SKIE's for the PAA mechanisms (Fig. 19) can be estimated, I must determine how replacing H_2O with D_2O will affect the speciation of PAA. This can be done by adopting acetic acid as a model for phenylacetic acid. Erickson et al. (2011) determined the dissociation constant of acetic acid in H_2O and D_2O, and found that the dissociation constant ratio $K_a^{D_2O} / K_a^{H_2O}$ has a value of 0.37 between 150 and 275°C. I use this ratio to perform a textbook equilibrium calculation (e.g., Kotz & Treichel, 1999)

$$\frac{\left[D^+\right]}{\left[H^+\right]} = \frac{\left[PA^-\right]_{D_2O}}{\left[PA^-\right]_{H_2O}} = \left(\frac{\left[PAA\right]_{D_2O}}{\left[PAA\right]_{H_2O}} \frac{K_a^{D_2O}}{K_a^{H_2O}}\right)^{1/2} = \left(\frac{0.92}{1.04} \times 0.37\right)^{1/2} = 0.57, \qquad (9)$$

where brackets indicate molal concentration. The H_2O and D_2O experiments in Table 2 had nearly identical molarities, but their molalities differ by ca. 10% as indicated in Eq. (9). The slight difference in molalities should not affect the interpretation of the experimental results, as the determination of rate constants for reactions that follow first-order kinetics does not depend on the initial concentration of the reactant. Equation (9) rests on the assumptions that PAA undergoes minimal dissociation, the concentration of OH^-/OD^- is negligible, and the activity coefficients of the species in the acid dissociation equilibrium are similar in H_2O and D_2O; all are very reasonable assumptions (e.g., Table 7). Equation (9) shows that the concentrations of lyonium ion and PA$^-$ should decrease by ca. 43% going from H_2O to D_2O. Because only a minuscule fraction of PAA molecules dissociate in both solvents, the relative concentration of PAA is insensitive to replacement of H_2O with D_2O. These estimates do not depend on the pK_a of PAA being identical to that of acetic acid; instead, they rely upon the more robust assumption that the ratio $K_a^{D_2O} / K_a^{H_2O}$ of PAA is similar to that of acetic acid.

SKIE's for Mechanisms A, B, and E can be predicted by inputting the result from Eq. (9) into the appropriate rate equation in Table 6. Notice that the estimate of k_{D_2O} / k_{H_2O} for Mechanism E is less than 0.3. This value is an upper limit because the rate-limiting step in Mechanism E involves proton transfer, which will be subject to a primary kinetic isotope effect of unknown magnitude. Estimation of SKIE's for Mechanisms C and D is more difficult because of the complex form of the rate equations. The preferred strategy is to make estimates

111

for endmember kinetic scenarios. As an example, below are written the two endmember forms of the rate equation for Mechanism D

$$\text{rate} = k_{\text{D1}}\left[H^+\right]f_{PA^-}\left[\sum PA\right] \text{ or } K_{\text{D1}}k_{D2}\left[H^+\right]f_{PA^-}\left[\sum PA\right]. \tag{10}$$

In the first case (left side), protonation of the benzene ring is rate-limiting, while the second case (right side) features an equilibrium between the zwitterion, phenylacetate anion, and H^+ (Fig. 19), characterized by equilibrium constant K_{D1}. Setting an upper limit on the SKIE for the first case is straightforward as this case is kinetically equivalent to Mechanism E. The second case is trickier because estimation of its SKIE requires knowledge of the isotope effects on K_{D1} and k_{D2}. Step D2 does not involve breaking or forming bonds to hydrogen (Fig. 19), so k_{D2} can only have a small secondary kinetic isotope effect. This effect is commonly neglected in mechanistic investigations (e.g., Willi, 1977). The SKIE on K_{D1} can be estimated by considering changes in bonds to H within the framework of fractionation factor theory (Anslyn & Dougherty, 2006). Consider equilibrium D1 below.
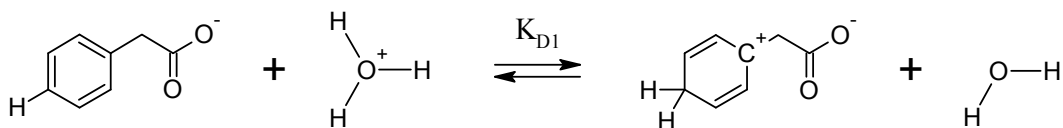
In the reactants, there is one sp^2 C-H bond and three O-H bonds in hydronium (H_3O^+ rather than H^+ must be considered to account for bonding changes). In the products, there are two sp^3 C-H bonds and two O-H bonds in water. Other C-H bonds do not change as much in terms of their chemical nature, so they approximately cancel out. According to fractionation factor theory

$$\frac{K_{D1}^{D_2O}}{K_{D1}^{H_2O}} = \frac{\prod \varphi (\text{product bonds to H})}{\prod \varphi (\text{reactant bonds to H})} = \frac{(0.9)^2 (1)^2}{(0.8)^1 (0.7)^3} \approx 3,$$ (11)

where the fractionation factors (φ) were taken from Schowen (1972). This is an idealized calculation, but the result is reasonable as many protonation equilibria have K^{D_2O} / K^{H_2O} between 2 and 3 (Laughton & Robertson, 1969). The above estimate corresponds to ambient temperature, but can be corrected to high temperature. Erickson et al. (2011) found that K^{D_2O} / K^{H_2O} for protonation of acetate anion at 275°C is ca. 15% less than that at 25°C. Assuming that the isotopic fractionation for equilibrium D1 scales similarly with temperature, a reasonable value for the SKIE on K_{D1} is 2.5 at 300°C. Using this value together with the result from Eq. (9), an estimate for the SKIE on the rate constant of decarboxylation of PAA for the pre-equilibrium endmember of Mechanism D can be made (Table 6). The isotope effect for the pre-equilibrium endmember of Mechanism C is predicted using the same procedure.

Experimentally, it was found that decarboxylation of PAA is ca. 30% slower in D_2O than in H_2O (Table 6). Hence, the SKIE is not large. This argues

113

against several kinetic scenarios. Both endmember scenarios of Mechanism C are inconsistent with the experimental SKIE (Table 6). The upper limit for the rate-limiting protonation scenario of Mechanism C should not be regarded as being compatible with observation, despite barely overlapping values of k_{D_2O} / k_{H_2O}. The upper limit is very conservative, and does not specify a primary kinetic isotope effect on rate constant k_{C1}. Consideration of studies of general acid-catalyzed protonation of unsaturated carbon-carbon bonds (Kresge & Chiang, 1967; Schubert & Keeffe, 1972; Willi, 1977) suggests that $k_{C1}(D_2O/H_2O)$ may be ca. 0.5. Hence, the upper limit is probably too large by about a factor of 2. This argument also applies to rate-limiting protonation scenarios in Mechanisms D and E, making them even less consistent with experiment. Conversely, Mechanism A seems unfavorable as it does not predict a large enough SKIE (Table 6), although there is neglect of a presumably small secondary effect from rehybridization of the benzyl carbon from sp^3 to sp^2. Note that while both endmember scenarios of Mechanism C are inconsistent with the observed SKIE, Mechanism C cannot be ruled out on the basis of the SKIE because there are kinetic scenarios between the endmembers that are consistent with the observed SKIE (Table 6). However, Mechanism C is already undesirable as it failed the HCl test (see Section 4.3).

Predicted SKIE's for Mechanism B and the pre-equilibrium endmember of Mechanism D are sufficiently consistent with the observed SKIE that these mechanisms may be regarded as acceptable on the basis of the solvent kinetic isotope test (Table 6). Of course, the predictions do not match the experimental value exactly, but they are close enough that slight discrepancies can be

114

reasonably attributed to uncertainties in the method of predicting SKIE's.

Mechanism B is not worth discussing further since it is clearly at odds with the

Hammett and HCl tests (Table 6). In contrast, it is informative to subject

Mechanism D to another D_2O test. If PAA decarboxylates via the pre-equilibrium

endmember of Mechanism D, deuterium should be incorporated into the benzene

ring of PAA. This is because the pre-equilibrium scenario implies that the

zwitterion of PAA reverts to PA⁻ faster than it decarboxylates to isotoluene and

CO_2 ($k_{-D1} \gg k_{D2}$; Fig. 19). This means that the benzene ring in the unreacted

starting material should be deuterated as shown in the following example.
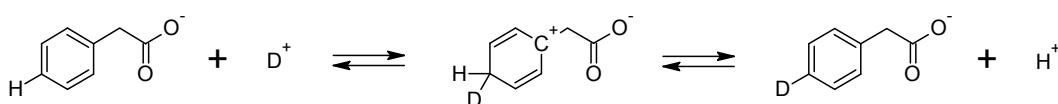
To test this, GC-MS analysis was performed on samples from the D_2O

experiments. I found that the benzene ring of PAA is indeed deuterated,

qualitatively consistent with the above prediction. Figure 23 shows the

quantitative data. Here, the focus is on the mass/charge (m/z) ratio of the benzyl

group of PAA rather than that of the molecular ion of PAA. The reason for this is

that the carboxyl group can readily exchange hydrogen with aqueous acid during

sample extraction, altering the molecular mass of PAA. Hydrogen atoms in the

benzyl group of PAA do not exchange with water during sample extraction as

they are not acidic enough.

I wish to call attention to five features in Fig. 23. First, the most abundant m/z at $t = 0$ is 93. This implies that the two hydrogens in the benzyl position of PAA exchange rapidly with the solvent during the heating phase of the experiments (the dominant m/z of the benzyl group in the starting material is 91). It is tempting to assume that interconversion between PAA and its enol leads to exchange of the two benzyllic hydrogens, but the GC-MS data do not reveal which hydrogens in the benzyl group were exchanged. Second, the presence of benzyl groups with m/z $\geq$ 94 proves that the benzene ring in PAA was deuterated, as deuteration of the ring is the only way to obtain m/z $\geq$ 94 in the present experimental system. Third, the entire benzene ring in some PAA molecules was deuterated (m/z = 98) at the longest durations, showing that the deuteration reaction is not highly selective to position on the ring. Fourth, the nearly identical isotopic compositions of the benzyl group at 50 and 72 h suggests that an equilibrium was reached, or that there is a kinetic impediment that prevents all molecules of PAA from being completely deuterated. Fifth, deuteration of the benzene ring of PAA does not appear to be markedly faster than decarboxylation of PAA, as both reactions take place over similar timescales (tens of hours). This finding seems significant for the mechanism of decarboxylation. If deuteration occurs via a conventional electrophilic aromatic substitution mechanism as illustrated above, it may be concluded that k_{-D1} (leading to deuteration) is not much larger than k_{D2} (leading to decarboxylation). This would mean that the pre-equilibrium endmember of Mechanism D ($k_{-D1} \gg k_{D2}$) does not correctly describe the kinetics of decarboxylation.

Together, the D_2O tests appear to give conflicting information regarding the viability of Mechanism D. On the one hand, the predicted SKIE for the pre-equilibrium endmember of the mechanism is consistent with the experimental effect. On the other hand, the rate of deuteration of PAA seems too slow (relative to decarboxylation) to be consistent with the pre-equilibrium. A plausible resolution to this apparent paradox is that Mechanism D exhibits complex kinetics, and the rate equation in Table 6 cannot be simplified to an endmember. In this model, the SKIE would lie between the two endmembers, and I must postulate that the kinetics of the mechanism is more similar to that of the pre-equilibrium endmember than to that of the rate-limiting protonation endmember, to account for the observed SKIE (Table 6). This may not be unreasonable as the D_2O experiments suggest that the rate of deuteration is ca. 4 times faster than the rate of decarboxylation.

Yet, there could be complications in making mechanistic deductions based on relative rates of deuteration and decarboxylation. One is that deuteration could be an Au-catalyzed reaction instead of an electrophilic aromatic substitution. This would make the pre-equilibrium case an even less viable possibility because k_{-D1} could be zero. Consequently, Mechanism D would simplify to the rate-limiting protonation endmember, and would no longer be consistent with the observed SKIE (Table 6). While Au catalysis of deuteration was not ruled out experimentally, this seems like a remote possibility because the sign and magnitude of ρ for decarboxylation of PAAs (Fig. 21) suggests that ring protonation occurs, arguing in favor of electrophilic aromatic substitution.

117

Another possibility is that both PAA and PA⁻ undergo deuteration and/or decarboxylation, which would mean that the relative rates of deuteration and decarboxylation cannot be equated to relative values of k_{-D1} and k_{D2}. I am ambivalent about this. On the one hand, thermochemical calculations show that the carboxylic acid should be more abundant than the carboxylate anion (Table 7). On the other hand, ring protonation of the anion should be faster than that of the acid, as σ_p^+ of the anion is -0.53 and that of the acid is -0.01 (Hansch et al., 1991). It is unclear how these opposing effects would combine in the present experiments. Overall, I think that Mechanism D with $k_{-D1} \approx k_{D2}$ seems reasonably consistent with all of the D_2O data, but this interpretation should be viewed with caution owing to a possible ambiguous relationship between relative rates of deuteration and decarboxylation.

Similar to the NaOH test, the D_2O kinetic isotope test does not provide clear discrimination between the candidate mechanisms for decarboxylation of Na-PA (Fig. 20). Small SKIE's are expected for Mechanisms F, H, and I because dissociation of the Na(PA) ion pair should not be sensitive to substitution of D_2O for H_2O, as evidenced by solubilities of salts in H_2O and D_2O that differ by less than 10% at high temperatures (Eddy & Menzies, 1940). Unlike for PAA in D_2O, the speciation of Na-PA in D_2O cannot be calculated as this system is characterized by more than one governing equilibrium (e.g., Table 7), and the necessary equilibrium constants are generally unavailable in D_2O at the experimental conditions of interest.

Two mechanisms that could have larger isotope effects are G and J. The decarboxylation rate for Mechanism G depends on the concentration of lyonium ion (Table 6), which will differ in H_2O and D_2O due to differing dissociation constants of the solvents (Mesmer & Herting, 1978). Like Mechanisms C and D, G has endmember kinetic regimes of rate-limiting protonation and pre-equilibrium, which further complicate prediction of the SKIE. However, further consideration of Mechanism G is not needed because it is already clear that G cannot be the correct mechanism for decarboxylation of Na-PA, as evidenced by the severe failure of G in both the Hammett and NaOH tests (see Sections 4.2 and 4.3, respectively).

Mechanism J will be subject to a primary kinetic isotope effect because an O-H bond is broken during the rate-limiting step (Fig. 20). An O-D bond will be broken more slowly. Therefore, Mechanism J should be slower in D_2O than in H_2O. It is difficult to predict the magnitude of the SKIE, however, because the extent of breaking of the O-H bond in the transition state is not known. If the bond is only slightly broken in the transition state, the SKIE would be small. A transition state with a lot of bond-breaking would also result in a small effect. The maximal SKIE would be produced if the bond is about halfway broken in the transition state (Schowen, 1972). A constraint on Mechanism J can be obtained by estimating the maximum isotope effect, corresponding to the difference in zero-point energy (ΔZPE) between O-H and O-D bonds in water. ΔZPE can be calculated using the quantum harmonic oscillator model (e.g., Atkins, 1998)

119

$$\Delta ZPE = 50hc\left(\tilde{v}_{OH} - \tilde{v}_{OD}\right), \tag{12}$$

where h stands for Planck's constant (6.626×10^{-34} J s; CODATA, 2010), c represents the speed of light (2.998×10^{8} m s^{-1}; CODATA, 2010), and $\tilde{v}$ signifies the wavenumber of the bond stretching vibration in cm^{-1}. The SKIE scales exponentially with ΔZPE as (Arrhenius dependence)

$$\left(\frac{k_{D_2O}}{k_{H_2O}}\right) = \exp\left(\frac{-\Delta ZPE}{k_B T}\right), \tag{13}$$

where k_B represents Boltzmann's constant (1.381×10^{-23} J K^{-1}; CODATA, 2010), and T refers to temperature in K. The symmetric O-H stretch in H_2O occurs at 3490 cm^{-1}, and the wavenumber of the symmetric O-D stretch in D_2O is 2540 cm^{-1} (Stuart, 2004). Using Eqs. (12) and (13), I calculate a maximum (i.e., greatest deviation from unity) isotope effect k_{D_2O} / k_{H_2O} of 0.3.

The observed SKIE for Na-PA appears to be small or possibly non-existent (Table 6). Thus, Mechanisms F, H, and I seem consistent enough with experiment. Mechanism J (Fig. 20) can be consistent with experiment if there is slight or substantial proton transfer from water to the benzyl carbon in the transition state. An intermediate amount of transfer would lead to a k_{D_2O} / k_{H_2O} that deviates too much from unity. Of the two options, the second seems less likely as a large amount of proton transfer would contribute more positive charge

to the benzyl carbon, which would probably lead to a ρ for decarboxylation of Na-PAs that is less positive than observed (Fig. 22). The extent of breaking of the O-H or O-D bond in the transition state of Mechanism J can be roughly estimated by constructing a simple model (Schowen, 1972). Here, x designates fractional extent of proton transfer. Isotope effect k_{D_2O}/k_{H_2O} starts at unity, and is assumed to vary linearly with x, reaching its limiting value of 0.3 at $x = 0.5$. Thus, $k_{D_2O}/k_{H_2O} = 1 - 1.4x$ for $0 \leq x \leq 0.5$. Combining this model with the experimental SKIE yields $x = 0.14 \pm 0.11$. This illustrative calculation reinforces the point that if decarboxylation of Na-PA occurs by Mechanism J, the benzyl carbon cannot be more than slightly protonated in the transition state.

While Mechanism J cannot be ruled out experimentally, Mechanism I (Fig. 20) appears to be a more attractive option (e.g., Segura et al., 1985). The issue of sequential versus concerted mechanisms is contentious as there is no sharp boundary between the two classifications (Jencks, 1981). Theoretically, a concerted mechanism would be preferred if the intermediate of the corresponding sequential mechanism cannot exist under the reaction conditions (Cox, 2011). The concerted mechanism allows the reaction to avoid forming the high-energy intermediate, leading to a lower activation energy (although presumably there is an entropic price to pay). In the case of decarboxylation, a concerted mechanism would be preferred if the carbanion intermediate were too unstable.

How unstable is too unstable? To help answer this question, I consider the study of Thibblin & Jencks (1979). These workers found that retroaldolization of 1-phenylcyclopropanol anion in water at 25°C is subject to general acid catalysis

with a Bronsted α of 0.25. This α indicates that there is some proton transfer in the transition state, consistent with a concerted mechanism (Thibblin & Jencks, 1979). This makes sense because the alternative sequential mechanism would produce a highly unstable primary carbanion, whose conjugate acid has a pK_a of ca. 50 (e.g., Jorgensen et al., 1987). Even in this extreme case, though, the extent of proton transfer in the transition state is only about 25% (Anslyn & Dougherty, 2006). The benzyl anion is a much more stable carbanion (pK_a of toluene, ca. 40; Streitwieser & Ni, 1985), so its formation probably does not need to be avoided by a concerted mechanism. Qualitatively, Mechanism I seems sufficient, and J seems unnecessarily complex. Indeed, Thibblin & Jencks (1979) also studied retroaldolization of trans-1,2-diphenylcyclopropanol anion, and observed weak general acid catalysis with a Bronsted α of less than 0.1. This α seems too small for a concerted mechanism, and it is likely that a hydrogen-bonded benzyllic anion is the reaction intermediate (Thibblin & Jencks, 1979).

To summarize, my interpretation is that Mechanisms B, C, and D probably pass the D_2O test for phenylacetic acid (Fig. 19), while A (probably) and E fail the test. For sodium phenylacetate (Fig. 20), Mechanisms F, H, and I probably pass the D_2O test, while J probably fails the test. Mechanism G was not tested because it is difficult to estimate the isotope effect for this mechanism, and the D_2O test is unnecessary in this case.

4.5. Verdict on decarboxylation mechanisms

Based on physical organic chemical analyses of the candidate mechanisms in the above sections, I propose that phenylacetic acids decarboxylate by Mechanism D (Fig. 19), and sodium phenylacetates decarboxylate by Mechanism I (Fig. 20), in water at 300°C and 1034 bar. These mechanisms are completely different, thus speciation dictates mechanism in the studied systems. Other mechanisms that were considered (Figs. 19 and 20) are rejected owing to inconsistencies with experimental data (Table 6) and relevant information from the literature. Here, I address several details pertaining to the proposed mechanisms and related topics.

First, what if decarboxylation occurs by a mechanism that was not considered? This is possible and deserves further attention. However, new candidates will need to be consistent with all of the mechanistic tests in Table 6 to contend with Mechanisms D and I. Thus, they may only differ in details from the proposed mechanisms. One possible variant is that a carbonic acid or carbonate species rather than CO_2 is the leaving group of decarboxylation (Mundle et al., 2010). However, an argument against carbonic acid is that CO_2 and H_2O are more thermodynamically stable than carbonic acid in aqueous solution (Adamczyk et al., 2009), and they should be even more stable at higher temperatures, where dehydration becomes more favorable (Shock, 1993). Another possibility is that Na^+ catalyzes decarboxylation of PA^- by electrostatically stabilizing negatively charged carbon in the transition state of the reaction. However, elevated concentrations of Na^+ in Na-PA + NaOH experiments (Table 7) did not give faster rates of decarboxylation (Table 5). Thus, this possibility seems unlikely

123

unless the electrostatic interaction is very weak, or Na$^+$ also causes a rate-retarding effect of approximately equal magnitude.

A more promising possibility is that internal return is an important detail that is currently missing from Mechanism I (Fig. 20), where the benzyl anion and CO_2 recombine to regenerate phenylacetate anion (e.g., Kluger & Mundle, 2010). In this model, the primary product of decarboxylation is a geminate pair consisting of the benzyl anion and CO_2 that is surrounded by water molecules. Because the benzyl anion and CO_2 are both confined to a solvent cage immediately after carbon-carbon bond heterolysis, they may recombine to regenerate phenylacetate anion. Internal return would be important if recombination is faster than in-cage protonation of the benzyl anion by water, and diffusional separation of the geminate pair into bulk solution. The occurrence of internal return could provide a quantitative explanation for the solvent kinetic isotope effect for decarboxylation of sodium phenylacetate. If it is assumed that the rates of in-cage protonation and diffusional separation are limited by the dynamical behavior of water molecules, the rates of these processes can be approximated by the dielectric relaxation rate of water (Richard et al., 2001). Significantly, the dielectric relaxation (reorganization) rate of D_2O is 80% of that of H_2O over nearly the whole liquid range (Okada et al., 1999), which is intriguingly close to the experimental SKIE (Table 6).

However, the protonation rate could be slower than the rate of solvent reorganization. Bockrath & Dorfman (1974) determined a rate constant of 5.3×10^7 M^{-1} s^{-1} for protonation of the benzyl anion by water in tetrahydrofuran at 24°C,

which is much smaller than the rate constant for a diffusion-controlled reaction (ca. 10^{10} M^{-1} s^{-1}; Atkins, 1998). This shows that the protonation rate is controlled by chemical factors rather than molecular dynamics at ambient temperature. Nevertheless, protonation of the benzyl anion by water could be limited by solvent reorganization at sufficiently high temperatures, if the protonation rate increases with temperature more rapidly than does the rate of solvent reorganization. This seems possible as the dielectric relaxation rate of water is a not a strong function of temperature (Okada et al., 1997).

Second, assuming that the proposed mechanisms are correct, could there be multiple mechanisms occurring simultaneously? This is possible but mystery mechanisms would most likely need to be minor. Otherwise, the Hammett plots in Figs. 21 and 22 would probably not exhibit linear behavior. Substituents would affect the kinetics of competing mechanisms differently, and curvature would be observed in the plots (Johnson, 1973) if an unknown mechanism were a major contributor to the rate of decarboxylation. Therefore, I do not expect, say, Mechanism B to be competitive with D in PAA systems (Fig. 19), or Mechanism G to be competitive with I in Na-PA systems (Fig. 20). Why does Mechanism D operate in PAA systems, but the nearly identical Mechanism G not operate in Na-PA systems? An analogous question can be asked about the relationship between Mechanisms B and I. These questions underscore the importance of composition in controlling the mechanisms. The rate of Mechanism G is proportional to the concentration of H^+ (Table 6), and the concentration of H^+ should be very low in Na-PA systems (Table 7). Thus, Mechanism G cannot compete with I. Similarly,

125

Mechanism B is uncompetitive in PAA systems presumably because the rate of this mechanism is proportional to the concentration of PA⁻ (Table 6), and only a small fraction of PAA molecules will dissociate to PA⁻ (Table 7).

Third, how do literature values of ρ for reactions that generate a protonated benzene ring or a benzyl anion compare to the values derived in this study? In general, the ρ for decarboxylation of PAAs (ca. -3; Fig. 21) is less negative than those for classic electrophilic aromatic substitution reactions. Hydrogen isotope exchange in H_2O-H_2SO_4 at 100°C has a ρ of -7.5 (Clementi & Katritzky, 1973). Decarboxylation of 4-substituted salicyclic acids in water at 50°C has a ρ of -4.4 (Willi, 1959). Nitration in nitromethane or acetic anhydride at ambient temperature has a ρ of ca. -6, and chlorination and bromination in acetic acid at 25°C have even more negative ρ's of ca. -8 and -12, respectively (Brown & Okamoto, 1958). Caution must be exercised in comparing the ρ values because the magnitude of ρ depends on the solvent and temperature (Jaffe, 1953).

At first glance, the ρ for decarboxylation of PAAs does not seem negative enough for a reaction that has an intermediate with a protonated benzene ring. I do not think that this is an inconsistency, however, because Mechanism D (Fig. 19) exhibits different kinetics from common electrophilic aromatic substitution reactions, where the reaction rate is generally determined by generation of the electrophile or electrophilic attack on the aromatic system (Anslyn & Dougherty, 2006). In Mechanism D, the reaction rate is determined by competitive rates of steps D1, -D1, and D2 (Table 6). Step D1 will have a large, negative ρ because the benzene ring is protonated, consistent with conventional wisdom. However,

126

steps -D1 and D2 should have positive ρ's because positive charge is removed from the benzene ring in these steps. The observed ρ will reflect all of these contributions (Johnson, 1973), so positive ρ's for steps -D1 and D2 may partially cancel the large negative ρ for step D1, yielding a moderately negative observed ρ. Presumably, decarboxylation of PAAs exhibits different kinetics from typical electrophilic aromatic substitution reactions because electrophilic substitution takes place on the benzyl carbon rather than on one of the ring carbons.

The ρ for decarboxylation of Na-PAs (ca. 3; Fig. 22) agrees well with literature values derived from rates of reactions that proceed via the benzyl anion. Streitwieser & Koch (1964) reported a ρ of 4.0 for cyclohexylamide-catalyzed hydrogen exchange of toluenes in cyclohexylamine at 50°C. Retroaldolization of 1-phenyl-2-arylcyclopropanol anions in H_2O-CH_3CN at 25°C has a ρ of 4-5 (Thibblin & Jencks, 1979). Straub & Bender (1972) studied decarboxylation of α-cyanophenylacetate anions in water at 60.4°C, and determined a ρ of 2.44. Agreement between this value and the ρ for decarboxylation of Na-PAs may be unsurprising given the structural similarities between phenylacetate and α-cyanophenylacetate anions, but the corresponding benzyl anions will have dramatically different stabilities as the cyano group stabilizes carbanions enormously (e.g., Richard et al., 1999). Indeed, stabilization of a benzyl anion-like transition state by the α-cyano substituent allows decarboxylation of α-cyanophenylacetate anions to occur at a relatively low temperature. The similarity in ρ values suggests that the distribution of negative charge in the transition state is not sensitive to α substitution. Note that Hammett analysis of the pK_a's of

127

toluenes in acetonitrile at ambient temperature gave an anomalously large ρ of 12.0 (Sim et al., 1990), but this value reflects substituent effects on the benzyl anion (i.e., thermodynamics), whereas the other values reflect substituent effects on transition states with benzyl anion character (i.e., kinetics). Presumably, kinetic ρ values are less positive because substituents are exposed to less negative charge in the transition states.

Fourth, why does para substitution give anomalously slow rates for PAAs (Fig. 21), and ortho substitution give anomalously fast rates for Na-PAs (Fig. 22). The first question is difficult to answer, as Mechanism D (Fig. 19) does not appear to provide an obvious explanation for the para effect. p-Me-PAA decarboxylates ca. 2.2 times slower than predicted by the Hammett plot, and p-F-PAA decarboxylates ca. 1.4 times slower than predicted. Thus, the effect is not large and does not appear to have an electronic origin because p-Me is electron-donating and p-F is electron-withdrawing in this reaction, yet the substituents cause similar kinetic effects. The small size of the para effect suggests that the effect reflects a subtle mechanistic feature. Perhaps the effect is caused by kinetic differences between para and ortho protonation of phenylacetate anion in Mechanism D (Fig. 19). Partitioning of para versus ortho protonation may depend on substitution. Alternatively, para substitution could affect solvation of the reactant and transition state differently (e.g., Arnett, 1985). However, why should differential solvation be restricted to para substituents? Another possibility is that tautomerization of isotoluenes to toluene proceeds via the benzyl anion, which is destabilized by both p-Me and p-F substituents. The tautomerization step can

affect the reaction rate only if the decarboxylation step in Mechanism D is reversible (internal return). It is unclear whether internal return can compete with tautomerization of isotoluene and diffusional separation of isotoluene and CO_2, because isotoluene may not have sufficient nucleophilicity to react with CO_2 fast enough since isotoluene is not negatively charged.

It is understandable that ortho substitution gives anomalously fast rates of decarboxylation for Na-PAs. Ortho effects are observed in many organic reactions, and they represent a combination of inductive, resonance, and steric effects (e.g., Gould, 1959; Segura, 1985). Ortho substituents are generally excluded from Hammett plots because ortho effects are reaction-dependent (Johnson, 1973). While it is presently not possible to account for the ortho effects on decarboxylation of Na-PAs in a quantitative sense, reasonable explanations that are consistent with Mechanism I (Fig. 20) can be put forth. Na-o-Me-PA decarboxylates slightly faster than Na-PA (Table 5), but the Hammett plot in Fig. 22 implies that Na-o-Me-PA should decarboxylate slower than the parent. o-Me is expected to cause inductive and resonance effects that impede decarboxylation, as electron donation by o-Me will destabilize the benzyl anion (Streitwieser & Koch, 1964). A steric effect is presumably responsible for the higher than expected reactivity of Na-o-Me-PA. Most likely, electron repulsion between adjacent CH_3 and $CH_2CO_2^-$ groups destabilizes the reactant, which leads to a lower energy barrier for decarboxylation. In effect, decarboxylation relieves steric strain.

The ortho effect for Na-o-F-PA probably has a different origin. Na-o-F-PA decarboxylates ca. 14 times faster than it should (Fig. 22). However, I used

129

σ_p^- for o-F (Table 5) in the Hammett plot, which means that I significantly underestimated inductive stabilization of the benzyl anion by o-F (ortho is much closer to the benzyl carbon than is para). It appears that the rate-enhancing inductive effect dominates the rate-retarding resonance effect for Na-o-F-PA. Streitwieser & Koch (1964) also observed this behavior; they found that o-F-toluene is easier to deprotonate than toluene, although they found that m-F-toluene reacts faster than o-F-toluene, which is apparently opposite to what I found (Table 5). This difference suggests that, compared to the toluene deprotonation reaction, inductive effects are more important in the decarboxylation reaction, or o-F also causes rate-enhancing steric or solvation effects in the decarboxylation reaction.

4.6. Recommendations for future work

This work revealed much about mechanisms of decarboxylation of phenylacetic acids and their sodium salts in water at high temperature and pressure. However, there is still a great deal that remains to be learned. As an example, it is an open question whether mechanisms like the proposed mechanisms (D in Fig. 19 and I in Fig. 20) occur at significant rates in natural systems. Sedimentary environments are much more chemically complex than the experimental systems studied here, so it is possible that carboxylic acids in the subsurface are broken down by mechanisms that are different from the proposed mechanisms.

130

Phenylacetic acid has a special structure with a benzyllic carbon that is adjacent (α) to the carboxyl group, so phenylacetic acid could decarboxylate by special mechanisms. Mechanisms of decarboxylation in nature presumably depend on the structure and speciation of the carboxylic acid, and on the geochemical environment. The present study on phenylacetic acid showed that, in general, decarboxylation can occur in hydrothermal fluids if the α or β carbon of the carboxylic acid can be an electron sink. The α carbon can be an electron sink if a sufficiently stable carbanion can form, and zwitterion formation can turn the β carbon into an electron sink if the acid possesses β,γ-unsaturation. These are fundamental mechanistic concepts that can serve as pillars for future models of decarboxylation in natural systems.

Below are some suggested topics for future studies that could lead to an improved understanding of mechanisms of decarboxylation and the geochemistry of carboxylic acids in hydrothermal systems.

1) Further details about the mechanisms of decarboxylation of phenylacetic acid and sodium phenylacetate in water at high temperatures and pressures. Additional experimental information is desired, such as the enthalpy and entropy of activation, volume of activation, and fractionation of carbon isotopes in the carboxyl group during decarboxylation. It would also be informative to determine the regiochemistry of protonation of the benzene ring in Mechanism D (Fig. 19) by performing ^{1}H nuclear magnetic resonance studies. The importance of internal return in Mechanism I (Fig. 20) could be assessed by adding a reagent that can

trap the benzyl anion (e.g., NH_4Cl, Br_2, or a carbonyl compound), and seeing if the presence of the trap increases the rate of decarboxylation.

2) Decarboxylation of structurally diverse carboxylic acids and carboxylate salts inside non-catalytic containers. A useful starting point would be experimental studies of decarboxylation of benzoic acid and sodium benzoate in high temperature-pressure water, to complement the present data for phenylacetate systems (Table 5) and the data of Palmer & Drummond (1986) for acetate systems. This would provide broad information about how the nature of the carbon atom that is adjacent to the carboxyl group affects the rate of decarboxylation. It would also be useful to determine how α-alkylation affects the rate by studying decarboxylation of α-alkylated (e.g., α-t-butyl) phenylacetic acids and phenylacetate salts. This would provide more detailed information about steric effects.

3) The thermochemical properties of carboxylic acids, carboxylate anions, and metal-carboxylate complexes in water at high temperatures and pressures. With these quantities, evaluations could be made on the speciation of carboxylates, and the thermodynamic potential for decarboxylation and other reactions of carboxylates in natural and experimental systems. Useful work has been done in this area (e.g., Shock & Koretsky, 1993; Shock, 1995), but there are innumerable carboxylates for which thermochemical properties are unavailable in high temperature-pressure water, including phenylacetate. More experiments would

certainly help, but the development of methods for estimating thermochemical properties of carboxylates of arbitrary structure (i.e., group contribution methods) would be most useful (e.g., Amend & Helgeson, 1997).

4) The thermochemical properties and reactions of carbocations and carbanions in hydrothermal fluids. Carbocations and carbanions can be intermediates in mechanisms of decarboxylation. Now, it is necessary to learn more about these species under hydrothermal conditions. A useful starting point would be to determine the pK_a's of protonated benzenes and simple hydrocarbons such as toluene. How do the pK_a's change with temperature and pressure, and how does aqueous solvation of carbocations and carbanions change with temperature, pressure, and structure? How quickly do carbocations and carbanions react with water (i.e., lifetimes), and are the reaction rates limited by physical processes such as solvent reorganization or diffusion? What are the reduction/oxidation potentials of carbocations and carbanions in high temperature-pressure water, and how do they compare to geological redox buffers?

5) The development of computational chemistry models of decarboxylation in hydrothermal fluids. To model decarboxylation computationally, accurate values of the free energies of species and transition states in solution are required. This is especially challenging for aqueous systems at high temperatures and pressures, because quantum mechanical solvation models are generally parameterized to ambient conditions (e.g., Marenich et al., 2009). Nevertheless, the prize is worth

133

the effort because, if successful, this approach will allow rate constants to be obtained without performing experiments! A recent computational model at 25°C is the no barrier theory of Guthrie et al. (2010). Members of the hydrothermal organic geochemistry group at Arizona State University are presently assessing the accuracy of various polarizable continuum models by applying them to Mechanism I (Fig. 20).

6) Kinetics and mechanisms of decarboxylation in the presence of geochemical additives. In addition to water, carboxylic acids can interact with a variety of organic and inorganic compounds in natural systems (e.g., in sediments), and some of these compounds may promote or catalyze decarboxylation. It would be useful to expand upon the works of Fein et al. (1994) and Miksa et al. (2002) by determining how the nature of the counterion affects rates of decarboxylation of different phenylacetate salts. This would provide information about the importance of ion pairing. Ionic strength and mineral effects could also be studied. Bell et al. (1994) and McCollom & Seewald (2003) found that the common minerals magnetite (Fe_3O_4) and hematite (Fe_2O_3) facilitate decarboxylation and oxidative decarboxylation of acetate, respectively, at hydrothermal conditions. However, the mechanisms of these reactions are unknown. Tools from the field of physical organic chemistry (e.g., substituent effects) may help in elucidating the mechanisms of mineral-catalyzed decarboxylation reactions.

7) Further analyses of the compositions of hydrothermal systems containing carboxylates. This will provide better information about synthesis and degradation reactions that control the abundances of carboxylates. For sedimentary systems, the goal would be to obtain as much information as possible on the compositions of coexisting aqueous fluids, petroleum, natural gas, mineral assemblages, and microbial communities (where appropriate). Measurements of carbon (e.g., Franks et al., 2001) and hydrogen isotopes in organic and inorganic species would also be helpful. Carboxylates can be produced and consumed by oxidation reactions (Seewald, 2001), so it would be informative to compare the abundances of carboxylates and hydrocarbons as functions of the oxidation state of subsurface systems, which can be estimated using alkane-alkene equilibria (Seewald, 1994). Samples should be taken from a broad range of environments to assess the effects of different geochemical conditions.

Table 1. Ring-substituted phenylacetic acids studied here.
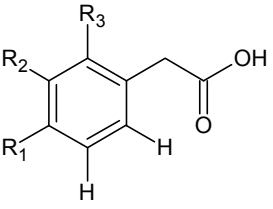
R_1	R_2	R_3	Name of Compound	Abbreviation
H	H	H	Phenylacetic acid	PAA
CH$_3$	H	H	p-Methylphenylacetic acid	p-Me-PAA
H	CH$_3$	H	m-Methylphenylacetic acid	m-Me-PAA
H	H	CH$_3$	o-Methylphenylacetic acid	o-Me-PAA
F	H	H	p-Fluorophenylacetic acid	p-F-PAA
H	F	H	m-Fluorophenylacetic acid	m-F-PAA
H	H	F	o-Fluorophenylacetic acid	o-F-PAA

Table 2. Abundances of organic compounds from experiments with phenylacetic acid or sodium phenylacetate in H_2O or D_2O (200 μL) at 1034 bar in Au capsules. PAA and TOL stand for phenylacetic acid or sodium phenylacetate, and toluene, respectively. Analytical uncertainties in initial amounts correspond to a weighing uncertainty of 0.3 mg, and uncertainties in final amounts correspond to the standard deviation from three gas chromatograph injections.

Temp. (°C)	Duration (h)	Initial PAA (μmol)	Final PAA (μmol)	Final TOL (μmol)	Mass Balance (%) [a]
Phenylacetic acid + H_2O					
298	2	203±2	185±2	15.4±0.1	99±1
300	6	209±2	153±3	41.9±0.2	93±2
302	11	220±2	137±4	83.2±0.3	100±2
299	16	212±2	118±3	88.1±0.8	97±2
300	18.7	202±2	81±2	117.7±0.8	98±1
302	23	211±2	66±4	140.2±0.1	98±2
301 [b]	23	204±2	66±2	132.9±0.6	97±1
301	23	203±2	77.5±0.3	122.6±0.4	98±1
301	29	209±2	59±3	148±1	99±2
300	40.1	212±2	42±2	166.2±0.5	98±1
301	50	207±2	22.1±0.3	179.7±0.8	97±1
300	55.6	203±2	13.9±0.5	175.8±0.5	93±1
300	72.5	205±2	10±2	201±3	103±2
Phenylacetic acid + H_2O + 707 mg Au					
301 [b]	23	206±2	72±4	136.8±0.8	101±2
Phenylacetic acid + 0.987 M HCl					
297	0	211±2	191±1	8.7±0.3 (C_6H_6 not detected)	94±1
299	6	205±2	127±3	74±1 (1.07±0.03 C_6H_6) [c]	99±2
301	13.7	207±2	73.0±0.5	123±1 (1.48±0.02 C_6H_6) [c]	96±1
300	19	199±2	52.4±0.2	139±2 (2.18±0.04 C_6H_6) [c]	97±1
301	23	186±2	20.9±0.2	155.7±0.6 (2.37±0.03 C_6H_6) [c]	96±1
Phenylacetic acid + D_2O					
297	0	204±2	196±1	3.8±0.1	98±1

301	6	205±2	160±1	45.0±0.9	100±1
301	23	199±2	85.0±0.3	114±1	100±1
301	50	207±2	58.1±0.3	142.4±0.4	97±1
300	72	202±2	25.3±0.5	172±1	98±1
Sodium phenylacetate + H$_2$O					
297	0	208±2	185±2	13.1±0.2	96±1
299	2	202±2	150±2	54.5±0.1	101±1
301	6	202±2	78±3	123±1	100±2
301 [d]	6	205±2	89±1	110±1	97±1
301	6	210±2	72±2	131±2	97±2
300	12.2	200±2	29±3	160±3	94±2
301	16	200±2	7.8±0.1	181±2	95±1
302	23	207±2	2.9±0.1	197.8±0.6	97.0±0.9
Sodium phenylacetate + 648 mg Au					
301 [d]	6	200±2	93.2±0.4	105±5	99±3
Sodium phenylacetate + 0.999 M NaOH					
297	0	206±2	187±2	9.4±0.1	95±1
298	2	204±2	153.2±0.7	46.7±0.4	98±1
299	6	203±2	84±1	119.3±0.7	100±1
301	6	199±2	100.0±0.7	94±2	97±2
300	9	197±2	65.9±0.5	123±2	96±1
301	19	201±2	9.9±0.2	182.3±0.8	96±1
Sodium phenylacetate + D$_2$O					
297	0	202±2	174±1	17.6±0.3	95±1
300	6	206±2	94±2	106±2	97±2
301	16	208±2	21.1±0.2	176.8±0.6	94.9±0.9
300	23	200±2	8.7±0.1	183±1	96±1

[a], Mass balance was computed in terms of number of benzene rings in the reactant and products; [b,d], Experiments were performed in the same run to ensure optimal comparability; [c], Benzene was detected and μmol of benzene was determined in most PAA + HCl experiments.

Table 3. Abundances of organic compounds from experiments with ring-methylated phenylacetic acids or sodium phenylacetates in H_2O (200 μL) at 1034 bar in Au capsules. PAA and TOL stand for the appropriate substituted phenylacetic acid and toluene, respectively (the initial stereochemistry is preserved), and ND means not detected (<0.1 μmol). Analytical uncertainties in initial amounts correspond to a weighing uncertainty of 0.3 mg, and uncertainties in final amounts correspond to the standard deviation from three gas chromatograph injections.

Temp. (°C)	Duration (h)	Initial PAA (μmol)	Final PAA (μmol)	Final TOL (μmol)	Mass Balance (%) [a]
p-Methylphenylacetic acid					
299	2	206±2	195±1	11.95±0.03	101±1
300	12.9	209±2	143.1±0.2	61.8±0.1	98.2±0.9
302	23	205±2	104±3	99.5±0.3	99±2
300	23	202±2	104±1	95.7±0.1	99±1
300	52.8	207±2	51±5	156.4±0.8	100±2
Sodium p-methylphenylacetate					
298	2	198±2	186±2	9.23±0.06	99±1
300	6	204±2	174±2	31.6±0.2	101±1
300	23	204±2	99±2	104.5±0.3	99±1
300	23	204±2	80.1±0.2	115.9±0.3	96.3±0.8
300	52.5	205±2	37.1±0.6	158.9±0.7	95.7±0.9
m-Methylphenylacetic acid					
296	0	202±2	169.4±0.5	35.4±0.1	101±1
300	2	199±2	72±5	127.9±0.4	100±3
299	4	210±2	42±2	169.9±0.1	101±1
300	9	202±2	4.6±0.1	194.8±0.5	99±1
300	23	197±2	ND	184.9±0.2	94±1
Sodium m-methylphenylacetate					
300	2	202±2	144±3	56.4±0.9	99±2
300	6	208±2	107.2±0.3	97.9±0.4	98.4±0.9
300	14	203±2	58±1	139.3±0.3	97±1
300	23	213±2	21.9±0.8	182.5±0.5	95.8±0.9
o-Methylphenylacetic acid					
300	2	206±2	170±3	33.0±0.1	98±2
300	5	211±2	152±1	54.7±0.4	98±1
301	7.5	205±2	95±5	100.9±0.1	96±3
301	15.5	197±2	65±4	125.7±0.7	97±3
300	23	207±2	34±1	166.5±0.2	97±1
300	23	203±2	34.3±0.1	164±1	98±1

300	31	201±2	7.9±0.2	179.7±0.5	93±1
Sodium o-methylphenylacetate					
296	0	208±2	192±3	17.3±0.2	101±2
300	2	207±2	111.7±0.4	96.8±0.6	100.8±0.9
301	3.5	199±2	97.3±0.7	100.7±0.7	99±1
300	6	218±2	49.0±0.8	162±1	97±1

[a], Mass balance was computed in terms of number of benzene rings in the reactant

and products.

Table 4. Abundances of organic compounds from experiments with ring-fluorinated phenylacetic acids or sodium phenylacetates in H_2O (200 μL) at 1034 bar in Au capsules. PAA, TOL, and CRE stand for the appropriate substituted phenylacetic acid, toluene, and cresol, respectively (the initial stereochemistry is preserved), and ND means not detected (<0.1 μmol). Analytical uncertainties in initial amounts correspond to a weighing uncertainty of 0.3 mg, and uncertainties in final amounts correspond to the standard deviation from three gas chromatograph injections.

Temp. (°C)	Duration (h)	Initial PAA (μmol)	Final PAA (μmol)	Final TOL (μmol)	Final CRE (μmol)	Mass Balance (%) [a]
p-Fluorophenylacetic acid						
300	2	213±2	211±5	1.49±0.03	ND	100±3
301	23	204±2	185±5	11.5±0.2	0.54±0.04	97±3
300	23	199±2	183.4±0.2	12.3±0.1	0.48±0.01	99±1
299	167	204±2	121±2	71.4±0.3	4.51±0.08	96±1
299	526	202±2	46.2±0.7	134.9±0.4	8.7±0.1	94±1
Sodium p-fluorophenylacetate						
300	2	195±2	164±2	24.2±0.3	3.0±0.3	98±2
300	6	206±2	135±1	54.2±0.4	12.8±0.3	98±1
302	15	203±2	67.0±0.1	96±1	27.3±0.6	94±1
300	23.03	202±2	43.3±0.4	107.8±0.7	39±3	94±2
300	31.5	198±2	24.2±0.6	116±1	43.8±0.4	93±1
m-Fluorophenylacetic acid						
301	2	204±2	169±1	32.7±0.4	ND	99±1
299	5	211±2	138±2	67.9±0.4	0.6±0.1	98±1
300	12.2	203±2	94±2	106.5±0.4	1.4±0.1	99±2
301	16	198±2	54.5±0.6	137±1	2.32±0.03	98±1
301	23	204±2	32±3	161±2	3.6±0.2	97±2
300	32.5	204±2	20±1	176±4	3.2±0.1	97±2
Sodium m-fluorophenylacetate						
296	0	206±2	123.7±0.4	73±3	3.0±0.5	97±2
299	0.5	210±2	66±2	133±4	8±1	98±3
298	1	207±2	48.0±0.5	140±1	10.4±0.1	96±1
300	2	209±2	12.4±0.1	167±2	18.1±0.2	94±1
300	6	203±2	ND	149±2	38.7±0.7	92±1
o-Fluorophenylacetic acid						
301	2	207±2	198±4	3.74±0.05	ND	98±2
300	23	206±2	166.1±0.1	24.7±0.1	2.16±0.02	93.9±0.9
300	97	202±2	107±5	74.7±0.4	12.6±0.3	96±3
299	265.67	205±2	36±2	125±1	26.3±0.6	91±1

Sodium o-fluorophenylacetate						
297	0	209±2	86±1	97±1	2.02±0.06	88±1
297	0	205±2	90.1±0.2	88.1±0.2	1.76±0.05	87.8±0.7
300	0.75	206±2	28.0±0.2	144.0±0.7	7.71±0.04	87.1±0.8
298	1	194±2	30.4±0.2	144.9±0.4	7.6±0.1	94.5±0.9
300	2	202±2	6.1±0.1	159.0±0.8	18.3±0.3	90.8±2
300	6	205±2	ND	161±1	33.9±0.4	95±1

[a], Mass balance was computed in terms of number of benzene rings in the reactant

and products.

Table 5. First-order rate constants for decarboxylation of phenylacetic acids or sodium phenylacetates in water at 300°C and 1034 bar, and Hammett substituent parameters used here.

Experimental System	$100 \times k_{decarb}$ (h^{-1})	k_{salt}/k_{acid} [b]	σ [c]
Phenylacetic acid + H$_2$O	4.4±0.5	-	0 [d]
Phenylacetic acid + D$_2$O	2.9±0.5	-	-
Phenylacetic acid + HCl [a]	7±1	-	-
p-Methylphenylacetic acid [a]	2.8±0.4	-	-0.07 [e]
m-Methylphenylacetic acid [a]	39±6	-	-0.31 [f]
o-Methylphenylacetic acid [a]	8±2	-	-0.07 [e]
p-Fluorophenylacetic acid [a]	0.27±0.03	-	0.34 [e]
m-Fluorophenylacetic acid [a]	7±1	-	-0.07 [f]
o-Fluorophenylacetic acid [a]	0.58±0.09	-	0.34 [e]
Sodium phenylacetate + H$_2$O	14.5±2	3.3±0.6	0 [d]
Sodium phenylacetate + D$_2$O	12±1.5	4.1±0.9	-
Sodium phenylacetate + NaOH [a]	12±2	-	-
Sodium p-methylphenylacetate [a]	3.5±0.7	1.25±0.3	-0.17 [g]
Sodium m-methylphenylacetate [a]	8±1.5	0.205±0.05	-0.07 [e]
Sodium o-methylphenylacetate [a]	21±5	2.6±0.9	-0.17 [g]
Sodium p-fluorophenylacetate [a]	5.6±0.9	21±4	-0.03 [g]
Sodium m-fluorophenylacetate [a]	110±25	16±4	0.34 [e]
Sodium o-fluorophenylacetate [a]	125±30	216±62	-0.03 [g]

[a], in H$_2$O; [b], k_{decarb} of the sodium phenylacetate of interest relative to that of the corresponding phenylacetic acid; [c], Hammett substituent parameters from Hansch et al. (1991); [d], Defined as zero by convention; [e], σ_m; [f], σ_p^+; [g], σ_p^-.

Table 6. Summary of kinetic tests of the candidate mechanisms for decarboxylation of phenylacetic acid or sodium phenylacetate in water at 300°C and 1034 bar.

Acid Mechanisms				
Mechanism [a]	ρ [b]	Rate Equation [c]	$\dfrac{k_{HCl}}{k_{H_2O}}$ [e]	$\dfrac{k_{D_2O}}{k_{H_2O}}$ [g]
A	-1	$k_{A1}f_{PAA}\left[\sum PA\right]$	1	1
B	≥ 3	$k_{B1}f_{PA^-}\left[\sum PA\right]$	0.0076	0.6
C	≤ -3	$\dfrac{k_{C1}k_{C2}\left[H^+\right]f_{PAA}\left[\sum PA\right]}{k_{-C1}+k_{C2}}$ [d]	560	<0.6 [h] 1.4 [i]
D	≤ -3	$\dfrac{k_{D1}k_{D2}\left[H^+\right]f_{PA^-}\left[\sum PA\right]}{k_{-D1}+k_{D2}}$ [d]	4.3	<0.3 [h] 0.8 [i]
E	≤ -3	$k_{E1}\left[H^+\right]f_{PA^-}\left[\sum PA\right]$	4.3	<0.3
Observed	-3.0±0.5	$k_{decarb}\left[\sum PA\right]$	1.6±0.3	0.7±0.1
Salt Mechanisms				
Mechanism [a]	ρ [b]	Rate Equation [c]	$\dfrac{k_{NaOH}}{k_{H_2O}}$ [f]	$\dfrac{k_{D_2O}}{k_{H_2O}}$ [g]
F	-1	$k_{F1}f_{PA^-}\left[\sum PA\right]$	0.7	1
G	≤ -3	$\dfrac{k_{G1}k_{G2}\left[H^+\right]f_{PA^-}\left[\sum PA\right]}{k_{-G1}+k_{G2}}$ [d]	0.0022	Not Estimated
H	≥ 3	$k_{H1}f_{NaPA}\left[\sum PA\right]$	1.3	1
I	≥ 3	$k_{I1}f_{PA^-}\left[\sum PA\right]$	0.7	1
J	≥ 3	$k_{J1}\left[H_2O\right]f_{PA^-}\left[\sum PA\right]$	0.7	>0.3 <1
Observed	2.9±0.7	$k_{decarb}\left[\sum PA\right]$	0.8±0.2	0.8±0.15

[a], The acid and salt mechanisms are shown in Figs. 19 and 20, respectively; [b], Hammett reaction constant; [c], k represents rate constant, f designates mole fraction of phenylacetate species, brackets indicate concentration of species, and $\sum PA$

stands for total phenylacetate; [d], Rate equation was derived using the steady-state approximation (e.g., Anslyn & Dougherty, 2006); [e], The rate constant for decarboxylation of phenylacetic acid in 1 m HCl relative to that in H_2O; [f], The rate constant for decarboxylation of sodium phenylacetate in 1 m NaOH relative to that in H_2O; [g], The rate constant for decarboxylation of the acid or salt in D_2O relative to that in H_2O; [h], For the rate-limiting protonation endmember ($k_2 \gg k_{-1}$); [i], For the pre-equilibrium endmember ($k_2 \ll k_{-1}$).

Table 7. Equilibrium molal concentrations of aqueous species in acetic acid or sodium acetate systems at 300°C and 1034 bar, computed using the GEOCHEQ code (Zolotov et al., 2006; Mironenko et al., 2008). Entries in the top row represent different bulk compositions. Only species in the leftmost column were considered in speciation calculations. Ac stands for acetate.

| Species	1 m HAc	1 m HAc + 1 m HCl	1 m NaAc	1 m NaAc + 1 m NaOH
HAc	9.99×10^{-1}	1.00×10^{0}	1.99×10^{-3}	3.16×10^{-6}
Ac⁻	1.08×10^{-3}	8.25×10^{-6}	1.60×10^{-1}	1.13×10^{-1}
Na(Ac)	-	-	3.12×10^{-1}	4.13×10^{-1}
Na(Ac)$_2$⁻	-	-	2.63×10^{-1}	2.37×10^{-1}
H⁺	1.08×10^{-3}	6.09×10^{-1}	5.58×10^{-8}	1.73×10^{-10}
OH⁻	2.27×10^{-8}	1.69×10^{-10}	1.69×10^{-3}	7.47×10^{-1}
HCl	-	3.91×10^{-1}	-	-
Cl⁻	-	6.09×10^{-1}	-	-
NaOH	-	-	3.04×10^{-4}	2.53×10^{-1}
Na⁺	-	-	4.25×10^{-1}	1.10×10^{0}
Ionic Strength	0.0011	0.6090	0.4249	1.0969

Fig. 1. Yields of phenylacetic acid (PAA) and toluene (TOL) as functions of time (denoted by symbols), from experiments with PAA in H_2O at 300°C and 1034 bar. The starting concentration of PAA was 1.04±0.03 molal. A 3% uncertainty in yields was assigned based on analysis of replicates in the entire dataset. First-order (exponential) kinetic curves were generated by performing least squares regression, and the best-fit apparent rate constant for disappearance of PAA is $(4.4\pm0.5)\times10^{-2}$ h^{-1}. The uncertainty in the rate constant was estimated by graphical analysis.
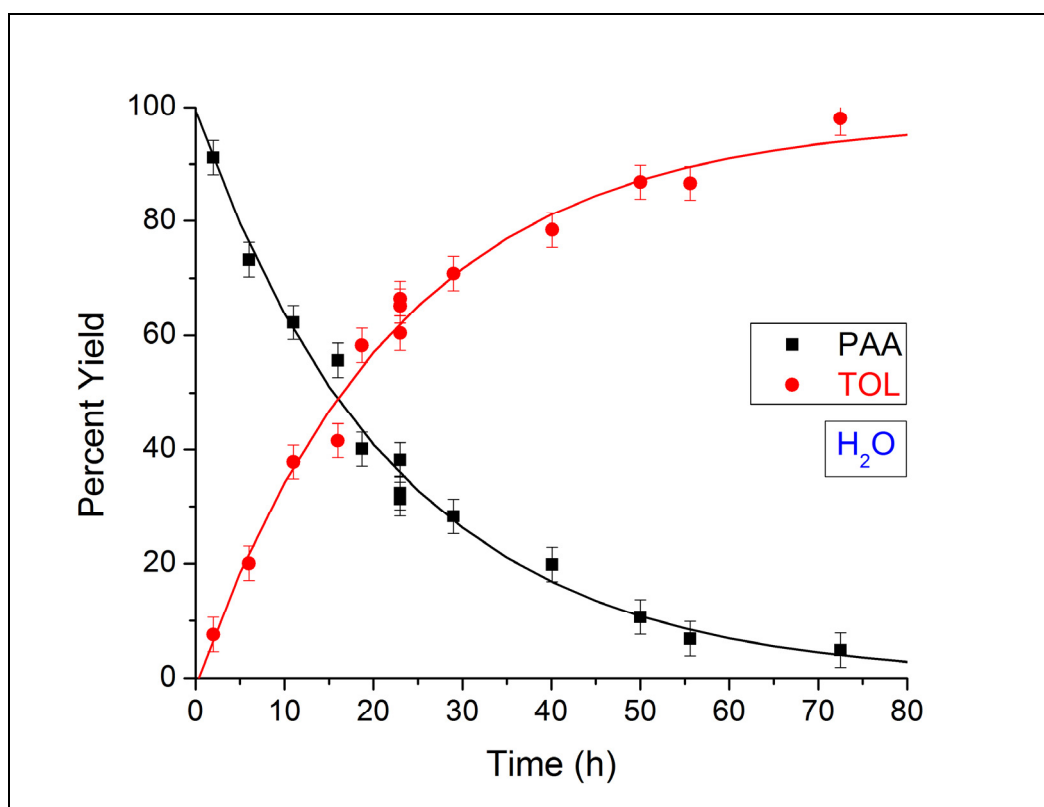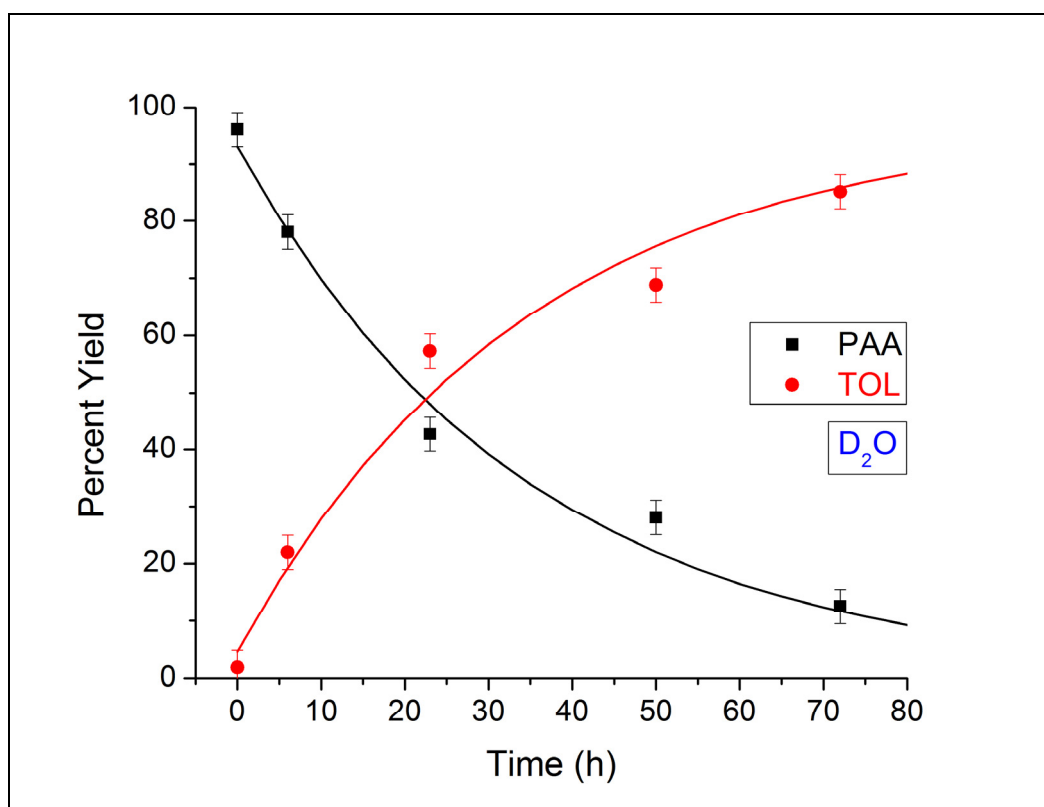
Fig. 2. Yields of phenylacetic acid (PAA) and toluene (TOL) + benzene (BEN) as functions of time (denoted by symbols), from experiments with PAA in 1 m aqueous HCl at 300°C and 1034 bar. The starting concentration of PAA was 1.01±0.05 molal. A 3% uncertainty in yields was assigned based on analysis of replicates in the entire dataset. First-order (exponential) kinetic curves were generated by performing least squares regression, and the best-fit apparent rate constant for disappearance of PAA is $(7\pm1)\times10^{-2}$ h^{-1}. The uncertainty in the rate constant was estimated by graphical analysis.
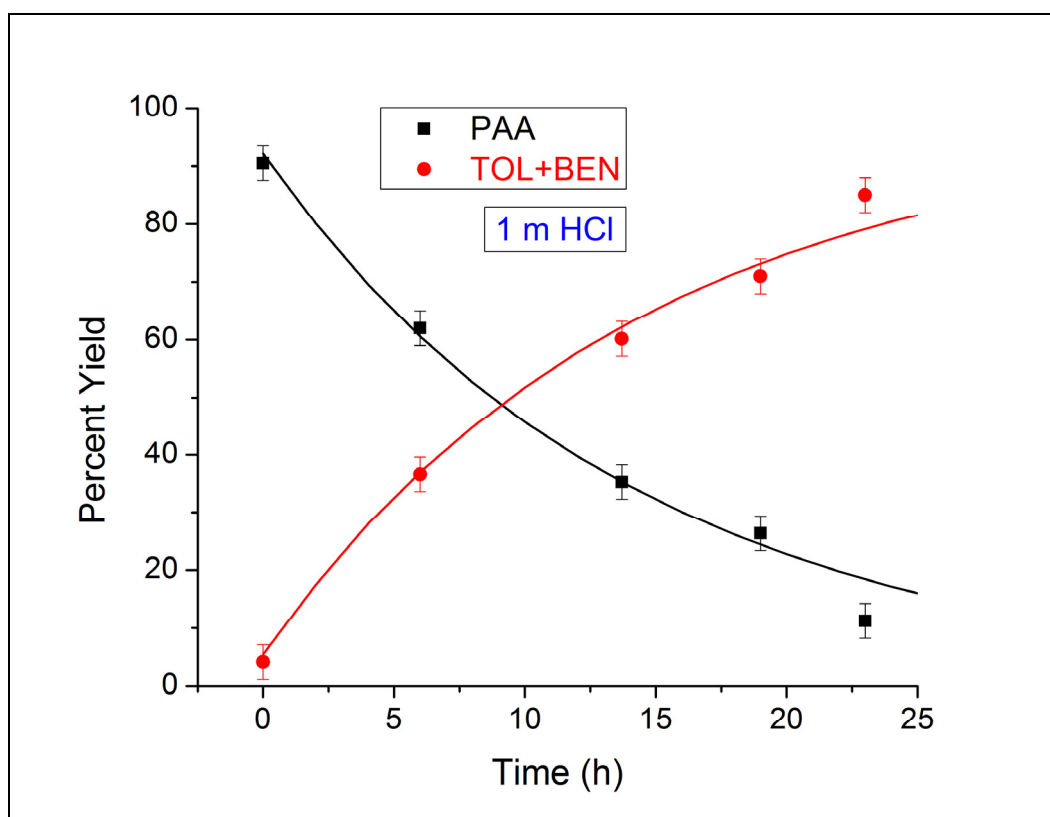
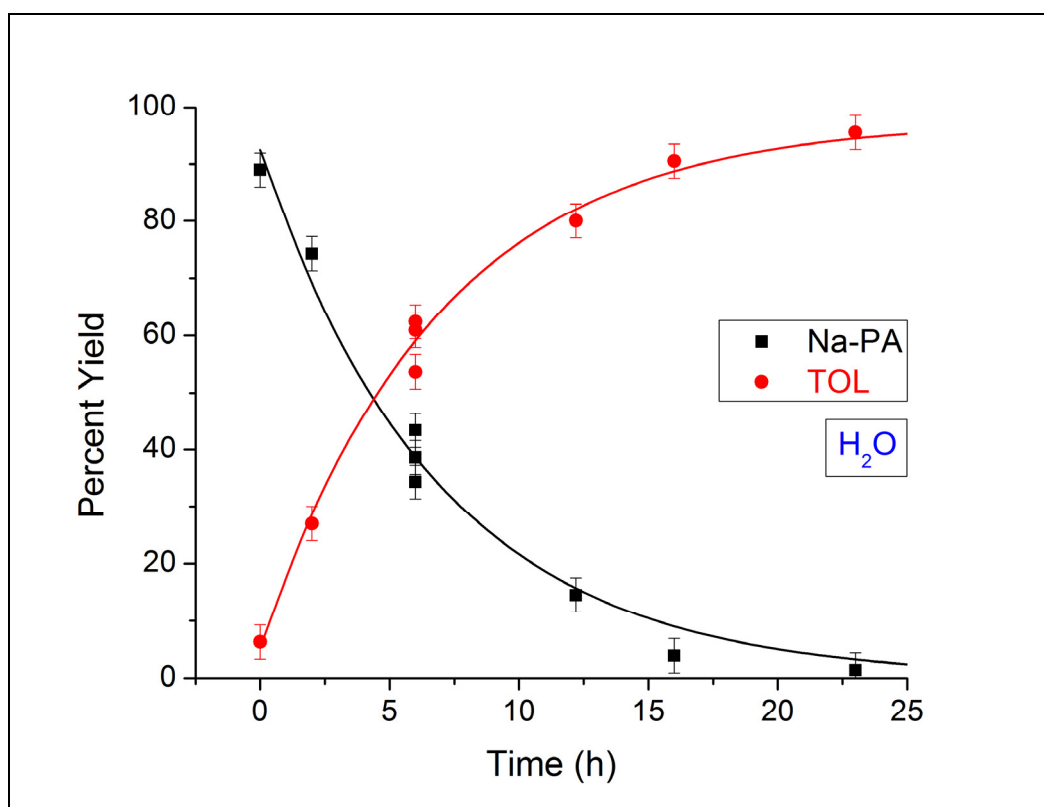Fig. 3. Yields of phenylacetic acid (PAA) and toluene (TOL) as functions of time (denoted by symbols), from experiments with PAA in D_2O at 300°C and 1034 bar. The starting concentration of PAA was 0.92±0.01 molal. A 3% uncertainty in yields was assigned based on analysis of replicates in the entire dataset. First-order (exponential) kinetic curves were generated by performing least squares regression, and the best-fit apparent rate constant for disappearance of PAA is $(2.9\pm0.5)\times10^{-2}$ h^{-1}. The uncertainty in the rate constant was estimated by graphical analysis.
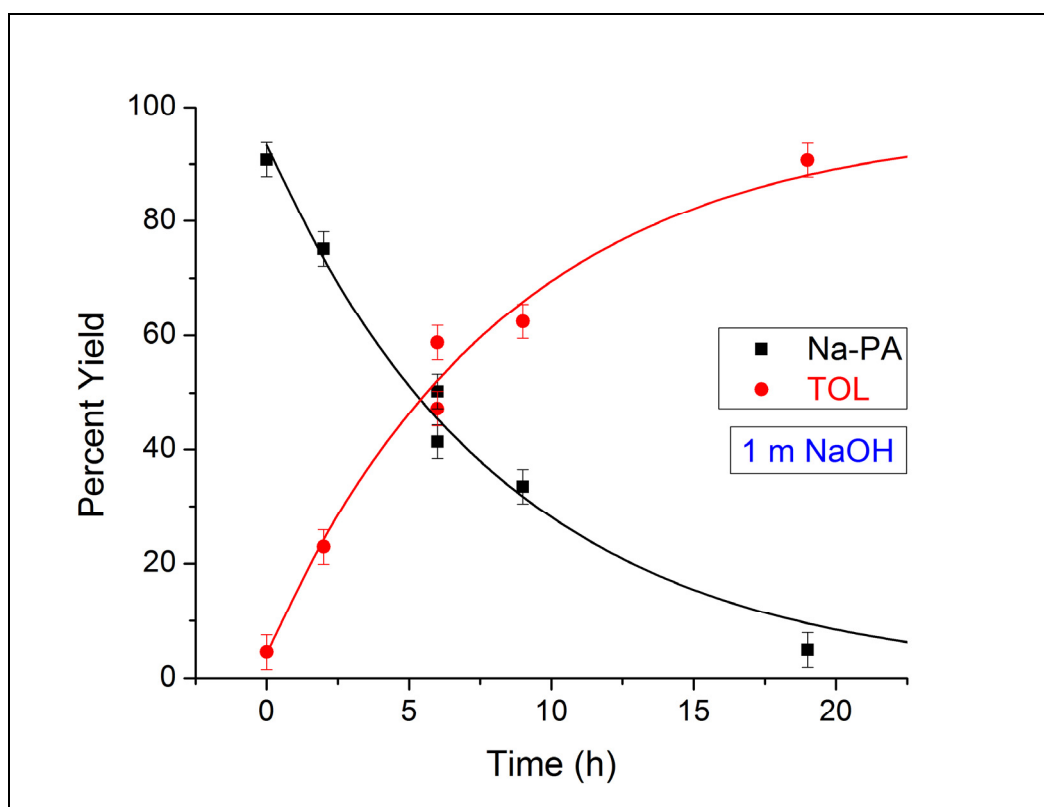
Fig. 4. Yields of sodium phenylacetate (Na-PA) and toluene (TOL) as functions of time (denoted by symbols), from experiments with Na-PA in H_2O at 300°C and 1034 bar. The starting concentration of Na-PA was 1.02±0.02 molal. A 3% uncertainty in yields was assigned based on analysis of replicates in the entire dataset. First-order (exponential) kinetic curves were generated by performing least squares regression, and the best-fit apparent rate constant for disappearance of Na-PA is $(1.45\pm0.2)\times10^{-1}$ h^{-1}. The uncertainty in the rate constant was estimated by graphical analysis.

Fig. 5. Yields of sodium phenylacetate (Na-PA) and toluene (TOL) as functions of time (denoted by symbols), from experiments with Na-PA in 1 m NaOH at 300°C and 1034 bar. The starting concentration of Na-PA was 1.01±0.02 molal. A 3% uncertainty in yields was assigned based on analysis of replicates in the entire dataset. First-order (exponential) kinetic curves were generated by performing least squares regression, and the best-fit apparent rate constant for disappearance of Na-PA is $(1.2\pm0.2)\times10^{-1}$ h^{-1}. The uncertainty in the rate constant was estimated by graphical analysis.
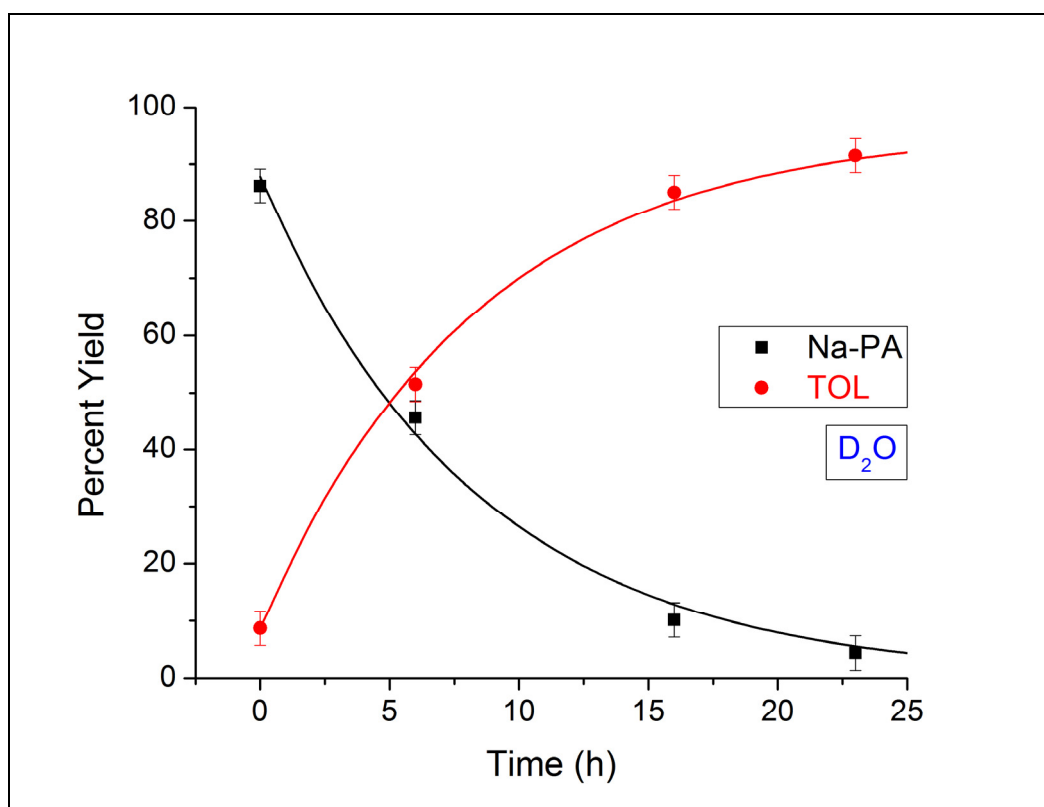
Fig. 6. Yields of sodium phenylacetate (Na-PA) and toluene (TOL) as functions of time (denoted by symbols), from experiments with Na-PA in D_2O at 300°C and 1034 bar. The starting concentration of Na-PA was 0.92±0.02 molal. A 3% uncertainty in yields was assigned based on analysis of replicates in the entire dataset. First-order (exponential) kinetic curves were generated by performing least squares regression, and the best-fit apparent rate constant for disappearance of Na-PA is $(1.2\pm0.15)\times10^{-1}$ h^{-1}. The uncertainty in the rate constant was estimated by graphical analysis.
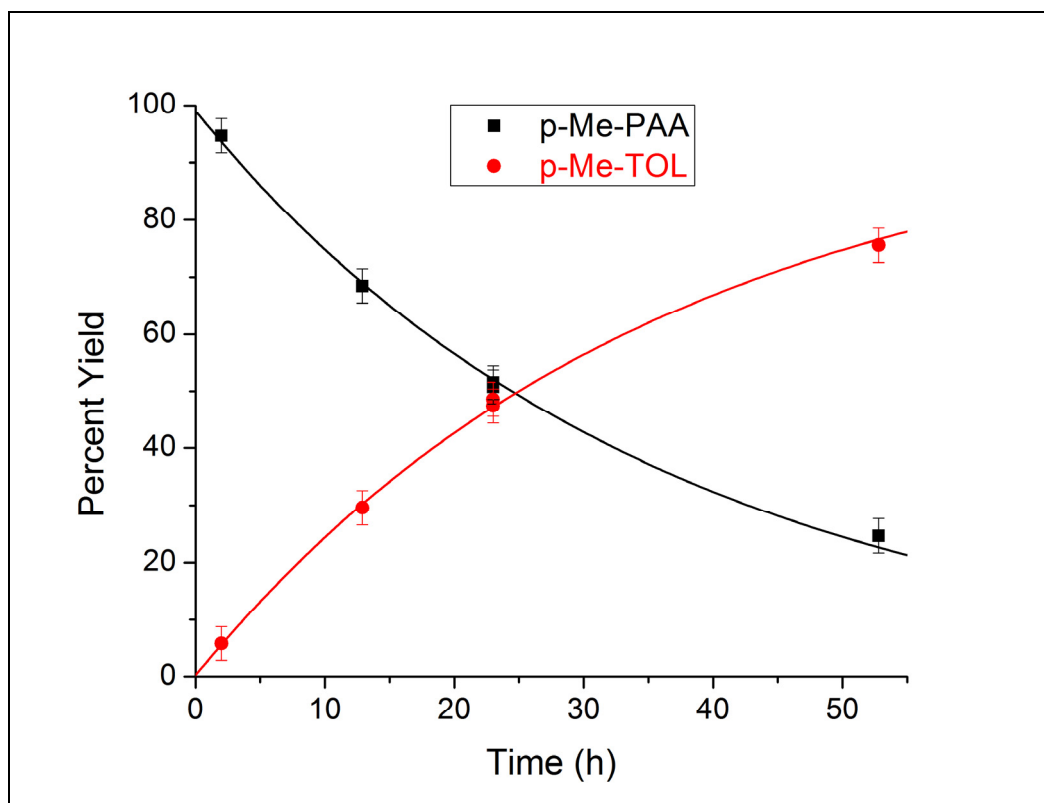
Fig. 7. Yields of p-methylphenylacetic acid (p-Me-PAA) and p-methyltoluene (p-Me-TOL) as functions of time (denoted by symbols), from experiments with p-Me-PAA in H_2O at 300°C and 1034 bar. The starting concentration of p-Me-PAA was 1.03±0.01 molal. A 3% uncertainty in yields was assigned based on analysis of replicates in the entire dataset. First-order (exponential) kinetic curves were generated by performing least squares regression, and the best-fit apparent rate constant for disappearance of p-Me-PAA is $(2.8\pm0.4)\times10^{-2}$ h^{-1}. The uncertainty in the rate constant was estimated by graphical analysis. p-Methyltoluene is also known as p-xylene.

Fig. 8. Yields of sodium p-methylphenylacetate (Na-p-Me-PA) and p-methyltoluene (p-Me-TOL) as functions of time (denoted by symbols), from experiments with Na-p-Me-PA in H_2O at 300°C and 1034 bar. The starting concentration of Na-p-Me-PA was 1.02±0.01 molal. A 3% uncertainty in yields was assigned based on analysis of replicates in the entire dataset. First-order (exponential) kinetic curves were generated by performing least squares regression, and the best-fit apparent rate constant for disappearance of Na-p-Me-PA is $(3.5\pm0.7)\times10^{-2}$ h^{-1}. The uncertainty in the rate constant was estimated by graphical analysis. p-Methyltoluene is also known as p-xylene.
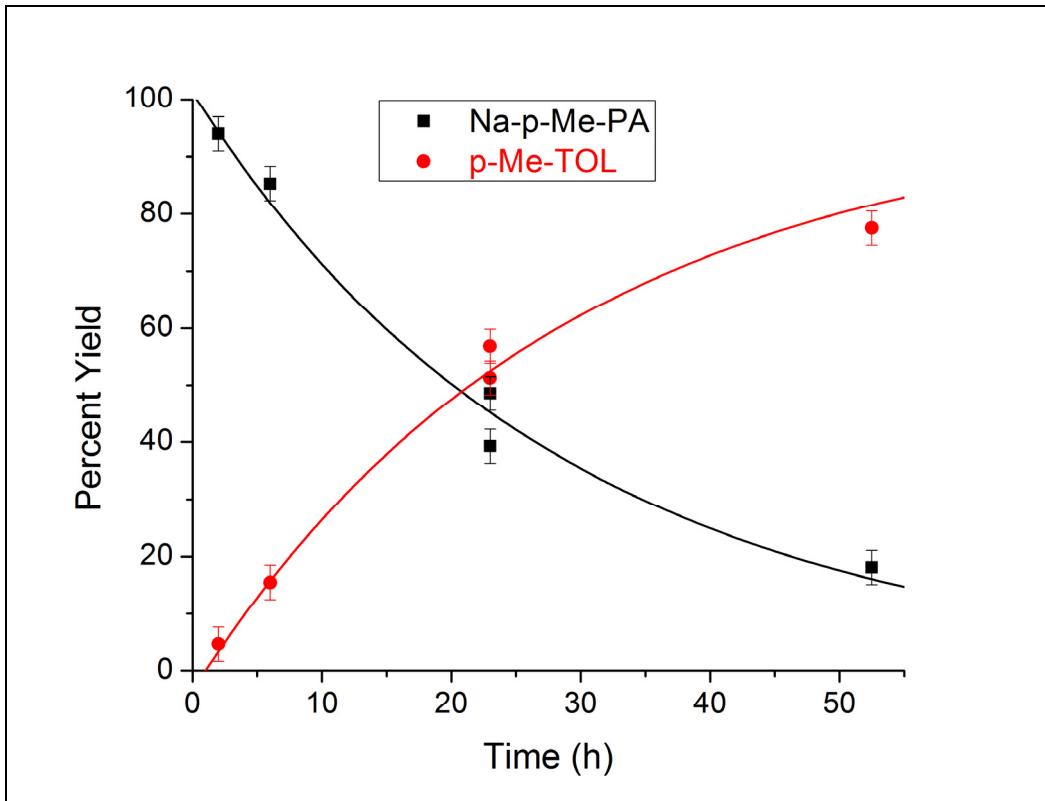
Fig. 9. Yields of m-methylphenylacetic acid (m-Me-PAA) and m-methyltoluene (m-Me-TOL) as functions of time (denoted by symbols), from experiments with m-Me-PAA in H_2O at 300°C and 1034 bar. The starting concentration of m-Me-PAA was 1.01±0.02 molal. A 3% uncertainty in yields was assigned based on analysis of replicates in the entire dataset. First-order (exponential) kinetic curves were generated by performing least squares regression, and the best-fit apparent rate constant for disappearance of m-Me-PAA is $(3.9\pm0.6)\times10^{-1}$ h^{-1}. The uncertainty in the rate constant was estimated by graphical analysis. m-Methyltoluene is also known as m-xylene.
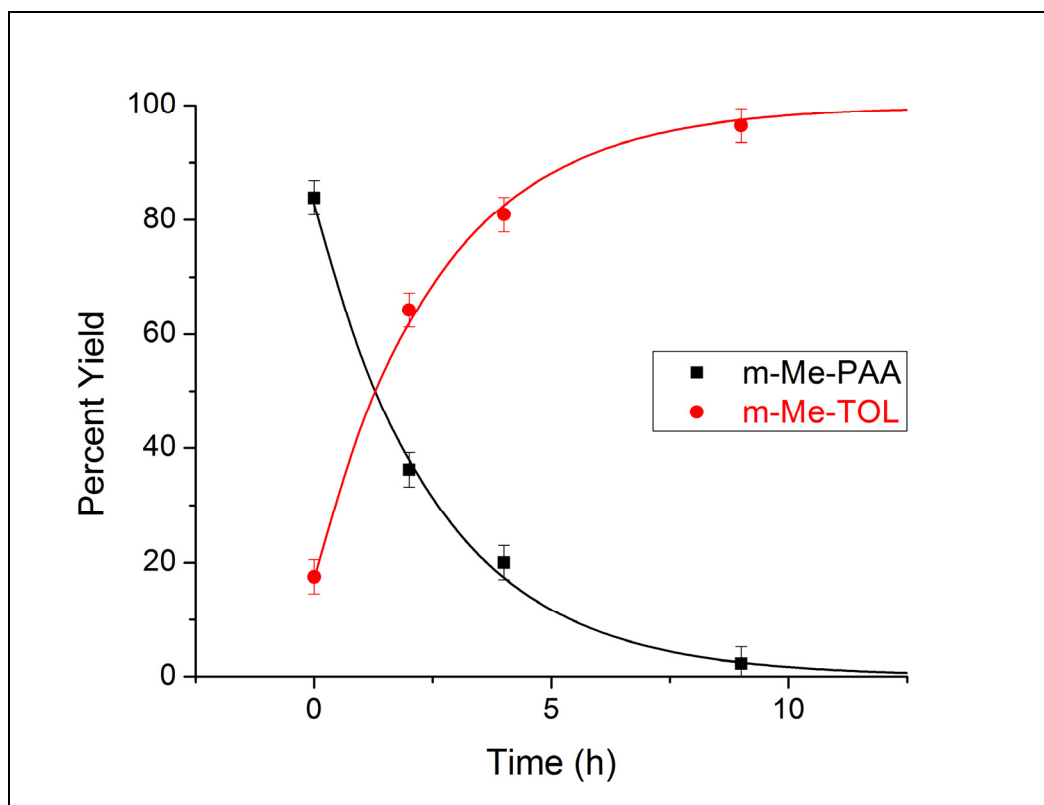
Fig. 10. Yields of sodium m-methylphenylacetate (Na-m-Me-PA) and m-methyltoluene (m-Me-TOL) as functions of time (denoted by symbols), from experiments with Na-m-Me-PA in H_2O at 300°C and 1034 bar. The starting concentration of Na-m-Me-PA was 1.04±0.03 molal. A 3% uncertainty in yields was assigned based on analysis of replicates in the entire dataset. First-order (exponential) kinetic curves were generated by performing least squares regression, and the best-fit apparent rate constant for disappearance of Na-m-Me-PA is $(8\pm1.5)\times10^{-2}$ h^{-1}. The uncertainty in the rate constant was estimated by graphical analysis. m-Methyltoluene is also known as m-xylene.
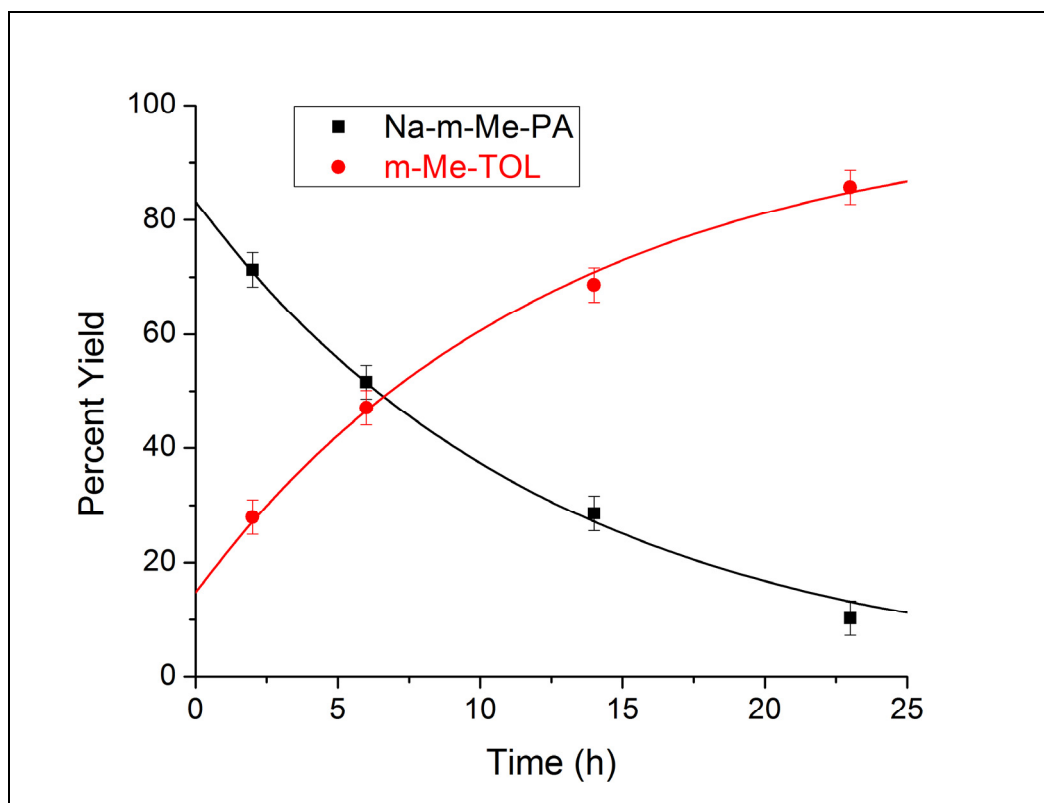
Fig. 11. Yields of o-methylphenylacetic acid (o-Me-PAA) and o-methyltoluene (o-Me-TOL) as functions of time (denoted by symbols), from experiments with o-Me-PAA in H_2O at 300°C and 1034 bar. The starting concentration of o-Me-PAA was 1.02±0.02 molal. A 3% uncertainty in yields was assigned based on analysis of replicates in the entire dataset. First-order (exponential) kinetic curves were generated by performing least squares regression, and the best-fit apparent rate constant for disappearance of o-Me-PAA is $(8\pm2)\times10^{-2}$ h^{-1}. The uncertainty in the rate constant was estimated by graphical analysis. o-Methyltoluene is also known as o-xylene.
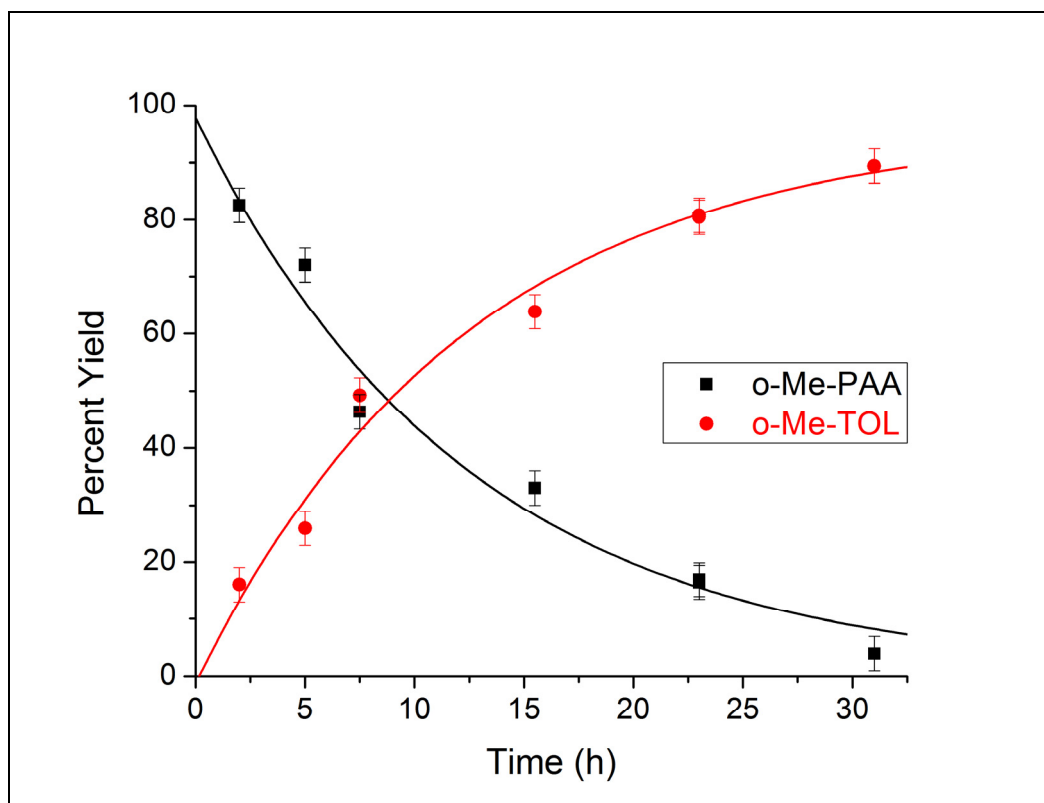
Fig. 12. Yields of sodium o-methylphenylacetate (Na-o-Me-PA) and o-methyltoluene (o-Me-TOL) as functions of time (denoted by symbols), from experiments with Na-o-Me-PA in H_2O at 300°C and 1034 bar. The starting concentration of Na-o-Me-PA was 1.04±0.04 molal. A 3% uncertainty in yields was assigned based on analysis of replicates in the entire dataset. First-order (exponential) kinetic curves were generated by performing least squares regression, and the best-fit apparent rate constant for disappearance of Na-o-Me-PA is $(2.1\pm0.5)\times10^{-1}$ h^{-1}. The uncertainty in the rate constant was estimated by graphical analysis. o-Methyltoluene is also known as o-xylene.
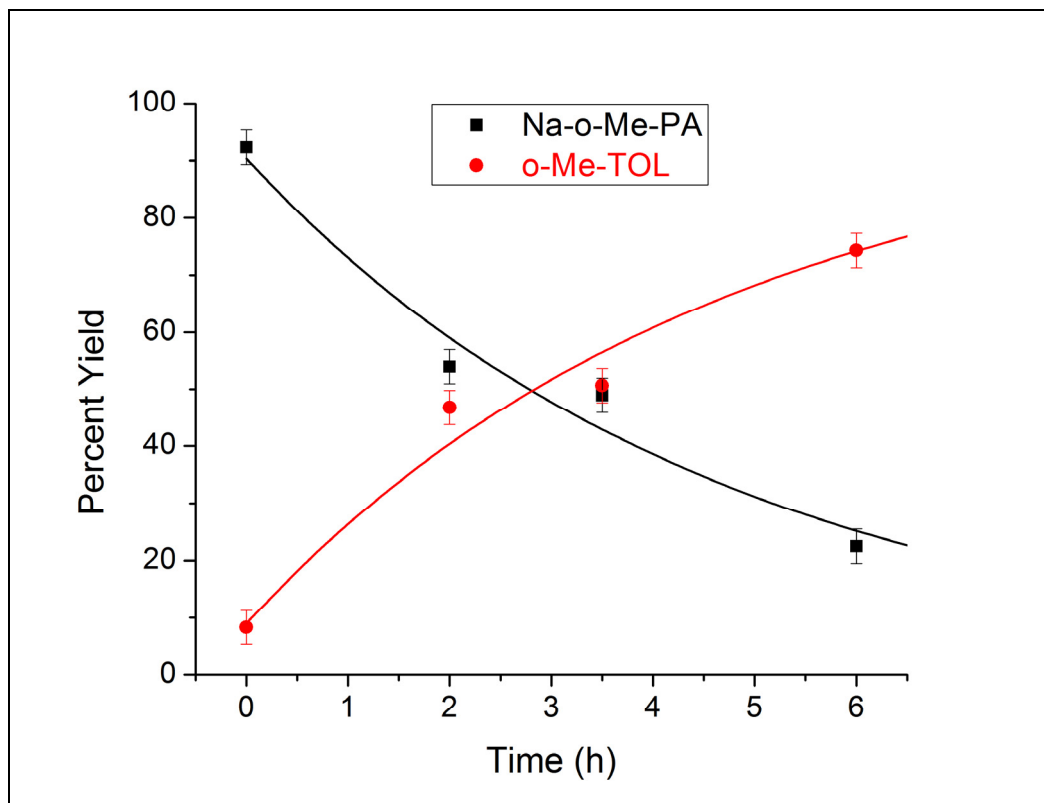
Fig. 13. Yields of p-fluorophenylacetic acid (p-F-PAA) and p-fluorotoluene (p-F-TOL) + p-cresol (p-CRE) as functions of time (denoted by symbols), from experiments with p-F-PAA in H_2O at 300°C and 1034 bar. The starting concentration of p-F-PAA was 1.03±0.03 molal. A 3% uncertainty in yields was assigned based on analysis of replicates in the entire dataset. First-order (exponential) kinetic curves were generated by performing least squares regression, and the best-fit apparent rate constant for disappearance of p-F-PAA is $(2.8\pm0.3)\times10^{-3}$ h^{-1}. The uncertainty in the rate constant was estimated by graphical analysis.
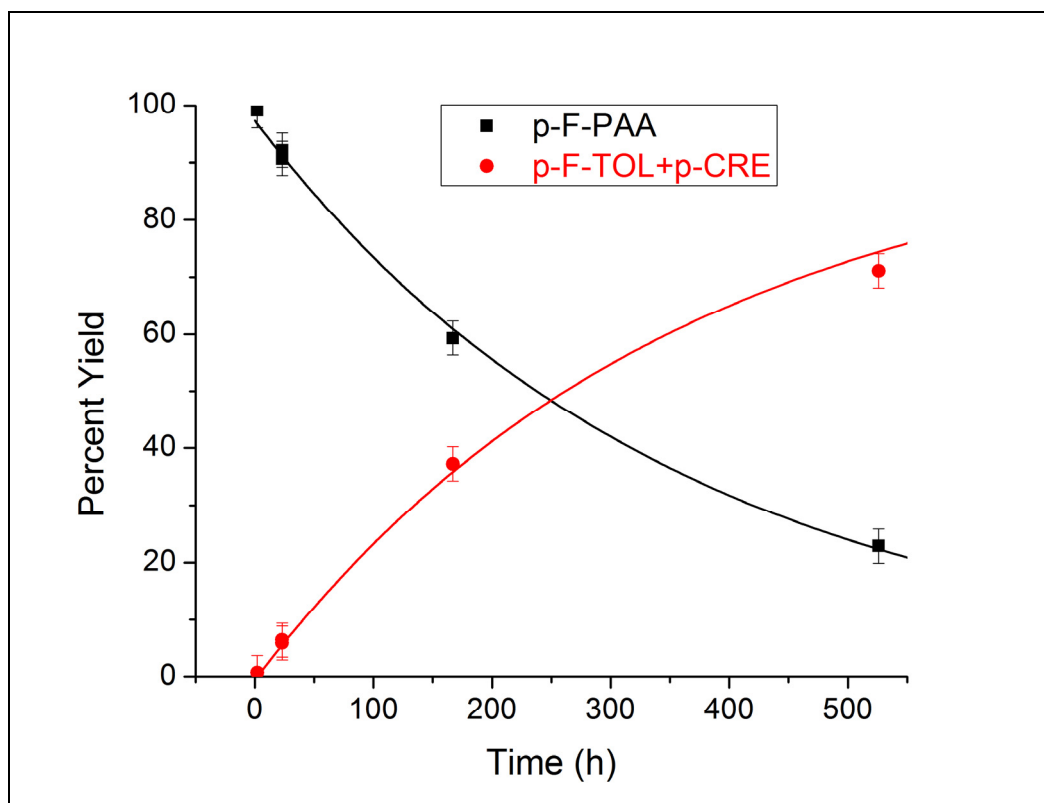
Fig. 14. Yields of sodium p-fluorophenylacetate (Na-p-F-PA) and p-fluorotoluene (p-F-TOL) + p-cresol (p-CRE) as functions of time (denoted by symbols), from experiments with Na-p-F-PA in H_2O at 300°C and 1034 bar. The starting concentration of Na-p-F-PA was 1.01±0.02 molal. A 3% uncertainty in yields was assigned based on analysis of replicates in the entire dataset. First-order (exponential) kinetic curves were generated by performing least squares regression, and the best-fit apparent rate constant for disappearance of Na-p-F-PA is $(6.5\pm0.7)\times10^{-2}$ h^{-1}. The uncertainty in the rate constant was estimated by graphical analysis.
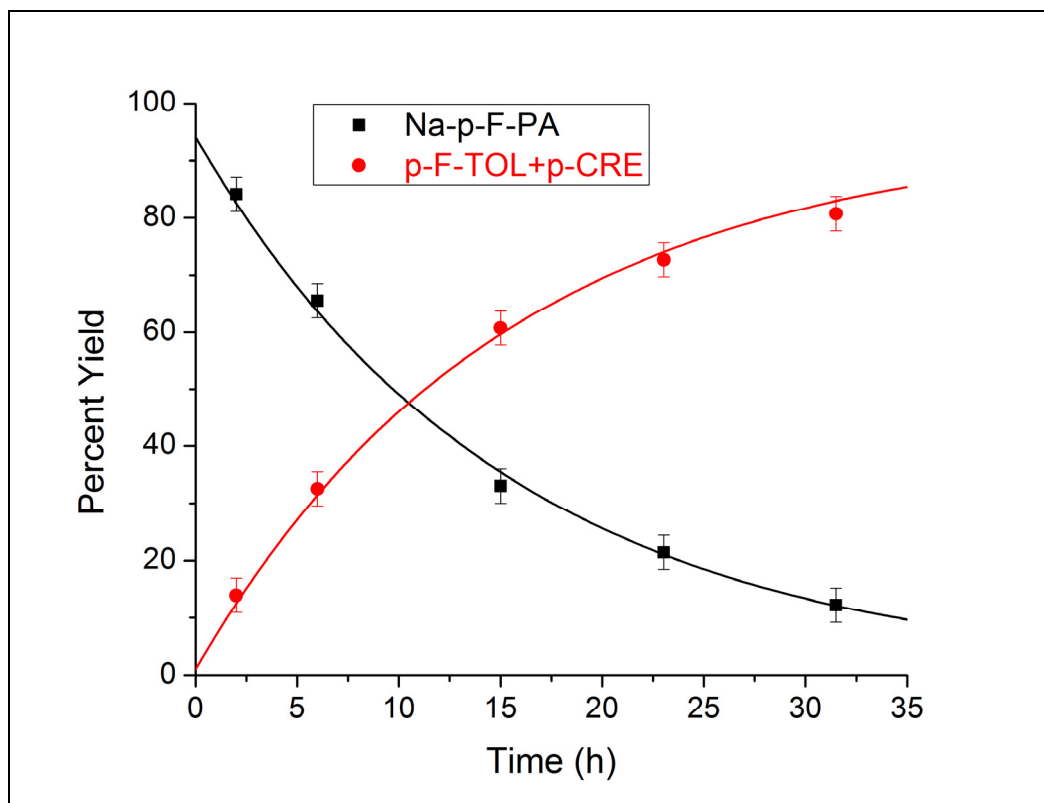
Fig. 15. Yields of m-fluorophenylacetic acid (m-F-PAA) and m-fluorotoluene (m-F-TOL) + m-cresol (m-CRE) as functions of time (denoted by symbols), from experiments with m-F-PAA in H_2O at 300°C and 1034 bar. The starting concentration of m-F-PAA was 1.02±0.02 molal. A 3% uncertainty in yields was assigned based on analysis of replicates in the entire dataset. First-order (exponential) kinetic curves were generated by performing least squares regression, and the best-fit apparent rate constant for disappearance of m-F-PAA is $(7\pm1)\times10^{-2}$ h^{-1}. The uncertainty in the rate constant was estimated by graphical analysis.
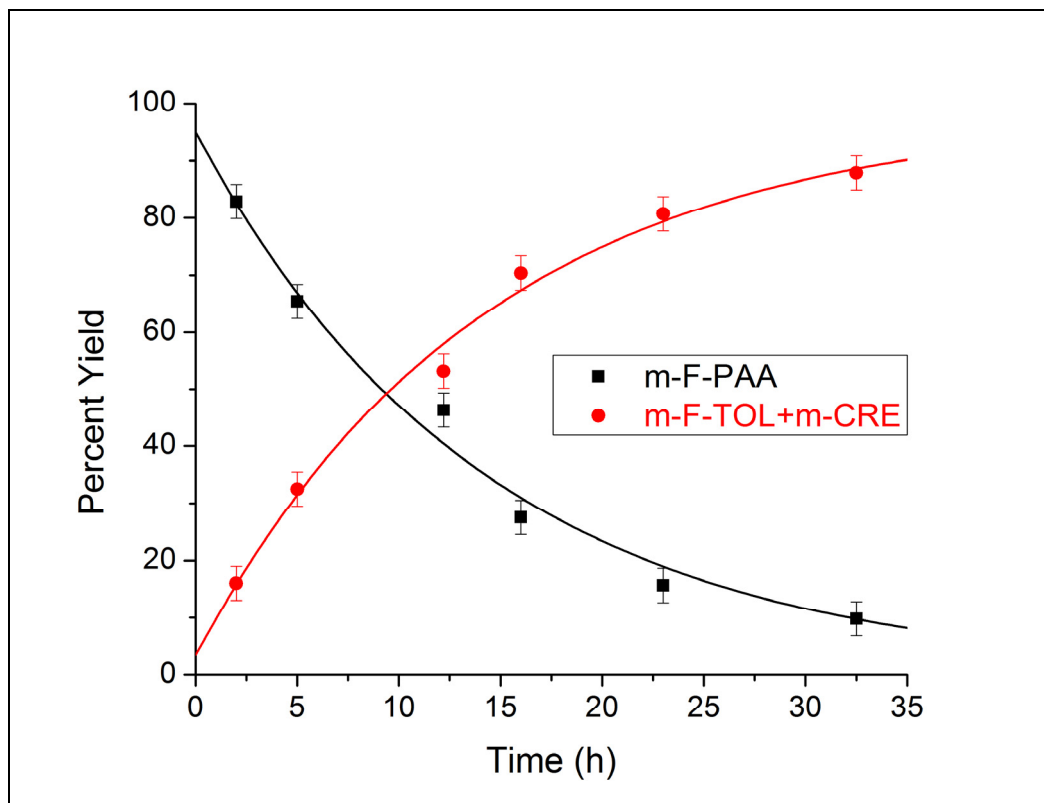
Fig. 16. Yields of sodium m-fluorophenylacetate (Na-m-F-PA) and m-fluorotoluene (m-F-TOL) + m-cresol (m-CRE) as functions of time (denoted by symbols), from experiments with Na-m-F-PA in H_2O at 300°C and 1034 bar. The starting concentration of Na-m-F-PA was 1.04±0.01 molal. A 3% uncertainty in yields was assigned based on analysis of replicates in the entire dataset. First-order (exponential) kinetic curves were generated by performing least squares regression, and the best-fit apparent rate constant for disappearance of Na-m-F-PA is $(1.1\pm0.2)\times10^{0}$ h^{-1}. The uncertainty in the rate constant was estimated by graphical analysis.
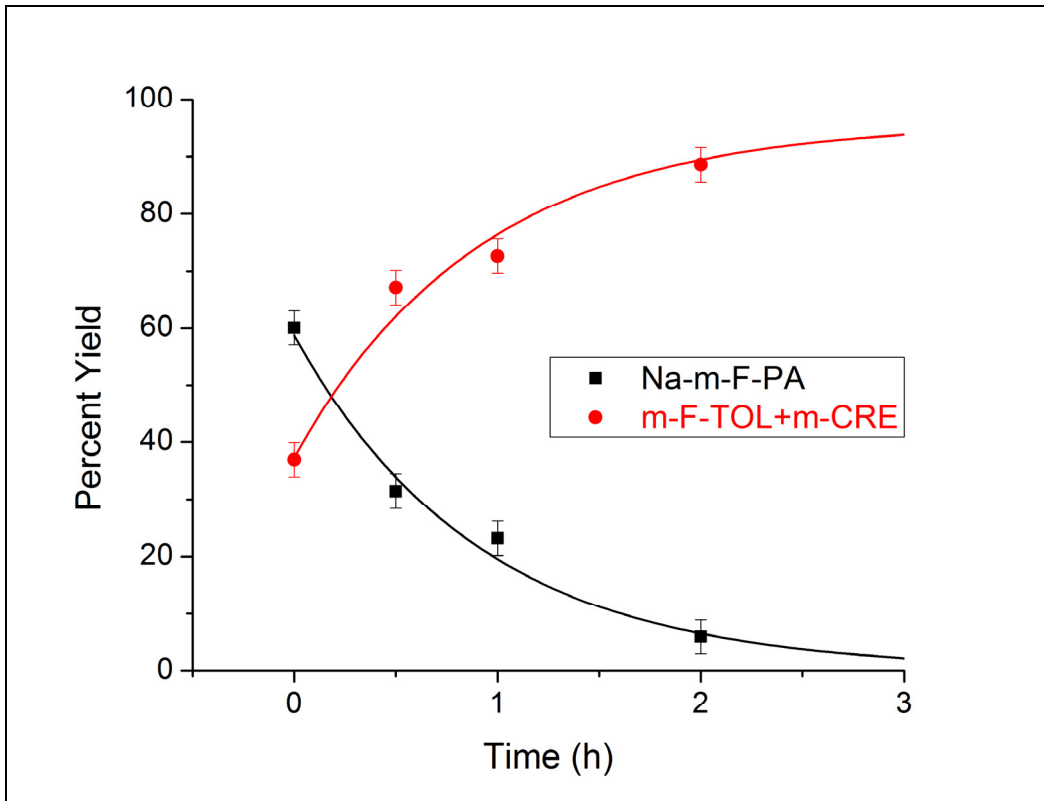
Fig. 17. Yields of o-fluorophenylacetic acid (o-F-PAA) and o-fluorotoluene (o-F-TOL) + o-cresol (o-CRE) as functions of time (denoted by symbols), from experiments with o-F-PAA in H_2O at 300°C and 1034 bar. The starting concentration of o-F-PAA was 1.03±0.01 molal. A 3% uncertainty in yields was assigned based on analysis of replicates in the entire dataset. First-order (exponential) kinetic curves were generated by performing least squares regression, and the best-fit apparent rate constant for disappearance of o-F-PAA is $(6.1\pm0.8)\times10^{-3}$ h^{-1}. The uncertainty in the rate constant was estimated by graphical analysis.

Fig. 18. Yields of sodium o-fluorophenylacetate (Na-o-F-PA) and o-fluorotoluene

(o-F-TOL) + o-cresol (o-CRE) as functions of time (denoted by symbols), from

experiments with Na-o-F-PA in H_2O at 300°C and 1034 bar. The starting

concentration of Na-o-F-PA was 1.02±0.03 molal. A 3% uncertainty in yields was

assigned based on analysis of replicates in the entire dataset. First-order

(exponential) kinetic curves were generated by performing least squares

regression, and the best-fit apparent rate constant for disappearance of Na-o-F-PA

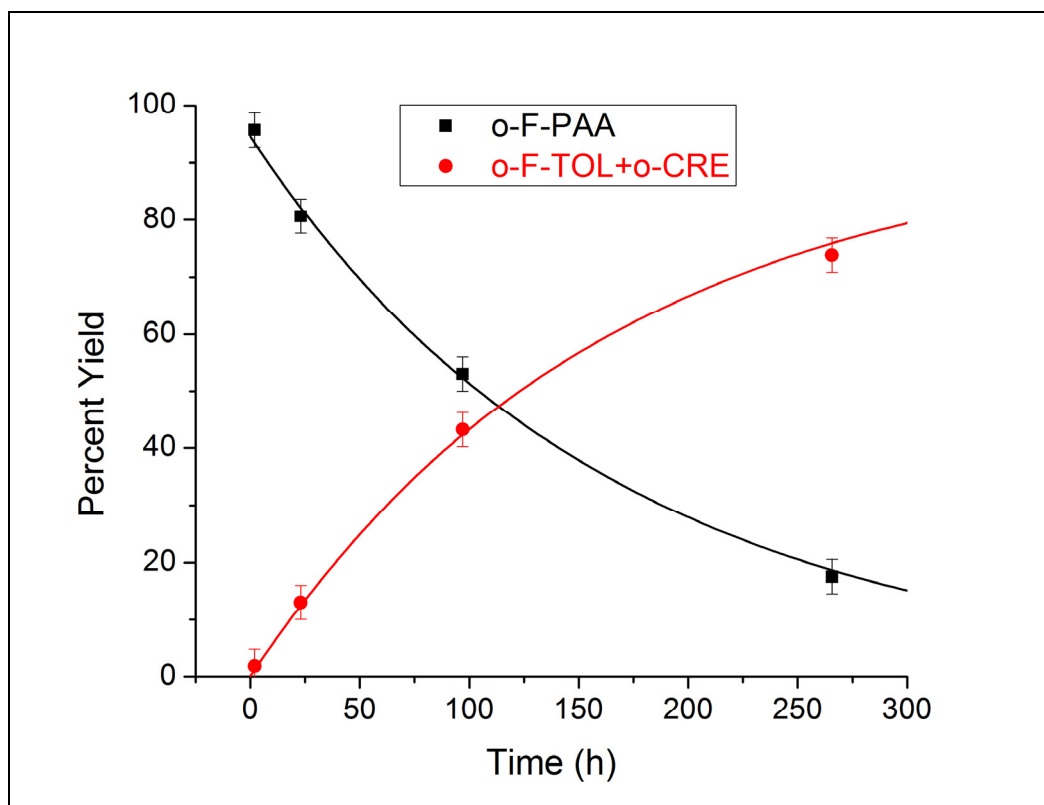is $(1.3\pm0.3)\times10^0$ h^{-1}. The uncertainty in the rate constant was estimated by
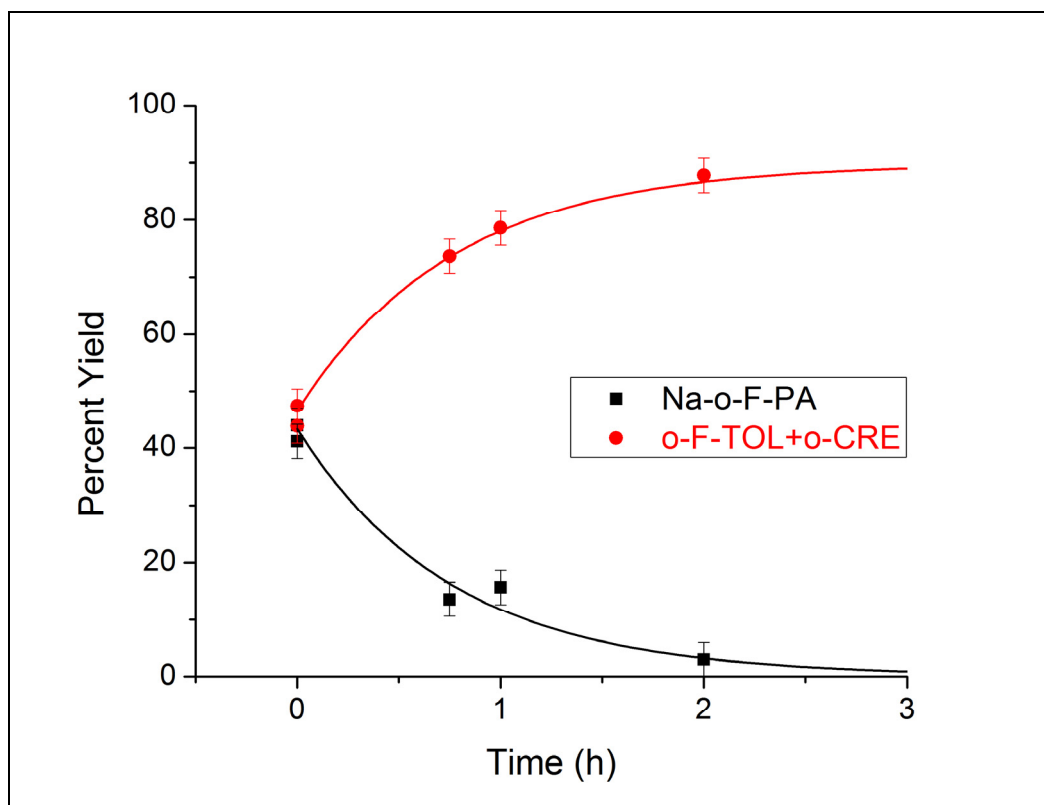
graphical analysis.

Fig. 19. Candidate mechanisms for decarboxylation of phenylacetic acid in water. The mechanisms are labeled alphabetically on the right side of the figure, and are separated by dashed black lines. Phenylacetic acid is the starting point for all mechanisms. Lowercase k's represent rate constants, and uppercase K's denote equilibrium constants. By assumption, single arrows designate irreversible steps, and double arrows designate reversible steps. Only one canonical resonance structure is shown for species with resonance. The bracketed structure with a double dagger at the upper-right corner of the bracket corresponds to a transition state, with bonds in red being broken and bonds in green being formed, and δ signifying fractional electric charge. In Mechanisms C-E, para protonation is shown for illustration, but ortho protonation is also possible.
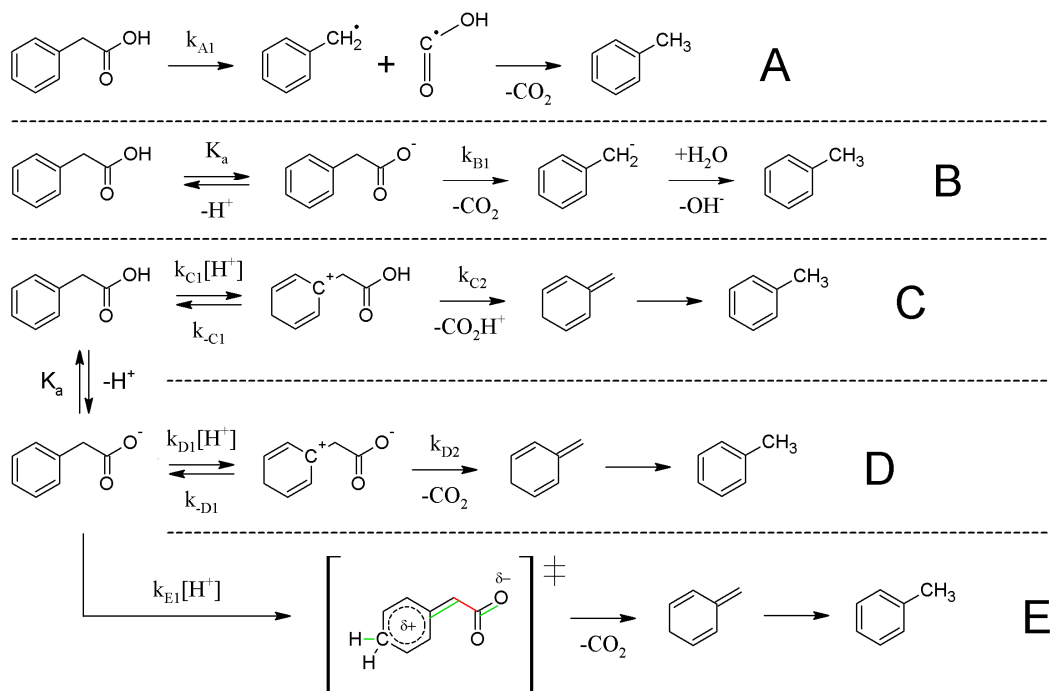
Fig. 20. Candidate mechanisms for decarboxylation of sodium phenylacetate in water. The mechanisms are labeled alphabetically on the right side of the figure, and are separated by dashed black lines. Sodium phenylacetate is the starting point for all mechanisms. Lowercase k's represent rate constants, and uppercase K's denote equilibrium constants. By assumption, single arrows designate irreversible steps, and double arrows designate reversible steps. Only one canonical resonance structure is shown for species with resonance. The bracketed structure with a double dagger at the upper-right corner of the bracket corresponds to a transition state, with bonds in red being broken and bonds in green being formed, and δ signifying fractional electric charge.

166
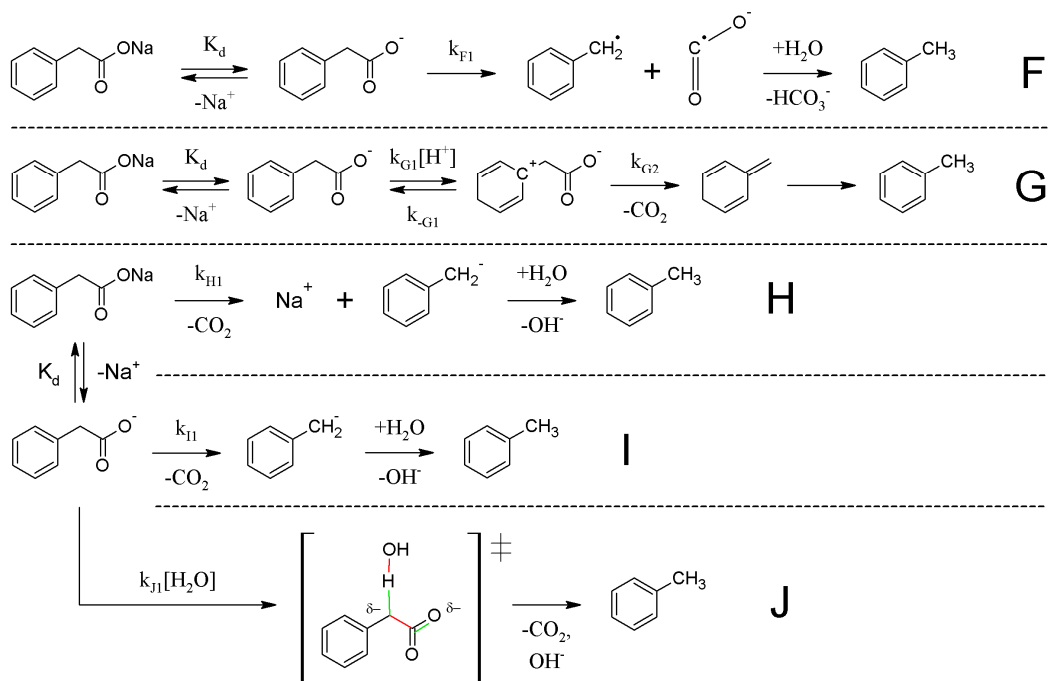
Fig. 21. Hammett plot for decarboxylation of phenylacetic acids (PAAs) in water at 300°C and 1034 bar. Logarithms of rate constants of decarboxylation are plotted as a function of Hammett substituent parameter σ^+, and symbols represent data from Table 5. The red line shows the best linear fit to the data, and the Hammett reaction constant ρ corresponds to the slope of the line. The uncertainty in ρ was estimated by graphical analysis.
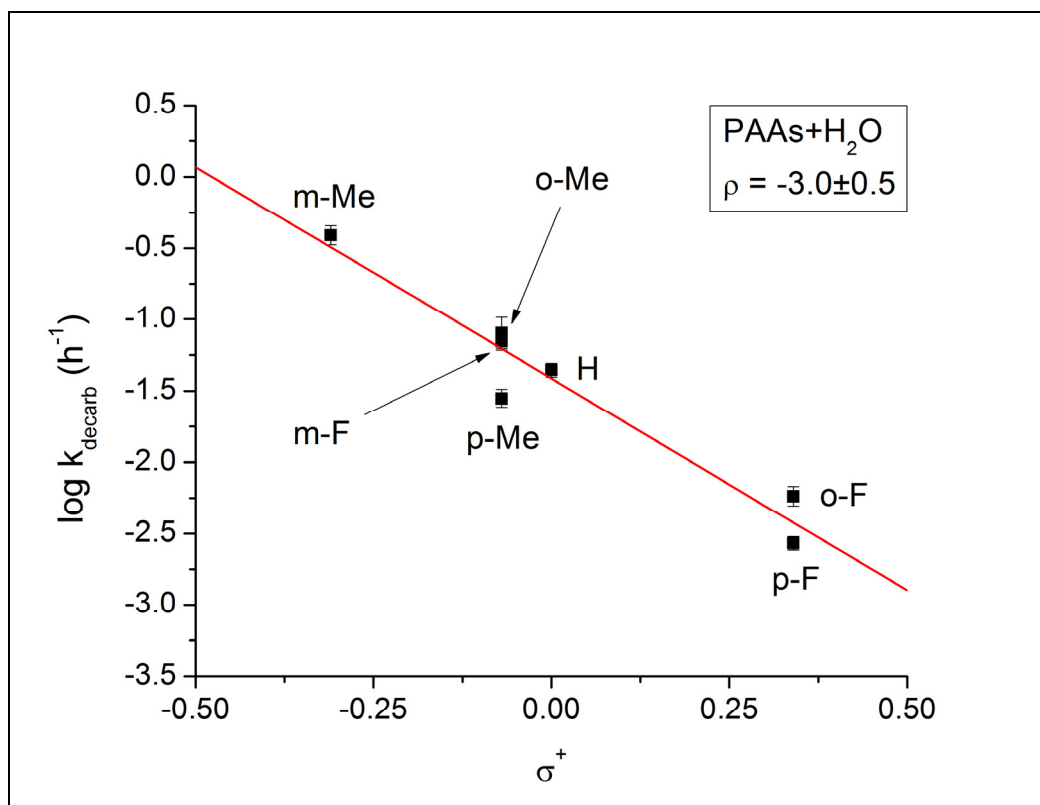
Fig. 22. Hammett plot for decarboxylation of sodium phenylacetates (Na-PAs) in water at 300°C and 1034 bar. Logarithms of rate constants of decarboxylation are plotted as a function of Hammett substituent parameter σ^-, and symbols represent data from Table 5. The red line shows the best linear fit to the data excluding the ortho substituents, and the Hammett reaction constant ρ corresponds to the slope of the line. The uncertainty in ρ was estimated by graphical analysis.
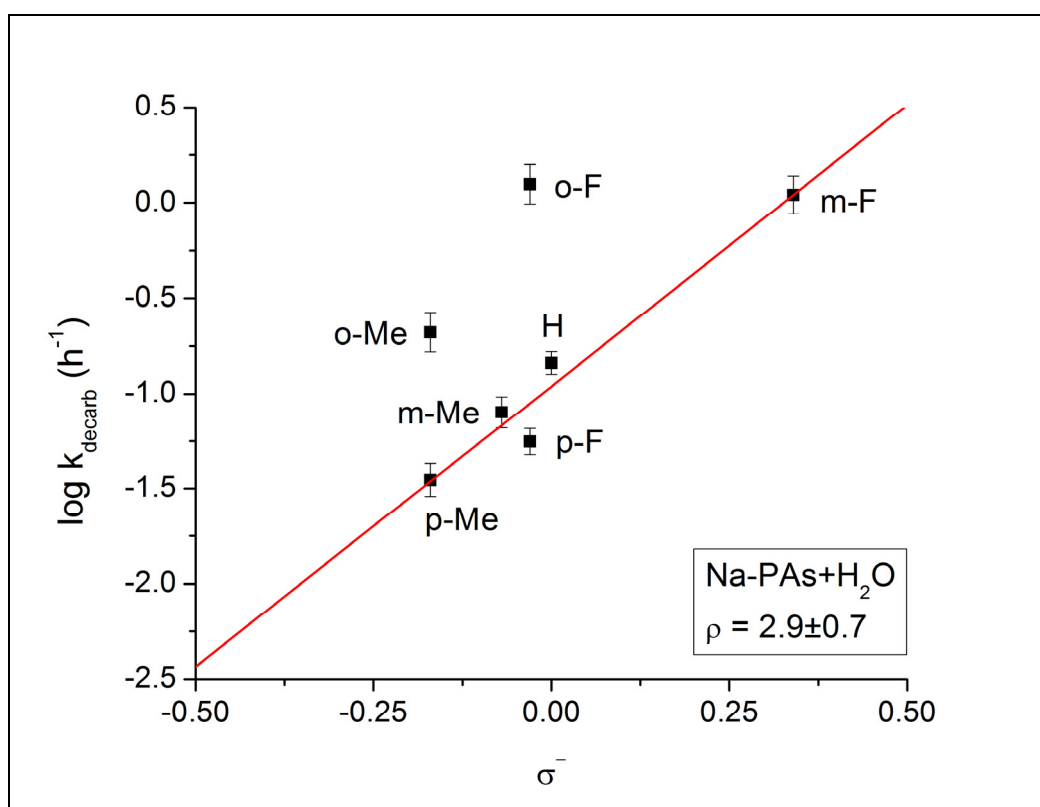
Fig. 23. Mass spectra of phenylacetic acid + D_2O experiments at 300°C and 1034 bar. Symbols denote relative abundances of tropylium cations derived from fragmentation of phenylacetic acid in the mass spectrometer. Before fragmentation, the tropylium cation was the benzyl group in phenylacetic acid. Points are connected by lines to clarify changes in the distribution, and lines correspond to experiments with different durations. The dashed orange line represents the m/z of $C_7H_7^+$, and the dashed violet line indicates the m/z of $C_7D_7^+$.
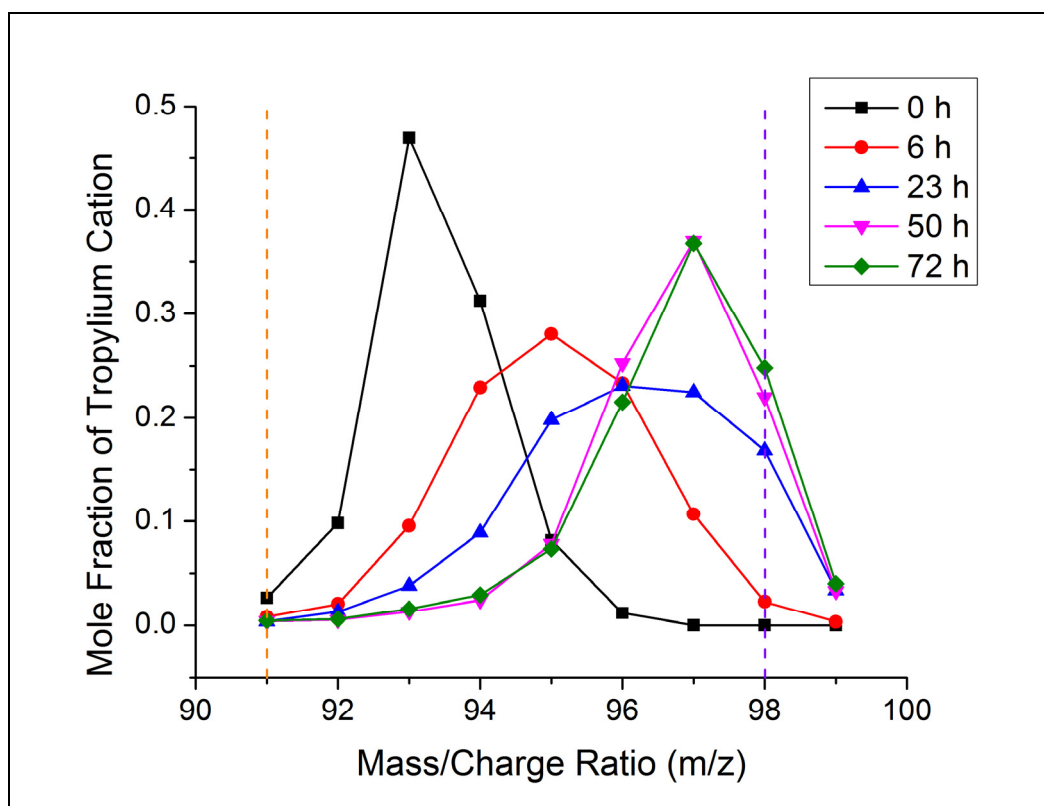
REFERENCES

Adamczyk K., Premont-Schwarz M., Pines D., Pines E. and Nibbering E. T. J. (2009) Real-time observation of carbonic acid formation in aqueous solution. *Science* **326**, 1690-1694.

Aharonson O. and 5 colleagues. (2009) An asymmetric distribution of lakes on Titan as a possible consequence of orbital forcing. *Nat. Geosci.* **2**, 851-854.

Ambrose D. (1956) The vapour pressures and critical temperatures of acetylene and carbon dioxide. *Trans. Faraday Soc.* **52**, 772-781.

Ambrose D. and Townsend R. (1964) Vapour pressure of acetylene. *Trans. Faraday Soc.* **60**, 1025-1029.

Amend J. P. and Helgeson H. C. (1997) Group additivity equations of state for calculating the standard molal thermodynamic properties of aqueous organic species at elevated temperatures and pressures. *Geochim. Cosmochim. Acta* **61**, 11-46.

Anderson G. M. (2005) *Thermodynamics of Natural Systems*. Cambridge University Press, New York.

Anslyn E. V. and Dougherty D. A. (2006) *Modern Physical Organic Chemistry*. University Science Books, Sausalito, California.

Arnett E. M. (1985) Solvation energies of organic ions. *J. Chem. Ed.* **62**, 385-391.

Atkins P. W. (1998) *Physical Chemistry*. Oxford University Press, New York.

Back M. H. and Sehon A. H. (1960) The thermal decomposition of phenylacetic acid. *Can. J. Chem.* **38**, 1261-1270.

Barker J. A. (1953) Determination of activity coefficients from total pressure measurements. *Aust. J. Chem.* **6**, 207-210.

Barnes J. W. and 16 colleagues. (2011) Organic sedimentary deposits in Titan's dry lakebeds: Probable evaporite. *Icarus* **216**, 136-140.

Barrett T. J., Anderson G. M. and Lugowski J. (1988) The solubility of hydrogen sulphide in 0-5 m NaCl solutions at 25°-95°C and one atmosphere. *Geochim. Cosmochim. Acta* **52**, 807-811.

Barth T. (1991) Organic acids and inorganic ions in waters from petroleum reservoirs, Norwegian continental shelf: A multivariate statistical analysis and comparison with American reservoir formation waters. *Appl. Geochem.* **6**, 1-15.

Bartlett P. D. and Ruchardt C. (1960) Peresters. IV. Substituent effects upon the concerted decomposition of t-butyl phenylperacetates. *J. Am. Chem. Soc.* **82**, 1756-1762.

Bell J. L. S. and Palmer D. A. (1994) Experimental studies of organic acid decomposition. In *Organic Acids in Geological Processes* (eds. E. D. Pittman and M. D. Lewan). Springer-Verlag, Berlin. pp. 226-269.

Bell J. L. S., Palmer D. A., Barnes H. L. and Drummond S. E. (1994) Thermal decomposition of acetate: III. Catalysis by mineral surfaces. *Geochim. Cosmochim. Acta* **58**, 4155-4177.

Belsky A. J., Maiella P. G. and Brill T. B. (1999) Spectroscopy of hydrothermal reactions. 13. Kinetics and mechanisms of decarboxylation of acetic acid derivatives at 100-260°C under 275 bar. *J. Phys. Chem. A* **103**, 4253-4260.

Bethke C. M. (2008) *Geochemical and Biogeochemical Reaction Modeling.* Cambridge University Press, New York.

Black C. (1958) Phase equilibria in binary and multicomponent systems: Modified van Laar-type equation. *Ind. Eng. Chem.* **50**, 403-412.

171

Bockrath B. and Dorfman L. M. (1974) Submicrosecond formation and observation of reactive carbanions. *J. Am. Chem. Soc.* **96**, 5708-5715.

Bourbo P. S. (1943) Vapor pressure of solid acetylene. *J. Phys.-USSR.* **7**, 286-288.

Brown B. R. (1951) The mechanism of thermal decarboxylation. *Q. Rev. Chem. Soc.* **5**, 131-146.

Brown H. C. and Okamoto Y. (1958) Electrophilic substituent constants. *J. Am. Chem. Soc.* **80**, 4979-4987.

Brown R. H. and 9 colleagues. (2008) The identification of liquid ethane in Titan's Ontario Lacus. *Nature* **454**, 607-610.

Bucker D. and Wagner W. (2006) A reference equation of state for the thermodynamic properties of ethane for temperatures from the melting line to 675 K and pressures up to 900 MPa. *J. Phys. Chem. Ref. Data* **35**, 205-266.

Buncel E., Venkatachalam T. K. and Menon B. C. (1984) A spectrophotometric study of 4-nitro-, 2,4-dinitro- and 2,4,6-trinitrobenzyl carbanions. Decarboxylation of (nitrophenyl)acetate anions. *J. Org. Chem.* **49**, 413-417.

Button R. G. and Taylor P. J. (1973) The decarboxylation of some heterocyclic acetic acids. Part II. Direct and indirect evidence for the zwitterionic mechanism. *J. Chem. Soc. Perk. Trans. II* **5**, 557-567.

Calado J. C. G., Garcia G. A. and Staveley L. A. K. (1974) Thermodynamics of the liquid system methane+propane. *J. Chem. Soc. Farad. Trans. I* **70**, 1445-1451.

Callahan B. P. and Wolfenden R. (2004) Charge development in the transition state for decarboxylations in water: Spontaneous and acetone-catalyzed decarboxylation of aminomalonate. *J. Am. Chem. Soc.* **126**, 4514-4515.

Carothers W. W. and Kharaka Y. K. (1978) Aliphatic acid anions in oil-field waters – Implications for origin of natural gas. *Am. Assoc. Petr. Geol. Bull.* **62**, 2441-2453.

Chang S. D. and Lu B. C. Y. (1967) Vapor-liquid equilibria in the nitrogen-methane-ethane system. *Chem. Eng. Prog. S. Ser.* **63**, 18-27.

Chao J., Wilhoit R. C. and Zwolinski B. J. (1973) Ideal gas thermodynamic properties of ethane and propane. *J. Phys. Chem. Ref. Data* **2**, 427-437.

Chase M. W., Jr. (1998) *NIST-JANAF Thermochemical Tables*, J. Phys. Chem. Ref. Data, Monograph No. 9. American Institute of Physics, New York.

Cheung H. and Wang D. I. J. (1964) Solubility of volatile gases in hydrocarbon solvents at cryogenic temperatures. *Ind. Eng. Chem. Fund.* **3**, 355-361.

Chien H. H. Y. and Null H. R. (1972) Generalized multicomponent equation for activity coefficient calculation. *Am. Inst. Chem. Eng. J.* **18**, 1177-1183.

Clark L. W. (1969) The decarboxylation reaction. In *The Chemistry of Carboxylic Acids and Esters* (ed. S. Patai). Interscience-Publishers, Hungary. pp. 589-622.

Clark R. N. and 15 colleagues. (2010) Detection and mapping of hydrocarbon deposits on Titan. *J. Geophys. Res.* **115**, E10005, doi:10.1029/2009JE003369.

Clementi S. and Katritzky A. R. (1973) The kinetics and mechanism of the electrophilic substitution of heteroaromatic compounds. Part XXXIII. Hammett treatment for hydrogen exchange of monosubstituted benzenes in sulphuric acid under standard conditions. *J. Chem. Soc. Perk. Trans. II* **7**, 1077-1080.

CODATA (Committee on Data for Science and Technology). (2010) *Internationally Recommended Values of Fundamental Physical Constants*. 21 Mar. 2012 < http://physics.nist.gov/cuu/Constants/index.html>.

Cordier D., Mousis O., Lunine J. I., Lavvas P. and Vuitton V. (2009) An estimate of the chemical composition of Titan's lakes. *Astrophys. J. Lett.* **707**, L128-L131.

Cordier D. and 6 colleagues. (2010) About the possible role of hydrocarbon lakes in the origin of Titan's noble gas atmospheric depletion. *Astrophys. J. Lett.* **721**, L117-L120.

Cordier D. and 7 colleagues. (2012) Titan's lakes chemical composition: Sources of uncertainties and variability. *Planet. Space Sci.* **61**, 99-107.

Coustenis A. and 155 colleagues. (2009) TandEM: Titan and Enceladus mission. *Exp. Astron.* **23**, 893-946.

Coustenis A. and 12 colleagues. (2010) Titan trace gaseous composition from CIRS at the end of the Cassini-Huygens prime mission. *Icarus* **207**, 461-476.

Cox R. A. (1991) Isotope effects in acid-catalyzed aromatic hydrogen exchange. *J. Phys. Org. Chem.* **4**, 233-241.

Cox R. A. (2011) A greatly under-appreciated fundamental principle of physical organic chemistry. *Int. J. Mol. Sci.* **12**, 8316-8332.

Craig H. (1961) Isotopic variations in meteoric waters. *Science* **133**, 1702-1703.

Crossey L. J. (1991) Thermal degradation of aqueous oxalate species. *Geochim. Cosmochim. Acta* **55**, 1515-1527.

Cutler A. J. B. and Morrison J. A. (1965) Excess thermodynamic functions for liquid mixtures of methane+propane. *Trans. Faraday Soc.* **61**, 429-442.

Dippy J. F. J. and Williams F. R. (1934) Chemical constitution and the dissociation constants of monocarboxylic acids. Part I. Some substituted phenylacetic acids. *J. Chem. Soc.*, 161-166.

Djordjevich L. and Budenholzer R. A. (1970) Vapor-liquid equilibrium data for ethane-propane system at low temperatures. *J. Chem. Eng. Data* **15**, 10-12.

Drever J. I. (1997) *The Geochemistry of Natural Waters: Surface and Groundwater Environments*. Prentice Hall, Upper Saddle River, New Jersey.

Dubouloz N., Raulin F., Lellouch E. and Gautier D. (1989) Titan's hypothesized ocean properties: The influence of surface temperature and atmospheric composition uncertainties. *Icarus* **82**, 81-96.

Eby G. N. (2004) *Principles of Environmental Geochemistry*. Brooks/Cole, Belmont, California.

Eddy R. D. and Menzies A. W. C. (1940) The solubilities of certain inorganic compounds in ordinary water and in deuterium water. *J. Phys. Chem.* **44**, 207-235.

Elachi C. and 34 colleagues. (2006) Titan Radar Mapper observations from Cassini's T$_3$ fly-by. *Nature* **441**, 709-713.

Ellington R. T., Eakin B. E., Parent J. D., Gami D. C. and Bloomer O. T. (1959) Vapor-liquid phase equilibria in the binary systems of methane, ethane and nitrogen. In *Thermodynamic and Transport Properties of Gases, Liquids and Solids* (ed. Y. S. Touloukian). The American Society of Mechanical Engineers, New York. pp. 180-194.

Epling G. A. and Lopes A. (1977) Fragmentation pathways in the photolysis of phenylacetic acid. *J. Am. Chem. Soc.* **99**, 2700-2704.

Erickson K. M., Arcis H, Raffa D., Zimmerman G. H. and Tremaine P. R. (2011) Deuterium isotope effects on the ionization constant of acetic acid in H_2O and D_2O by AC conductance from 368 to 548 K at 20 MPa. *J. Phys. Chem. B* **115**, 3038-3051.

Fedorova M. F. (1940) Solubility of acetylene and carbon dioxide in liquid nitrogen and liquid oxygen. *Zh. Fiz. Khim.* **14**, 422-426.

Fein J. B., Yane L. and Handa T. (1994) The effect of aqueous complexation on the decarboxylation rate of oxalate. *Geochim. Cosmochim. Acta* **58**, 3975-3981.

Fisher J. B. (1987) Distribution and occurrence of aliphatic acid anions in deep subsurface waters. *Geochim. Cosmochim. Acta* **51**, 2459-2468.

Focke W. W. (2001) Local composition structured fluid model for the excess Gibbs energy of liquid mixtures. *Ind. Eng. Chem. Res.* **40**, 2971-2981.

Franks S. G. and 6 colleagues (2001) Carbon isotopic composition of organic acids in oil field waters, San Joaquin Basin, California, USA. *Geochim. Cosmochim. Acta* **65**, 1301-1310.

Fu J., Lu X. and Savage P. E. (2010) Catalytic hydrothermal deoxygenation of palmitic acid. *Energ. Environ. Sci.* **3**, 311-317.

Fuks S. and Bellemans A. (1967) Excess free energies and volumes of two simple binary liquid mixtures: Methane-krypton and nitrogen-methane. *B. Soc. Chim. Belg.* **76**, 290-299.

Fulchignoni M. and 42 colleagues. (2005) In situ measurements of the physical characteristics of Titan's environment. *Nature* **438**, 785-791.

Gabis D. H. (1991) Liquid-Vapor Equilibrium at 90-160 K for Systems containing Nitrogen, Methane, and Ethane. Ph. D. thesis, Cornell University.

Gajewski J. J. and Gortva A. M. (1982) Bimolecular thermal reactions of 5-methylene-1,3-cyclohexadiene (o-isotoluene) and 3-methylene-1,4-cyclohexadiene (p-isotoluene). *J. Am. Chem. Soc.* **104**, 334-335.

Garrels R. M. and Christ C. L. (1965) *Solutions, Minerals, and Equilibria*. Freeman, Cooper & Company, San Francisco, California.

Gasem K. A. M., Hiza M. J. and Kidnay A. J. (1981) Phase behavior in the nitrogen + ethylene system from 120 to 200 K. *Fluid Phase Equilibr.* **6**, 181-189.

Glein C. R., Desch S. J. and Shock E. L. (2009) The absence of endogenic methane on Titan and its implications for the origin of atmospheric nitrogen. *Icarus* **204**, 637-644.

Gomes de Azevedo E. J. S. and Calado J. C. G. (1989) Thermodynamics of liquid methane+ethane. *Fluid Phase Equilibr.* **49**, 21-34.

Goudie A. S. (1983) Calcrete. In *Chemical Sediments and Geomorphology: Precipitates and Residua in the Near-Surface Environment* (eds. A. S. Goudie and K. Pye). Academic Press, New York. pp. 93-131.

Gould E. S. (1959) *Mechanism and Structure in Organic Chemistry*. Holt, Rinehart and Winston, New York.

Griffith C. A. and 7 colleagues. (2012) Possible tropical lakes on Titan from observations of dark terrain. *Nature* **486**, 237-239.

Guedes H. J. R., Zollweg J. A., Filipe E. J. M., Martins L. F. G. and Calado J. C. G. (2002) Thermodynamics of liquid (nitrogen + ethane). *J. Chem. Thermodyn.* **34**, 669-678.

Guthrie J. P., Peiris S., Simkin M. and Wang Y. (2010) Rate constants for decarboxylation reactions calculated using no barrier theory. *Can. J. Chem.* **88**, 79-98.

Hansch C., Leo A. and Taft R. W. (1991) A survey of Hammett substituent constants and resonance and field parameters. *Chem. Rev.* **91**, 165-195.

Hayes A. and 13 colleagues. (2008) Hydrocarbon lakes on Titan: Distribution and interaction with a porous regolith. *Geophys. Res. Lett.* **35**, L09204, doi:10.1029/2008GL033409.

Hayes A. G. and 14 colleagues. (2011) Transient surface liquid in Titan's polar regions from Cassini. *Icarus* **211**, 655-671.

Heintz A. and Bich E. (2009) Thermodynamics in an icy world: The atmosphere and internal structure of Saturn's moon Titan. *Pure Appl. Chem.* **81**, 1903-1920.

Helgeson H. C. (1969) Thermodynamics of hydrothermal systems at elevated temperatures and pressures. *Am. J. Sci.* **267**, 729-804.

Helgeson H. C., Knox A. M., Owens C. E. and Shock E. L. (1993) Petroleum, oil field waters, and authigenic mineral assemblages: Are they in metastable equilibrium in hydrocarbon reservoirs? *Geochim. Cosmochim. Acta* **57**, 3295-3339.

Hildebrand J. H. and Scott R. L. (1950) *The Solubility of Nonelectrolytes*. Reinhold Publishing Corporation, New York.

Hiza M. J., Miller R. C. and Kidnay A. J. (1979) A review, evaluation, and correlation of the phase equilibria, heat of mixing, and change in volume on mixing for liquid mixtures of methane + ethane. *J. Phys. Chem. Ref. Data* **8**, 799-816.

Hiza M. J., Kidnay A. J. and Miller R. C. (1982) *Equilibrium Properties of Fluid Mixtures 2: A Bibliography of Experimental Data on Selected Fluids*. IFI/Plenum, New York.

Hodyss R., Johnson P. V. and Kanik I. (2010) Experimental determination of the solubilities of organics and rare gases in simulated Titan lake solutions. *Astrobio. Sci. Conf.*, #5294 (abstr.).

Hodyss R., Choukroun M., Sotin C. and Beauchamp P. (2012) The solubility of
    [40]Ar in liquid hydrocarbons: Implications for Titan's geological evolution.
    Titan Through Time 2 Workshop (eds. V. Cottini, C. Nixon and R.
    Lorenz), p.80 (abstr.).

Holland T. and Powell R. (2003) Activity-composition relations for phases in
    petrological calculations: An asymmetric multicomponent formulation.
    Contrib. Mineral. Petrol. **145**, 492-501.

Houssin-Agbomson D., Coquelet C., Richon D. and Arpentinier P. (2010)
    Equipment using a "static-analytic" method for solubility measurements in
    potentially hazardous binary mixtures under cryogenic temperatures.
    Cryogenics **50**, 248-256.

Hunter D. H., Hamity M., Patel V. and Perry R. A. (1978) Crown ether catalysis
    of decarboxylation: A general survey of reactivity and a detailed analysis
    of the triphenylacetate anion. *Can. J. Chem.* **56**, 104-113.

Ingold C. K. (1969) *Structure and Mechanism in Organic Chemistry.* Cornell
    University Press, Ithaca, New York.

Ishkin I. P. and Burbo P. Z. (1939) Solubility of solid acetylene and carbon
    dioxide in liquid oxygen, nitrogen and oxygen-nitrogen mixtures. *Zh. Fiz.
    Khim.* **13**, 1337-1339.

Jaffe H. H. (1953) A reexamination of the Hammett equation. *Chem. Rev.* **53**,
    191-261.

Jaumann R. and 10 colleagues. (2009) Geology and surface processes on Titan. In
    Titan from Cassini-Huygens (eds. R. H. Brown, J. P. Lebreton and J. H.
    Waite). Springer, New York. pp. 75-140.

Jencks W. P. (1981) How does a reaction choose its mechanism? *Chem. Soc. Rev.*
    10, 345-375.

Jennings D. E. and 19 colleagues. (2009) Titan's surface brightness temperatures. *Astrophys. J. Lett.* **691**, L103-L105.

Johnson C. D. (1973) *The Hammett Equation.* Cambridge University Press, London.

Johnson J. W. and Norton D. (1991) Critical phenomena in hydrothermal systems: State, thermodynamic, electrostatic, and transport properties of H_2O in the critical region. *Am. J. Sci.* **291**, 541-648.

Johnson J. W., Oelkers E. H. and Helgeson H. C. (1992) SUPCRT92: A software package for calculating the standard molal thermodynamic properties of minerals, gases, aqueous species, and reactions from 1 to 5000 bar and 0 to 1000°C. *Comput. Geosci.* **18**, 899-947.

Jorgensen W. L., Briggs J. M. and Gao J. (1987) A priori calculations of pK_a's for organic compounds in water. The pK_a of ethane. *J. Am. Chem. Soc.* **109**, 6857-6858.

Kanabus-Kaminska J. M., Gilbert B. C. and Griller D. (1989) Solvent effects on the thermochemistry of free-radical reactions. *J. Am. Chem. Soc.* **111**, 3311-3314.

Katritzky A. R., Balasubramanian M. and Siskin M. (1990a) Aqueous high-temperature chemistry of carbo- and heterocycles. 2. Monosubstituted benzenes: Benzyl alcohol, benzaldehyde, and benzoic acid. *Energ. Fuel.* **4**, 499-505.

Katritzky A. R., Luxem F. J. and Siskin M. (1990b) Aqueous high-temperature chemistry of carbo- and heterocycles. 5. Monosubstituted benzenes with a two carbon atom side chain oxygenated at the ß-position. *Energ. Fuel.* **4**, 514-517.

Katritzky A. R., Luxem F. J. and Siskin M. (1990c) Aqueous high-temperature chemistry of carbo- and heterocycles. 7. Monosubstituted benzenes with two carbon atom side chains oxygenated at the α- and ß-positions. *Energ. Fuel.* **4**, 525-531.

Kemp D. S. and Paul K. G. (1975) The physical organic chemistry of benzisoxazoles. III. The mechanism and the effects of solvents on rates of decarboxylation of benzisoxazole-3-carboxylic acids. *J. Am. Chem. Soc.* **97**, 7305-7318.

Kharaka Y. F., Carothers W. W. and Rosenbauer R. J. (1983) Thermal decarboxylation of acetic acid: Implications for origin of natural gas. *Geochim. Cosmochim. Acta* **47**, 397-402.

Kidnay A. J., Miller R. C., Sloan E. D. and Hiza M. J. (1985) A review and evaluation of the phase equilibria, liquid-phase heats of mixing and excess volumes, and gas-phase PVT measurements for nitrogen + methane. *J. Phys. Chem. Ref. Data* **14**, 681-694.

Kluger R. and Mundle S. O. C. (2010) The role of pre-association in Bronsted acid-catalyzed decarboxylation and related processes. *Adv. Phys. Org. Chem.* **44**, 357-375.

Kotz J. C. and Treichel P. Jr. (1999) *Chemistry and Chemical Reactivity.* Saunders College Publishing, Orlando, Florida.

Kouvaris L. C. and Flasar F. M. (1991) Phase equilibrium of methane and nitrogen at low temperatures: Application to Titan. *Icarus* **91**, 112-124.

Kremer H. and Knapp H. (1983) Three-phase conditions are predictable. *Hydrocarb. Process.* **62**, 79-83.

Kresge A. J. and Chiang Y. (1967) Aromatic protonation. III. Kinetic hydrogen isotope effects on acid-catalyzed aromatic hydrogen exchange in 1,3,5-trimethoxybenzene. *J. Am. Chem. Soc.* **89**, 4411-4417.

Kunz O., Klimeck R., Wagner W. and Jaeschke M. (2007) *The GERG-2004 Wide-Range Equation of State for Natural Gases and Other Mixtures*, GERG TM-15. Fortschr.-Ber. VDI, Reihe 6, Nr. 557, VDI Verlag, Dusseldorf, Germany.

Langhans M. H. and 13 colleagues. (2012) Titan's fluvial valleys: Morphology, distribution, and spectral properties. *Planet. Space Sci.* **60**, 34-51.

Lasaga A. C. (1998) *Kinetic Theory in the Earth Sciences*. Princeton University Press, Princeton, New Jersey.

Laughton P. M. and Robertson R. E. (1969) Solvent isotope effects for equilibria and reactions. In *Solute-Solvent Interactions* (eds. J. F. Coetzee and C. D. Ritchie). Marcel Dekker, New York. pp. 399-538.

Lavvas P. P., Coustenis A. and Vardavas I. M. (2008a) Coupling photochemistry with haze formation in Titan's atmosphere, Part I: Model description. *Planet. Space Sci.* **56**, 27-66.

Lavvas P. P., Coustenis A. and Vardavas I. M. (2008b) Coupling photochemistry with haze formation in Titan's atmosphere, Part II: Results and validation with Cassini/Huygens data. *Planet. Space Sci.* **56**, 67-99.

Lawlor D. A., More O'Ferrall R. A. and Rao S. N. (2008) Stabilities and partitioning of arenonium ions in aqueous media. *J. Am. Chem. Soc.* **130**, 17997-18007.

Lemmon E. W., McLinden M. O. and Wagner W. (2009) Thermodynamic properties of propane. III. A reference equation of state for temperatures from the melting line to 650 K and pressures up to 1000 MPa. *J. Chem. Eng. Data* **54**, 3141-3180.

Lemmon E. W., Huber M. L. and McLinden M. O. (2010) *NIST Standard Reference Database 23: Reference Fluid Thermodynamic and Transport Properties-REFPROP*, Version 9.0. National Institute of Standards and Technology, Standard Reference Data Program, Gaithersburg, Maryland.

Li J. and Brill T. B. (2003) Spectroscopy of hydrothermal reactions 23: The effect of OH substitution on the rates and mechanisms of decarboxylation of benzoic acid. *J. Phys. Chem. A* **107**, 2667-2673.

Llave F. M., Luks K. D. and Kohn J. P. (1985) Three-phase liquid-liquid-vapor equilibria in the binary systems nitrogen + ethane and nitrogen + propane. *J. Chem. Eng. Data* **30**, 435-438.

Llave F. M., Luks K. D. and Kohn J. P. (1987) Three-phase liquid-liquid-vapor equilibria in the nitrogen + methane + ethane and nitrogen + methane + propane systems. *J. Chem. Eng. Data* **32**, 14-17.

Lorenz R. D. and Lunine J. I. (1996) Erosion on Titan: Past and present. *Icarus* **122**, 79-91.

Lorenz R. D. and 39 colleagues. (2006) The sand seas of Titan: Cassini RADAR observations of longitudinal dunes. *Science* **312**, 724-727.

Lorenz R. D. and 15 colleagues. (2008a) Fluvial channels on Titan: Initial Cassini RADAR observations. *Planet. Space Sci.* **56**, 1132-1144.

Lorenz R. D. and 15 colleagues. (2008b) Titan's inventory of organic surface materials. *Geophys. Res. Lett.* **35**, L02206, doi:10.1029/2007GL032118.

Lundegard P. D. and Kharaka Y. K. (1994) Distribution and occurrence of organic acids in subsurface waters. In *Organic Acids in Geological Processes* (eds. E. D. Pittman and M. D. Lewan). Springer-Verlag, Berlin. pp. 40-69.

Lunine J. I. (1985) Volatiles in the Outer Solar System: I. Thermodynamics of Clathrate Hydrates. II. Ethane Ocean on Titan. III. Evolution of Primordial Titan Atmosphere. Ph. D. thesis, California Institute of Technology.

Lunine J. I. and Lorenz R. D. (2009) Rivers, lakes, dunes, and rain: Crustal processes in Titan's methane cycle. *Annu. Rev. Earth Planet. Sci.* **37**, 299-320.

Lunine J. I., Stevenson D. J. and Yung Y. L. (1983) Ethane ocean on Titan. *Science* **222**, 1229-1230.

MacGowan D. B. and Surdam R. C. (1990) Carboxylic acid anions in formation waters, San Joaquin Basin and Louisiana Gulf Coast, U.S.A. – Implications for clastic diagenesis. *Appl. Geochem.* **5**, 687-701.

Magee B. A. and 5 colleagues. (2009) INMS-derived composition of Titan's upper atmosphere: Analysis methods and model comparison. *Planet. Space Sci.* **57**, 1895-1916.

Maiella P. G. and Brill T. B. (1996) Spectroscopy of hydrothermal reactions. 5. Decarboxylation kinetics of malonic acid and monosodium malonate. *J. Phys. Chem.* **100**, 14352-14355.

Malaska M. and 5 colleagues. (2011) Surface dissolution model for Titan karst. *First Int. Planet. Cave Res. Worksh.*, #8018 (abstr.).

Marenich A. V., Cramer C. J. and Truhlar D. G. (2009) Universal solvation model based on solute electron density and on a continuum model of the solvent defined by the bulk dielectric constant and atomic surface tensions. *J. Phys. Chem. B* **113**, 6378-6396.

Marion G. M. and Kargel J. S. (2008) *Cold Aqueous Planetary Geochemistry with FREZCHEM: From Modeling to the Search for Life at the Limits.* Springer, Berlin.

Matteson D. S. (1984) Acetylene on Titan. *Science* **223**, 1131.

McClure D. W., Lewis K. L., Miller R. C. and Staveley L. A. K. (1976) Excess enthalpies and Gibbs free energies for nitrogen + methane at temperatures below the critical point of nitrogen. *J. Chem. Thermodyn.* **8**, 785-792.

McCollom T. M. and Seewald J. S. (2003) Experimental study of the hydrothermal reactivity of organic acids and acid anions: II. Acetic acid, acetate, and valeric acid. *Geochim. Cosmochim. Acta* **67**, 3645-3664.

McCollom T. M., Seewald J. S. and Simoneit B. R. T. (2001) Reactivity of monocyclic aromatic compounds under hydrothermal conditions. *Geochim. Cosmochim. Acta* **65**, 455-468.

McIntosh D. (1907) The physical properties of liquid and solid acetylene. *J. Phys. Chem.* **11**, 306-317.

McKay C. P. and Smith H. D. (2005) Possibilities for methanogenic life in liquid methane on the surface of Titan. *Icarus* **178**, 274-276.

McKay C. P., Pollack J. B., Lunine J. I. and Courtin R. (1993) Coupled atmosphere-ocean models of Titan's past. *Icarus* **102**, 88-98.

Mesmer R. E. and Herting D. L. (1978) Thermodynamics of ionization of D_2O and $D_2PO_4^-$. *J. Solution Chem.* **7**, 901-913.

Miksa D., Li J. and Brill T. B. (2002) Spectroscopy of hydrothermal reactions 22. The effects of cations on the decarboxylation kinetics of trifluoroacetate, cyanoacetate, propiolate, and malonate ions. *J. Phys. Chem. A* **106**, 11107-11114.

Miller R. C. and Staveley L. A. K. (1976) Excess enthalpies for some binary liquid mixtures of low-molecular-weight alkanes. *Adv. Cryog. Eng.* **21**, 493-500.

Miller R. C., Kidnay A. J. and Hiza M. J. (1980) A review, evaluation, and correlation of the phase equilibria, heat of mixing, and change in volume on mixing for liquid mixtures of methane + propane. *J. Phys. Chem. Ref. Data* **9**, 721-734.

Mironenko M. V., Melikhova T. Yu., Zolotov M. Yu. and Akinfiev N. N. (2008) GEOCHEQ_M: Program complex for thermodynamic and kinetic modeling of geochemical processes in rock-water-gas systems, Version 2008. *Herald DGGGMS RAS* 1(26).

Mitchell K. L. and Malaska M. (2011) Karst on Titan. *First Int. Planet. Cave Res. Worksh.*, #8021 (abstr.).

Mitchell K. L. and 11 colleagues. (2008) The formation of high latitude karst lakes on Titan and implications for the existence of polar caps. *Lunar Planet. Sci. Conf.*, #2170 (abstr.).

Mitri G., Showman A. P., Lunine J. I. and Lorenz R. D. (2007) Hydrocarbon lakes on Titan. *Icarus* **186**, 385-394.

Moriconi M. L. and 6 colleagues. (2010) Characterization of Titan's Ontario Lacus region from Cassini/VIMS observations. *Icarus* **210**, 823-831.

Morrison T. J. (1944) The salting-out effect. *Trans. Faraday Soc.* **40**, 43-48.

Mundle S. O. C., Lacrampe-Couloume G., Sherwood Lollar B. and Kluger R. (2010) Hydrolytic decarboxylation of carboxylic acids and the formation of protonated carbonic acid. *J. Am. Chem. Soc.* **132**, 2430-2436.

Nagaoka T., Berinstain A. B., Griller D. and Wayner D. D. M. (1990) Acidities of arenium ions in acetonitrile. *J. Org. Chem.* **55**, 3707-3708.

Neely B. J., Wagner J., Robinson R. L. and Gasem K. A. M. (2008) Mutual solubility measurements of hydrocarbon-water systems containing benzene, toluene, and 3-methylpentane. *J. Chem. Eng. Data* **53**, 165-174.

Neumann A. and Mann R. (1969) Solubility of solid acetylene in liquid methane-ethylene mixtures. *Chem.-Ing.-Tech.* **41**, 708-711.

Niemann H. B. and 9 colleagues. (2010) Composition of Titan's lower atmosphere and simple surface volatiles as measured by the Cassini-Huygens probe gas chromatograph mass spectrometer experiment. *J. Geophys. Res.* **115**, E12006, doi:10.1029/2010JE003659.

Okada K., Imashuku Y. and Yao M. (1997) Microwave spectroscopy of supercritical water. *J. Chem. Phys.* **107**, 9302-9311.

Okada K., Yao M., Hiejima Y., Kohno H. and Kajihara Y. (1999) Dielectric relaxation of water and heavy water in the whole fluid phase. *J. Chem. Phys.* **110**, 3026-3036.

Omar M. H., Dokoupil Z. and Schroten H. G. M. (1962) Determination of the solid-liquid equilibrium diagram for the nitrogen-methane system. *Physica* **28**, 309-329.

Palmer D. A. and Drummond S. E. (1986) Thermal decarboxylation of acetate. Part I. The kinetics and mechanism of reaction in aqueous solution. *Geochim. Cosmochim. Acta* **50,** 813-823.

Parrish W. R. and Hiza M. J. (1974) Liquid-vapor equilibria in the nitrogen-methane system between 95 and 120 K. *Adv. Cryog. Eng.* **19**, 300-308.

Pearson R. E. and Martin J. C. (1963) The mechanism of benzylic bromination with N-bromosuccinimide. *J. Am. Chem. Soc.* **85**, 354-355.

Peng D. Y. (2010) Extending the van Laar model to multicomponent systems. *Open Thermodyn. J.* **4**, 129-140.

Penteado P. F. and Griffith C. A. (2010) Ground-based measurements of the methane distribution on Titan. *Icarus* **206**, 345-351.

Pittman E. D. and Lewan M. D. (1994) *Organic Acids in Geological Processes*. Springer-Verlag, Berlin.

Poling B. E., Prausnitz J. M. and O'Connell J. P. (2001) *The Properties of Gases and Liquids*. McGraw-Hill, New York.

Poon D. P. L. and Lu B. C. Y. (1974) Phase equilibria for systems containing nitrogen, methane, and propane. *Adv. Cryog. Eng.* **19**, 292-299.

Prausnitz J. M., Lichtenthaler, R. N. and Gomes de Azevedo E. (1999) *Molecular Thermodynamics of Fluid-Phase Equilibria*. Prentice Hall PTR, Upper Saddle River, New Jersey.

Preston G. T. and Prausnitz J. M. (1970) Thermodynamics of solid solubility in cryogenic solvents. *Ind. Eng. Chem. Process Des. Develop.* **9**, 264-271.

Price L. C. (1981) Aqueous solubility of crude oil to 400°C and 2,000 bars pressure in the presence of gas. *J. Petrol. Geol.* **4**, 195-223.

Raulin F. (1987) Organic chemistry in the oceans of Titan. *Adv. Space Res.* **7**, 71-81.

Richard J. P., Williams G. and Gao J. (1999) Experimental and computational determination of the effect of the cyano group on carbon acidity in water. *J. Am. Chem. Soc.* **121**, 715-726.

Richard J. P., Amyes T. L. and Toteva M. M. (2001) Formation and stability of carbocations and carbanions in water and intrinsic barriers to their reactions. *Acc. Chem. Res.* **34**, 981-988.

Richardson W. H. and O'Neal H. E. (1972) The unimolecular decomposition and isomerization of oxygenated organic compounds (other than aldehydes and ketones). In *Comprehensive Chemical Kinetics: Decomposition and Isomerisation of Organic Compounds* (eds. C. H. Bamford and C. F. H. Tipper). Elsevier Publishing Company, Amsterdam. pp. 381-565.

Samuelson R. E., Nath N. R. and Borysow A. (1997) Gaseous abundances and methane supersaturation in Titan's troposphere. *Planet. Space Sci.* **45**, 959-980.

Schindler D. L., Swift G. W. and Kurata F. (1966) More low temperature V-L design data. *Hydrocarb. Process.* **45**, 205-210.

Schneider T., Graves S. D. B., Schaller E. L. and Brown M. E. (2012) Polar methane accumulation and rainstorms on Titan from simulations of the methane cycle. *Nature* **481**, 58-61.

Schowen R. L. (1972) Mechanistic deductions from solvent isotope effects. *Prog. Phys. Org. Chem.* **9**, 275-332.

Schubert W. M. and Keeffe J. R. (1972) The acid-catalyzed hydration of styrenes. *J. Am. Chem. Soc.* **94**, 559-566.

Seewald J. S. (1994) Evidence for metastable equilibrium between hydrocarbons under hydrothermal conditions. *Nature* **370**, 285-287.

Seewald J. S. (2001) Aqueous geochemistry of low molecular weight hydrocarbons at elevated temperatures and pressures: Constraints from mineral buffered laboratory experiments. *Geochim. Cosmochim. Acta* **65**, 1641-1664.

Segura P. (1985) Simultaneous use of empirical and semiempirical substituent parameters as a new method of analysis of the ortho effect. Application in reactions via aryl anion intermediates. *J. Org. Chem.* **50**, 1045-1053.

Segura P., Bunnett J. F. and Villanova L. (1985) Substituent effects on the decarboxylation of dinitrobenzoate ions. Representative aromatic S_E1 reactions. *J. Org. Chem.* **50**, 1041-1045.

Setzmann U. and Wagner W. (1991) A new equation of state and tables of thermodynamic properties for methane covering the range from the melting line to 625 K at pressures up to 1000 MPa. *J. Phys. Chem. Ref. Data* **20**, 1061-1155.

Shimoyama A. and Johns W. D. (1971) Catalytic conversion of fatty acids to petroleum-like paraffins and their maturation. *Nat. Phys. Sci.* **232**, 140-144.

Shipp J. and 5 colleagues. Organic functional group transformations in water at elevated temperature and pressure: Reversibility, reactivity, and mechanisms. *Geochim. Cosmochim. Acta*, submitted.

Shock E. L. (1988) Organic acid metastability in sedimentary basins. *Geology* **16**, 886-890.

Shock E. L. (1993) Hydrothermal dehydration of aqueous organic compounds. *Geochim. Cosmochim. Acta* **57**, 3341-3349.

Shock E. L. (1994) Application of thermodynamic calculations to geochemical processes involving organic acids. In *Organic Acids in Geological Processes* (eds. E. D. Pittman and M. D. Lewan). Springer-Verlag, Berlin. pp. 270-318.

Shock E. L. (1995) Organic acids in hydrothermal solutions: Standard molal thermodynamic properties of carboxylic acids and estimates of dissociation constants at high temperatures and pressures. *Am. J. Sci.* **295**, 496-580.

Shock E. L., Helgeson H. C. and Sverjensky D. A. (1989) Calculation of the thermodynamic and transport properties of aqueous species at high pressures and temperatures: Standard partial molal properties of inorganic neutral species. *Geochim. Cosmochim. Acta* **53**, 2157-2183.

Shock E. L. and Koretsky C. M. (1993) Metal-organic complexes in geochemical processes: Calculation of standard partial molal thermodynamic properties of aqueous acetate complexes at high pressures and temperatures. *Geochim. Cosmochim. Acta* **57**, 4899-4922.

Shock E. L., Sassani D. C., Willis M. and Sverjensky D. A. (1997) Inorganic species in geologic fluids: Correlations among standard molal thermodynamic properties of aqueous ions and hydroxide complexes. *Geochim. Cosmochim. Acta* **61**, 907-950.

Sim B. A., Milne P. H., Griller D. and Wayner D. D. M. (1990) Thermodynamic significance of ρ^+ and ρ^- from substituent effects on the redox potentials of arylmethyl radicals. *J. Am. Chem. Soc.* **112**, 6635-6638.

Smith M. B. and March J. (2007) *March's Advanced Organic Chemistry: Reactions, Mechanisms, and Structure.* Wiley-Interscience, Hoboken, New Jersey.

Smukala J., Span R. and Wagner W. (2000) New equation of state for ethylene covering the fluid region for temperatures from the melting line to 450 K at pressures up to 300 MPa. *J. Phys. Chem. Ref. Data* **29**, 1053-1121.

Soderblom L. A. and 18 colleagues. (2007) Topography and geomorphology of the Huygens landing site on Titan. *Planet. Space Sci.* **55**, 2015-2024.

Span R., Lemmon E. W., Jacobsen R. T., Wagner W. and Yokozeki A. (2000) A reference equation of state for the thermodynamic properties of nitrogen for temperatures from 63.151 to 1000 K and pressures to 2200 MPa. *J. Phys. Chem. Ref. Data* **29**, 1361-1433.

Sprow F. B. and Prausnitz J. M. (1966) Vapor-liquid equilibria for five cryogenic mixtures. *Am. Inst. Chem. Eng. J.* **12**, 780-784.

Stephan K. and 14 colleagues. (2010) Specular reflection on Titan: Liquids in Kraken Mare. *Geophys. Res. Lett.* **37**, L07104, doi:10.1029/2009GL042312.

Stermitz F. R. and Huang W. H. (1971) Thermal and photodecarboxylation of 2-, 3-, and 4-pyridylacetic acid. *J. Am. Chem. Soc.* **93**, 3427-3431.

Stoeckli H. F. and Staveley L. A. K. (1970) 231. Low temperature thermodynamics: The excess Gibbs function and the volumes of mixing for the system methane + propane at 90.68 K. *Helv. Chim. Acta* **53**, 1961-1964.

Stofan E. R. and 37 colleagues. (2007) The lakes of Titan. *Nature* **445**, 61-64.

Stofan E. R. and 16 colleagues. (2010) Exploring the seas of Titan: The Titan Mare Explorer (TiME) mission. *Lunar Planet. Sci. Conf.*, #1236 (abstr.).

Straub T. S. and Bender M. L. (1972) Cycloamyloses as enzyme models. The decarboxylation of phenylcyanoacetate anions. *J. Am. Chem. Soc.* **94**, 8875-8881.

Streitwieser A. Jr. and Koch H. F. (1964) Acidity of hydrocarbons. X. Exchange rates of ring-substituted toluene-α-t's with lithium cyclohexylamide in cyclohexylamine. *J. Am. Chem. Soc.* **86**, 404-409.

Streitwieser A. Jr. and Ni J. X. (1985) Base-catalyzed hydrogen isotope exchange and the aqueous acidity of toluene. *Tetrahedron Lett.* **26**, 6317-6320.

Strobel D. F. and 7 colleagues. (2009) Atmospheric structure and composition. In *Titan from Cassini-Huygens* (eds. R. H. Brown, J. P. Lebreton and J. H. Waite). Springer, New York. pp. 235-257.

Stryjek R., Chappelear P. S. and Kobayashi R. (1974) Low-temperature vapor-liquid equilibria of nitrogen-methane system. *J. Chem. Eng. Data* **19**, 334-339.

Stuart B. H. (2004) *Infrared Spectroscopy: Fundamentals and Applications*. John Wiley & Sons, Ltd, Chichester, England.

Stull D. R. (1947) Vapor pressure of pure substances: Organic compounds. *Ind. Eng. Chem.* **39**, 517-540.

Summerfield M. A. (1991) *Global Geomorphology: An Introduction to the Study of Landforms*. Pearson, Singapore.

Swain C. G. and Bader R. F. W. (1960) The nature of the structure difference between light and heavy water and the origin of the solvent isotope effect. *Tetrahedron* **10**, 182-199.

Szczepaniec-Cieciak E., Kondaurov V. A. and Melikova S. M. (1980) Study on the solubility light alkanes in liquid nitrogen. *Cryogenics* **20**, 48-51.

Taylor P. J. (1972a) The decarboxylation of some heterocyclic acetic acid. *J. Chem. Soc. Perk. Trans. II* **9**, 1077-1086.

Taylor R. (1972b) Kinetics of electrophilic aromatic substitution. In *Comprehensive Chemical Kinetics: Reactions of Aromatic Compounds*

(eds. C. H. Bamford and C. F. H. Tipper). Elsevier Publishing Company, Amsterdam. pp. 1-406.

Thibblin A. and Jencks W. P. (1979) Unstable carbanions. General acid catalysis of the cleavage of 1-phenylcyclopropanol and 1-phenyl-2-arylcyclopropanol anions. *J. Am. Chem. Soc.* **101**, 4963-4973.

Thompson W. R. (1985) Phase equilibria in N_2-hydrocarbon systems: Applications to Titan. In *The Atmospheres of Saturn and Titan* (eds. E. Rolfe and B. Battrick), ESA SP-241. ESA Publ. Div., Noordwijk, Netherlands. pp. 109-119.

Thompson W. R., Calado J. C. G. and Zollweg J. A. (1990) Liquid-vapor equilibrium of multicomponent cryogenic systems. In *First International Conference on Laboratory Research for Planetary Atmospheres* (eds. K. Fox, J. E. Allen, Jr., L. J. Stief and D. T. Quillen), NASA CP-3077. NASA, Washington, D.C. pp. 303-326.

Thompson W. R., Henry T. J., Schwartz J. M., Khare B. N. and Sagan C. (1991) Plasma discharge in $N_2 + CH_4$ at low pressures: Experimental results and applications to Titan. *Icarus* **90**, 57-73.

Thompson W. R., Zollweg J. A. and Gabis D. H. (1992) Vapor-liquid equilibrium thermodynamics of $N_2 + CH_4$: Model and Titan applications. *Icarus* **97**, 187-199.

Thurman E. M. (1985) *Organic Geochemistry of Natural Waters*. Martinus Nijhoff/Dr W. Junk Publishers, Dordrecht, Netherlands.

Tickner A. W. and Lossing F. P. (1951) The measurement of low vapor pressures by means of a mass spectrometer. *J. Phys. Colloid Chem.* **55**, 733-740.

Tiffin D. L., Kohn J. P. and Luks K. D. (1979) Solid hydrocarbon solubility in liquid methane-ethane mixtures along three-phase solid-liquid-vapor loci. *J. Chem. Eng. Data* **24**, 306-310.

Tissot B. P. and Welte D. H. (1984) *Petroleum Formation and Occurrence.* Springer-Verlag, Berlin.

Tokano T. (2009) Impact of seas/lakes on polar meteorology of Titan: Simulation by a coupled GCM-Sea model. *Icarus* **204**, 619-636.

Tomasko M. G. and 39 colleagues. (2005) Rain, winds and haze during the Huygens probe's descent to Titan's surface. *Nature* **438**, 765-778.

Tosca N. J. and McLennan S. M. (2006) Chemical divides and evaporite assemblages on Mars. *Earth Planet. Sci. Lett.* **241**, 21-31.

TSSM (Titan Saturn System Mission) Final Report on the NASA Contribution to a Joint Mission with ESA. 30 Jan. (2009) Task Order #NMO710851. *Outer Planet Flagship Mission Reports*. 21 Mar. 2012 <http://opfm.jpl.nasa.gov/library>.

Turtle E. P. and 7 colleagues. (2009) Cassini imaging of Titan's high-latitude lakes, clouds, and south-polar surface changes. *Geophys. Res. Lett.* **36**, L02204, doi:10.1029/2008GL036186.

Turtle E. P. and 13 colleagues. (2011a) Rapid and extensive surface changes near Titan's equator: Evidence of April showers. *Science* **331**, 1414-1417.

Turtle E. P., Perry J. E., Hayes A. G. and McEwen A. S. (2011b) Shoreline retreat at Titan's Ontario Lacus and Arrakis Planitia from Cassini Imaging Science Subsystem observations. *Icarus* **212**, 957-959.

van Laar J. J. (1906) *Sechs Vorträge über das Thermodynamische Potential (Six Lectures on the Thermodynamic Potential)*. Vieweg & Sohn, Braunschweig, Germany.

Vinatier S. and 10 colleagues. (2010) Analysis of Cassini/CIRS limb spectra of Titan acquired during the nominal mission: I. Hydrocarbons, nitriles and CO_2 vertical mixing ratio profiles. *Icarus* **205**, 559-570.

Watanabe M., Iida T. and Inomata H. (2006) Decomposition of a long chain saturated fatty acid with some additives in hot compressed water. *Energ. Convers. Manage.* **47** 3344-3350.

Watson A. (1983) Gypsum crusts. In *Chemical Sediments and Geomorphology: Precipitates and Residua in the Near-Surface Environment* (eds. A. S. Goudie and K. Pye). Academic Press, New York. pp. 133-161.

Wichterle I. and Kobayashi R. (1972) Vapor-liquid equilibrium of methane-ethane-propane system at low temperatures and high pressures. *J. Chem. Eng. Data* **17**, 13-18.

Willey L. M., Kharaka Y. K., Presser T. S., Rapp J. B. and Barnes I. (1975) Short chain aliphatic acid anions in oil field waters and their contribution to the measured alkalinity. *Geochim. Cosmochim. Acta* **39**, 1707-1711.

Willi A. V. (1959) Kinetics and mechanism of the decarboxylation of salicylic acids. *Trans. Faraday Soc.* **55**, 433-441.

Willi A. V. (1977) Homogeneous catalysis of organic reactions (mainly acid-base). In *Comprehensive Chemical Kinetics: Proton Transfer* (eds. C. H. Bamford and C. F. H. Tipper). Elsevier Scientific Publishing Company, Amsterdam. pp. 1-95.

Williams L. B., Hervig R. L., Holloway J. R. and Hutcheon I. (2001) Boron isotope geochemistry during diagenesis. Part I. Experimental determination of fractionation during illitization of smectite. *Geochim. Cosmochim. Acta* **65**, 1769-1782.

Wilson G. M. (1975) Vapor-liquid equilibria of nitrogen, methane, ethane, and propane binary mixtures at LNG temperatures from total pressure measurements. *Adv. Cryog. Eng.* **20**, 164-171.

Wilson E. H. and Atreya S. K. (2009) Titan's carbon budget and the case of the missing ethane. *J. Phys. Chem. A* **113**, 11221-11226.

Wohl K. (1946) Thermodynamic evaluation of binary and ternary liquid systems. *Trans. Am. Inst. Chem. Eng.* **42**, 215-249.

Yang Z., Gould I. R., Williams L., Hartnett H. E. and Shock E. L. The central role of ketones in reversible and irreversible hydrothermal organic functional group transformations. *Geochim. Cosmochim. Acta*, submitted.

Yu P., Elshayal I. M. and Lu B. C. Y. (1969) Liquid-liquid-vapor equilibria in the nitrogen-methane-ethane system. *Can. J. Chem. Eng.* **47**, 495-498.

Yung Y. L., Allen M. and Pinto J. P. (1984) Photochemistry of the atmosphere of Titan: Comparison between model and observations. *Astrophys. J. Suppl. S.* **55**, 465-506.

Zhou L. and 6 colleagues. (2010) Cosmic-ray-mediated formation of benzene on the surface of Saturn's moon Titan. *Astrophys. J.* **718**, 1243-1251.

Zolotov M. Y., Mironenko M. V. and Shock E. L. (2006) Thermodynamic constraints on fayalite formation on parent bodies of chondrites. *Meteorit. Planet. Sci.* **41**, 1775-1796.

APPENDIX A

DERIVATION OF THE MODIFIED VAN LAAR MODEL

The purpose of this section is to show how Scatchard-Hildebrand regular solution theory can be transformed into the modified van Laar (MVL) model. Regular solution theory provides a suitable basis for an empirical model of non-ideality in mixtures of nonpolar molecules. The theory assumes that the volume of a liquid mixture is the sum of pure-component volumes, and the entropy of mixing of pure components is equivalent to that of the corresponding ideal solution. The distribution and orientations of molecules in a regular solution are random, as a result of non-directional intermolecular interactions and thermal agitation. In general, these assumptions are appropriate for mixtures of nonpolar molecules (Hildebrand & Scott, 1950). The excess Gibbs energy of mixing (G^E) refers to the difference in free energy between a solution and its ideal counterpart. In Scatchard-Hildebrand theory, G^E for binary 1-2 is given by (Prausnitz et al., 1999)

$$\frac{G^E}{v_{mix}} = \left(\frac{\Delta U_1}{v_1} + \frac{\Delta U_2}{v_2} - 2\frac{\Delta U_{12}}{v_{12}} \right) \Phi_1 \Phi_2 , \qquad\qquad (A1)$$

where ΔU stands for internal energy of vaporization to the ideal gas state, v designates liquid volume, and Φ indicates volume fraction in the mixture. Parameters with subscript 12 are constants that are used with mixing rules to characterize mixtures in terms of pure-component properties.

Volume v_{12} can be decomposed using the van der Waals mixing rule for volume parameters: $v_{12} = (v_1+v_2)/2$. Substituting this into Eq. (A1) and rearranging, yields

$$\frac{G^E}{v_{mix}} = \frac{\omega_{12}\Phi_1\Phi_2}{(v_1+v_2)},$$
(A2)

with

$$\omega_{12} = \left(1+\tfrac{v_2}{v_1}\right)\Delta U_1 + \left(1+\tfrac{v_1}{v_2}\right)\Delta U_2 - 4\Delta U_{12},$$
(A3)

where ω_{12} is defined as the interaction energy for binary 1-2. To obtain optimal agreement with experimental data, ω_{12} is treated as an adjustable parameter (e.g., Peng, 2010). Theoretical evaluation of ω_{12} is hampered by the inability to formulate a suitable mixing rule for ΔU_{12} (arithmetic or geometric means are insufficient). A second modification of regular solution theory is to replace liquid volumes in Eq. (A2) with effective volumes (q), as suggested by Hildebrand & Scott (1950). This gives the MVL model more flexibility.

A simple expression for the excess Gibbs energy of mixing in multicomponent systems from the MVL model is

$$\frac{G^E}{q_{mix}} = \sum_{i=1}^{n-1}\sum_{j>i}^{n} \frac{\omega_{ij}z_i z_j}{q_i+q_j},$$
(A4)

199

where z represents effective volume fraction in the mixture. Activity coefficients (Eq. 3 in Chapter 1) can be derived from Eq. (A4) by differentiating Eq. (A4) with respect to the component of interest (see Prausnitz et al., 1999). This guarantees thermodynamic consistency by satisfaction of the Gibbs-Duhem equation. Summing binary contributions to non-ideal behavior in Eq. (A4) should provide reasonable approximations for nonpolar mixtures, in which two-body interactions are most important. This is because relatively weak dispersion forces between nonpolar molecules act over short distances.

The accuracy of the MVL model can be improved by accounting for ternary interactions. A logical extension of Eq. (A4) is (e.g., Wohl, 1946)

$$\frac{G^E}{q_{mix}} = \sum_{i=1}^{n-1}\sum_{j>i}^{n}\frac{\omega_{ij}z_i z_j}{q_i + q_j} + \sum_{a=1}^{n-2}\sum_{b>a}^{n-1}\sum_{c>b}^{n}\frac{\omega_{abc}z_a z_b z_c}{q_a + q_b + q_c}, \tag{A5}$$

where ω_{abc} specifies the interaction energy for ternary a-b-c. This is a more general form of the MVL model. The structure of this equation is reminiscent of that used in the formulation of the Pitzer equations (Anderson, 2005), which are used in geochemistry to calculate activity coefficients of components in saline solutions. There is also an analogy with the virial equation (Prausnitz et al., 1999). Differentiation of Eq. (A5) leads to Eq. (12) in Chapter 1. Adding further corrections, such as quaternary terms, seems unnecessary for nonpolar mixtures, and would make the model unwieldy.